論文 / 著書情報
Article / Book Information

題目(和文)	
Title(English)	Deployment of Wireless Multi-hop Networks in Practical Environments
著者(和文)	ﾗｰｽﾋﾞ ﾗﾑﾅﾑｼｰﾝﾌﾟ
Author(English)	Namzilp Lertwiram
出典(和文)	学位:博士(学術), 学位授与機関:東京工業大学, 報告番号:甲第9339号, 授与年月日:2013年9月25日, 学位の種別:課程博士, 審査員:荒木 純道,鈴木 博,高田 潤一,府川 和彦,松本 隆太郎,阪口 啓
Citation(English)	Degree:Doctor (Academic), Conferring organization: Tokyo Institute of Technology, Report number:甲第9339号, Conferred date:2013/9/25, Degree Type:Course doctor, Examiner:,,,,,
学位種別(和文)	博士論文
Type(English)	Doctoral Thesis

Doctoral Dissertation

Deployment of Wireless Multi-hop Networks in Practical Environments

August 2013

Supervisors

Professor Kiyomichi Araki

Associate Professor Kei Sakaguchi

Department of Communications and Integrated Systems

Graduate School of Engineering

Tokyo Institute of Technology

Namzilp Lertwiram

Contents

List of Figures

List of Tables

Abstract

Low latency and high reliability systems are required for future applications of Wireless Sensor Networks (WSNs) in autonomous systems. Since WSNs consist of numerous sensor nodes distributed in the target area, the deployment of relay nodes is necessary to help sensor nodes, which cannot directly connect to the sink, to transfer data. One of the efficient ways to deploy relay is to construct multi-hop relay networks as supporting backbone to the WSNs. To maximize the network performance, however, network designers still confront with challenges in deploying multi-hop networks in WSNs, especially the determination of optimum relay placement and the exploitation method of Multi-Input Multi-Output (MIMO). These two issues have been investigated in several researches based on theoretical models, which are almost impractical since they do not consider the effect of shadowing caused by obstacles typically existing in realistic environments. Therefore, the main contribution of this dissertation is to provide the deployment methodology of multi-hop relay networks in practical environments, mainly subject to optimize the relay node placement and network performance. To achieve this objective, we conduct the propagation measurement experiment and 3D ray-tracing simulation to obtain the information of MIMO propagation channels in realistic environments for using in our studies. In this dissertation, we first study the performance of MIMO multi-hop relay networks in a real shadowing environment by adapting several relaying schemes, which have been theoretically investigated so far, to verify the best method of achieving high network capacity. Together with the performance optimization of multi-hop networks based on different relaying schemes, we also investigate the optimum relay locations. Finally, with the similar analogy, we design a deployment methodology of backbone network for WSNs, which the network designers can use to find the best relay locations and fully exploit MIMO technology to obtain the best network performance.

Acknowledgments

My research works during the Ph.D program cannot be succeeded without the supports from several people. I would like to express my gratefulness to all of them.

First of all, I would like to show my deepest gratitude to Assoc. Prof. Kei Sakaguchi and Prof. Kiyomichi Araki, the academic supervisors of my graduate course, who always provide me several helpful suggestions in my research and support me several things during I spent my life in Japan. I also greatly indebted to Prof. Hiroshi Suzuki, Assoc. Prof. Kazuhiko Fukawa, Prof. Junichi Takada, and Assoc. Prof. Ryutaroh Matsumoto who are my dissertation committee members and provided me several critical comments to improve the quality of my research. Also, I would like to thank Assoc. Prof. Lunchakorn Wuttisittikulkij, the supervisor of my senior project when I studied at Chulalongkorn University, who recommended me to Araki-Sakaguchi laboratory.

In addition, during my Ph.D program, I had a chance to be an exchange researcher at Aalborg University, Denmark, in Autumn 2011. At that time, Assoc. Prof. Petar Popovski was my supervisor during the exchange program, and helped me a lot in the research topic that is not directly related to what I have been doing in the home university. It was my pleasure to have a research work with him.

There are also several people who have contributed their valuable time to my research work in this dissertation. First person I would like to thank is Assist. Prof. Gia Khanh Tran, who always provides me several advantageous comments, checks my manuscript of several papers, and teaches me lots of knowledge in my research field. Also, I would like to show my gratitude to Dr. Keiichi Mizutani, Mr. Jonghyong Lee, Mr. Minoru Komatsu, Mr. Shinichi Tajima, Mr. Naoki Kusashima, Mr. Ramamonjison Rindranirina and other members of Araki-Sakaguchi laboratory for helping me in the experiment of MIMO relay networks in L-shaped corridor.

Also, during my study in Japan, I also had a chance to become a board member of Thai

Students'Association in Japan (TSAJ) where I had a good experience and practiced my skills of working besides the academic part. In this chance, I would like to show my gratitude to the president of TSAJ in the fiscal year of 2012, Ms. Pitcha Jongvivatsakul, the other board members of financial affair division I worked in, Mr. Bancha Janthong, and Mr. Dejudom Kiatpanachart, and other people in TSAJ who supported the activities during my working term in TSAJ.

Finally, my success in Ph.D degree cannot be achieved if there is no encouragement from my family. I would like to acknowledge my parents, Mr. Apisit Lertwiram and Ms. Ariya Issaravinyakul, who are always taking care of me. Also, I would like to show my obligation to Mr. Vichai and Ms. Aksorn Issaravinyakul, who I stayed with during my study in Chulalongkorn University and gave me several suggestions in my life.

Chapter 1

Introduction

1.1 Background

In the past decades, wireless technologies have been developed to serve the need of people in several ways. The form of wireless technologies has been grown from "person-to-person (P2P)" communications, such as cellular systems, to "person-to-machine (P2M)" communications, such as Internet access via Wireless Local Area Networks (WLANs) or the third generation cellular systems (3G), and then recently to "machine-to-machine (M2M)" communications [1], such as Wireless Sensor Networks (WSNs) [2]- [4]. Nowadays, several researchers are paying a great attention to WSN technology since it simplifies the establishment and lowers the cost of autonomous systems, e.g. environment surveillance systems, from the conventional systems with wired-cable solutions.

WSN technology has been originally motivated by military applications such as battlefield surveillance. In the later time, by the advancement of wireless communications and electronics, WSNs have been employed to consumer uses such as health care monitoring, industrial process monitoring, traffic monitoring, etc. [2]. These applications, however, are typically for monitoring the environmental conditions. Nowadays, WSNs are expected to apply in autonomous systems, which provide both sensing and actuating features to not only monitor but also control the target environment condition, such as factory automation systems [5]- [8], smart energy-controlled building [9]- [11].

Traditionally, WSNs consist of numerous sensor nodes distributed over the interest area. In practical environments, some sensor nodes in the network cannot transfer their signal directly to the sink due to two main reasons, illustrated in Fig. 1.1. For the first reason, some

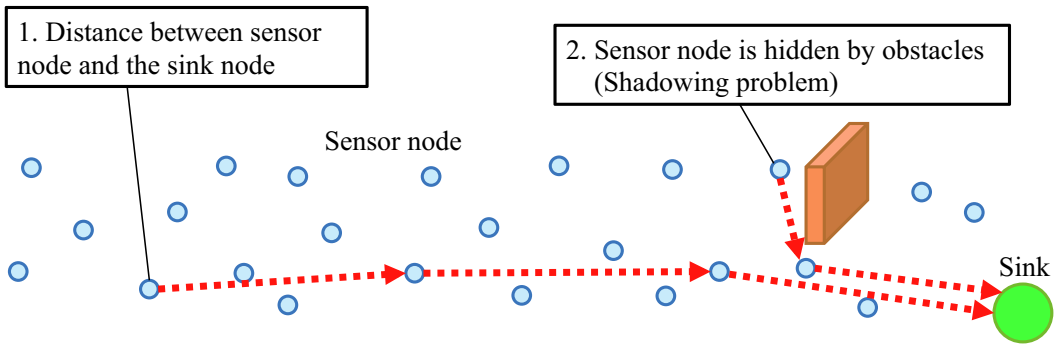

Figure 1.1 The problem of non-connectable sensor nodes in WSNs.

sensor nodes are located far from the sink node, or gateway node connected to the central server, so that the signals are significantly degraded due to distance loss. The second reason is that, in practical environment, some of sensor nodes are hidden from the sink by obstacles which weaken signal power received by the destination nodes. This kind of problem is also known as shadowing problem [12]. By these reasons, these sensor nodes need relays to help them transfer data to the sink [13]- [15].

Conventionally, a sensor node transfers signal to the sink node through other sensor nodes, which act as relays, in ad-hoc manner, where the determination of routing is made dynamically on the basis of connectivity between nodes in distance range. However, non-deterministic routing protocols [16] result in unpredictable performance bounds. To avoid this problem, the works in [17]- [18] suggest deploying the network in heterogeneous manner, and [19]- [20] suggest the deployment in cluster-tree topology. In both ways, relay nodes are hierarchically deployed over sensor nodes and take a role of cluster nodes to gather data from the nearby sensor nodes and transfer to the sink via cluster nodes in multi-hop relay manner. The multi-hop relay network over the clusters can be treated as a supporting backbone network for the WSN, as illustrated in Fig. 1.2. Therefore, it is necessary to deploy the backbone network with high capacity in order to construct a reliable and robust WSN. In this thesis, we aim to focus on the deployment of wireless multi-hop networks expected to be a backbone for WSNs in order to enhance network performance.

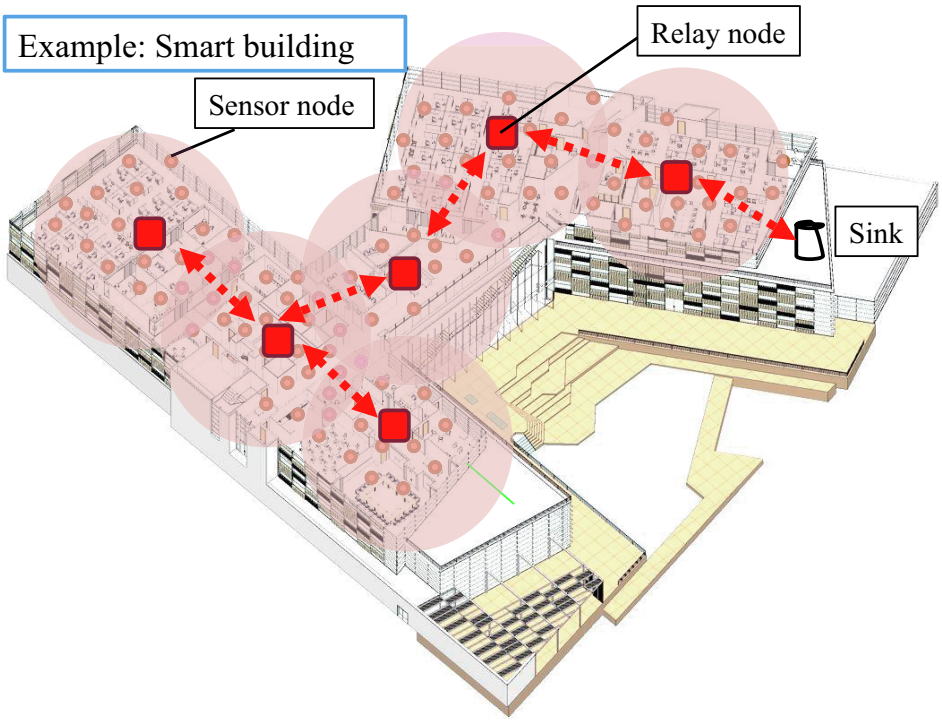

Figure 1.2 The deployment of backbone network for densely deployed WSNs.

1.2 Overview of wireless multi-hop networks

The effort of implementing multi-hop relay in wireless networks has long been an attention for researchers in several standardization working groups, including IEEE 802.15.4. The IEEE 802.15.4 standard [21] specifies physical layer and medium access layer protocol for Low-Rate Wireless Personal Area Networks (LR-WPAN) which is a basis for the extended standard such as ZigBee, WirelessHART, and ISA 100.11a [22]. IEEE 802.15.4 also suggests cluster-tree topology as an alternative way of network formation, where the connection between cluster nodes can be realized as multi-hop backbone network supporting the entire WSN.

As mentioned, the upcoming applications of WSNs require the backbone multi-hop networks with high capacity. Recently, Multiple-Input Multiple-Output (MIMO) is a technique to increase capacity by employing multiple antennas to transceivers [23]. To fulfill this requirement, MIMO is adopted to multi-hop relay networks in several ways. The idea of using multiple antennas is originally to exploit the spatial diversity to combat with deep fading in wireless channel [24]. In addition, multiple antennas at both transmitter (Tx) and receiver (Rx) sides also gain the additional degree-of-freedom to spatial domain which enables the system suppress co-channel interference and establishes the multiple parallel channels. This feature is known as spatial multiplexing and the improvement of spatial efficiency resulted by this feature is proved in [23] for the Rayleigh fading channels. Since the applications for autonomous systems are mostly in two-way manner, several researchers applied MIMO to enable multi-hop network simultaneously to relay data in bi-direction [25]- [27].

To the best of our knowledge, however, the researches of multi-hop relay networks are based on theoretical studies. In practical, the network designers still confront with the difficulties of deploying multi-hop networks in the target environment as follows. The first challenge is how to determine the optimum placement to deploy relay nodes in the realistic environment, which is typically full of obstacles causing shadowing problem. The studies in [28]- [34] indicate that relay locations have an important impact to the network performance in the realistic environments, especially when transceivers are in the condition of Non-Line-Of-Sight (NLOS). The assumption of theoretical channel model has been used in the studies of optimum relay placement [31]- [34]. However, there is still lack of study to verify the optimum relay placement in realistic environments where shadow fading exists. Moreover, several relaying schemes employing MIMO have been proposed, however, some of them, especially MIMO two-way relaying schemes, have not been evaluated in real shadowing environments. Also,

the study of how to maximally exploit the ability of MIMO in multi-hop networks to optimize the performance in the realistic environment is still challenging.

1.3 Contributions and outline of the dissertation

Due to the lack of studies addressed in the previous sections, the main contribution of this dissertation is to study the deployment methodology of wireless multi-hop networks in practical environments. To implement an efficient multi-hop network in the target environment, the deployment of multi-hop network must cover the following four main issues:

- Which transceiver nodes need relay to connect to their destination?
- Which relaying scheme is appropriate?
- Where the optimum location for each relay node is?
- How to optimize the network resource in the network?

Figure 1.3 shows the outline of remaining parts of the dissertation.

Chapter 2 briefly introduces the fundamental concept of MIMO communication systems and the exploitation of MIMO in multi-hop relay networks. This chapter presents several MIMO relaying schemes, which will be used for evaluation in the practical environment for the rest chapters. Also, the method for calculating Signal to Interference plus Noise Ratio (SINR) and end-to-end capacity, which will be used in the rest of this dissertation, is also explained.

Chapter 3 presents the design of basic two-hop MIMO relay networks in practical shadowing environment. Here, the study focuses on the role of relay as a solution for shadowing problem. In this chapter, MIMO propagation channel measurement in the realistic L-shaped corridor environment, where shadowing is dominant, is conducted. The degradation of network performance by shadowing and the improvement of network performance by employing relay will be discussed. Furthermore, this chapter also evaluates the capacity performance of various schemes as well as the optimum relay placement in the shadowing environment. By this study, the criteria of relay deployment in two-hop relay network configuration can be concluded. The results in this chapter are published in

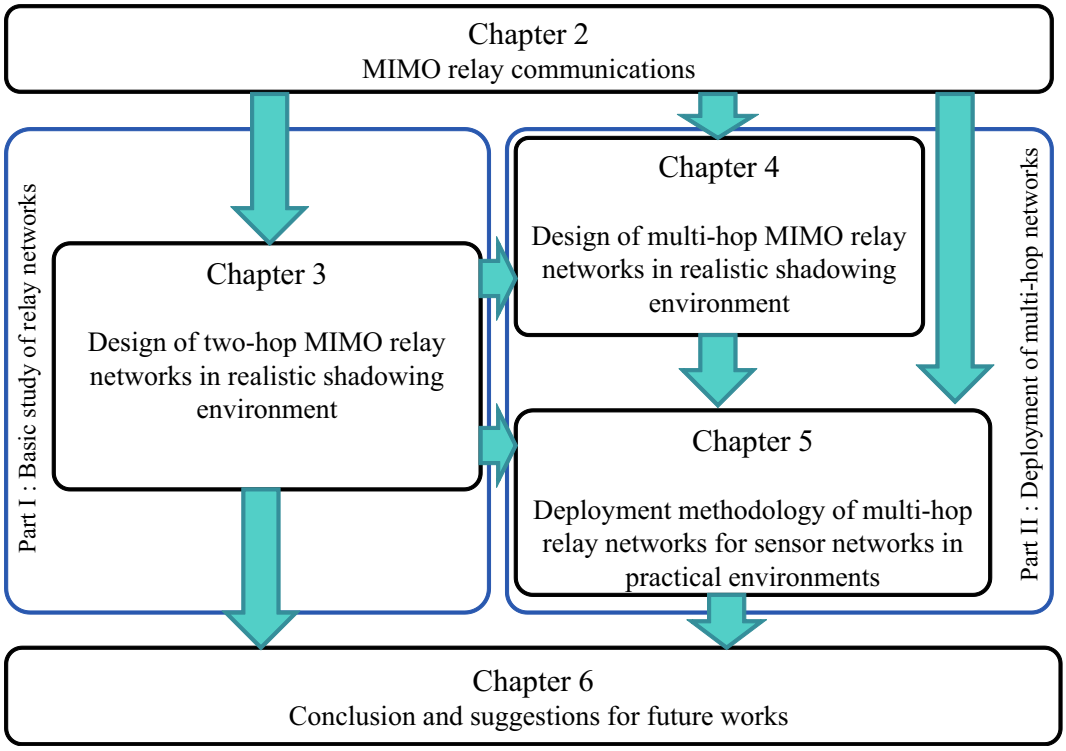

Figure 1.3 The organization of this dissertation.

- N. Lertwiram, G. K. Tran, K. Mizutani, K. Sakaguchi, K. Araki, "Performance Analysis of MIMO Relay Network via Propagation Measurement in L-shaped Corridor Environment", IEICE Trans. Commun., Vol. E95-B, No. 04, Apr. 2012.

- N. Lertwiram, G. K. Tran, K. Mizutani, K. Sakaguchi, K. Araki, "MIMO Radio Propagation Measurement for Two-Hop Relay Network on L-shaped Corridor with Network Performance Analysis", IEEE VTC2010-Spring, May. 2010.

- N. Lertwiram, G. K. Tran, K. Mizutani, K. Sakaguchi, K. Araki, "Propagation Measurement of MIMO Relay Network in Strong Shadowing Indoor Environment at 5 GHz Band", IEICE RCS Technical Conf., vol. 109, no. 440, pp. 161-166, Mar. 2010

Chapter 4 extends the consideration from basic two-hop relay networks discussed in Chapter 3 to multi-hop relay networks. The study is conducted by performing the 3D ray-tracing simulation in the U-shaped corridor environment. Different from two-hop relay networks, co-channel interference among nodes limits the network performance, so that the exploitation of MIMO as well as optimization of network resource and relay placement in order to deal with this problem is discussed. Similarly, the criteria of relay deployment in multi-hop network configuration can be concluded. The results in this chapter are published in

- N. Lertwiram, G. K. Tran, K. Sakaguchi, K. Araki, "An Efficient Relay Node Placement Scheme for Two-way MIMO Multi-hop Networks in Practical Environment", IEEE Trans.Wireless Commun., Vol. 12, No. 6, pp. 2977 - 2987, June 2013.

- N. Lertwiram, G. K. Tran, K. Sakaguchi, K. Araki, "Relay Placement of Two-Way Multi-Hop Relay Network with Power Adaptation in a Realistic Shadowing Environment", IEEE VTC2012-Spring, May. 2012.

- N. Lertwiram, G.K. Tran, K. Sakaguchi, K. Arkai, "Practical Relay Node Placement for MIMO Two-way Relay Networks in a U-Shaped Corridor Environment", IEICE SR Technical Conf., 2012-07-SR, Jul. 2012.

Chapter 5 proposes the deployment methodology of multi-hop relay networks for WSNs in practical environments by using the analogy learnt from Chapter 3 and 4. The results in this chapter are published in

- N. Lertwiram, G.K. Tran, K. Sakaguchi, K. Arkai, "Network Planning Methodology for Wireless Multi-hop Networks in Practical Environments", IEICE SR Technical Conf., 2013-07-SR, Jul. 2013.

Finally, Chapter 6 concludes the studies in this dissertation and provides suggestions for the future studies.

Chapter 2

MIMO relay communications

2.1 Introduction

In wireless systems, the rapid growth of demand for capacity has become challenges for system designers due to the limitation of the available radio spectrum. MIMO technique has been proposed to improve the network capacity. Owing to multiple antennas employed at both the Tx and Rx, MIMO systems can significantly improve spectral efficiency without sacrificing power and radio bandwidth [23].

In addition, the deployment of relay nodes in wireless networks becomes necessary in some practical environments where the Tx cannot directly transmit signal to Rx due to the existence of obstacles or distance between nodes. Recently, MIMO technique has been adapted to wireless relay networks in order to improve the network performance.

This chapter contains the basic idea of MIMO communications. After that, the adaptation of MIMO in basic two-hop relay networks is introduced before we consider the usage of MIMO in multi-hop networks in the following sections.

2.2 MIMO communication systems

2.2.1 MIMO system model

By having multiple transmit antennas and receive antennas, MIMO provides additional spatial dimensions for communication and yields a degree-of-freedom gain. These additional degrees of freedom can be exploited by spatially multiplexing several data streams via single

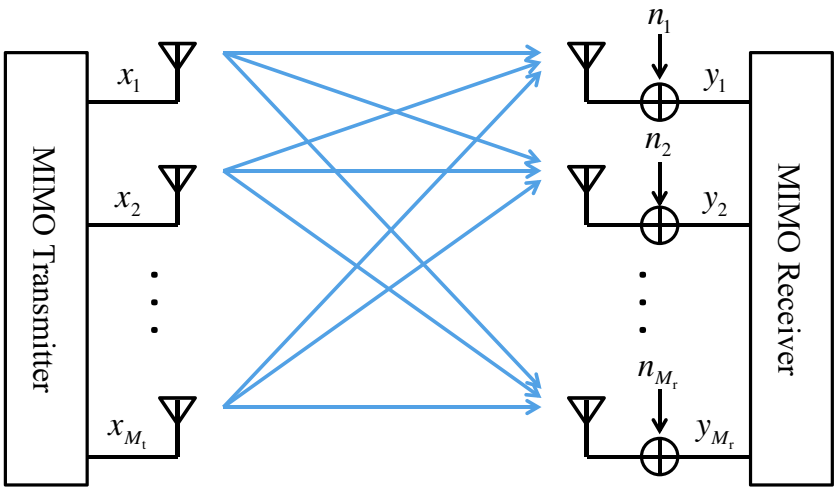

Figure 2.1 MIMO communication systems.

transmitter and receiver, and lead to an increase in capacity.

A general narrowband point-to-point MIMO communication system with Additive White Gaussian Noise (AWGN) is illustrated in Fig. 2.1. The transmitter and receiver are equipped with M_t and M_r antennas respectively. This system can be represented by the following discrete-time model as

$$\begin{bmatrix} y_1 \\ \vdots \\ y_{M_\mathrm{r}1} \end{bmatrix} = \begin{bmatrix} h_{11} & \dots & h_{1M_\mathrm{t}} \\ \vdots & \ddots & \vdots \\ h_{M_\mathrm{r}1} & \dots & h_{M_\mathrm{r}M_\mathrm{t}} \end{bmatrix} \begin{bmatrix} x_1 \\ \vdots \\ x_{M_\mathrm{t}} \end{bmatrix} + \begin{bmatrix} n_1 \\ \vdots \\ n_{M_\mathrm{r}} \end{bmatrix}, \tag{2.1}$$

or simply as

$$\mathbf{y} = \mathbf{H}\mathbf{x} + \mathbf{n}, \tag{2.2}$$

where, $\mathbf{y} \in \mathcal{C}^{M_\mathrm{r}}$ is the receive signal vector, $\mathbf{x} \in \mathcal{C}^{M_\mathrm{t}}$ is the transmit signal vector, $\mathbf{H} \in \mathcal{C}^{M_\mathrm{r} \times M_\mathrm{t}}$ is the matrix of channel responses where h_{ij} represents the channel response from transmit antenna j to receive antenna i, and $\mathbf{n} \in \mathcal{C}^{M_\mathrm{r}}$ is the noise signal vector. The noise vector is assumed to be complex AWGN with zero mean and σ^2 variance element vectors, where typically $\sigma^2 = \mathrm{E}[n_i^2]$.

There are several techniques to decode each independent stream from the receive signal. In this thesis, we consider the basic linear estimation algorithm of Zero Forcing (ZF). The idea of ZF is that the estimation of the transmit vector can be obtained by producing the

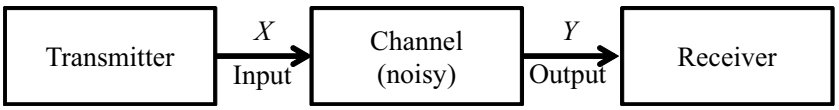

Figure 2.2 Diagram of a general communication channel.

receive weight which is the inverse matrix of MIMO channel, $(\mathbf{H}^H\mathbf{H})^{-1}\mathbf{H}^H$ and applying to the receive signal such that cross interference signal can be canceled out as,

$$\hat{\mathbf{x}} = (\mathbf{H}^H\mathbf{H})^{-1}\mathbf{H}^H\mathbf{y} = \mathbf{H}^+\mathbf{y} = \mathbf{x} + \mathbf{H}^+\mathbf{n}, \tag{2.3}$$

where $\hat{\mathbf{x}}$ represents the estimated signal of transmit vector, and $[.]^+$ represents the pseudo-inverse.

2.2.2 Capacity of MIMO channel

Basically, the performance of wireless communications is evaluated by using Shannon capacity [35]. Firstly, we consider a general communication system illustrated in Fig. 2.2. The relationship between input and output of the system can be expressed as $Y = X + N$, where X is the random input, Y is the random output, and N is noise in random process. Referring to information theory, the channel capacity is defined as

$$C = \max I(X;Y), \tag{2.4}$$

where $I(X;Y)$ is the mutual information between X and Y. From this concept, Shannon derived the capacity of AGWN wireless channel with bandwidth B as

$$C = \log_2(1+\gamma), [\text{bps/Hz}] \tag{2.5}$$

where γ is the Signal-to-Noise Ratio (SNR) of the corresponding channel. It is noted that the above Shannon capacity is originally created for a general Single-Input Single-Output (SISO) system; or a system where Tx and Rx are equipped with single antenna. In simple AWGN wireless channel, the receive signal can be written as $y = hx + n$, where y is the receive signal, x is the transmit signal, h is complex channel response and n is an AWGN with zero mean and σ^2 variance, so that the SNR of the channel can be expressed as $\frac{P|h|^2}{\sigma^2}$, where P is the transmit power, and the capacity of wireless channel becomes

$$C = \log_2(1 + \frac{P|h|^2}{\sigma^2}) \text{ [bps/Hz]}, \tag{2.6}$$

On the other hand, the concept of Shannon capacity is also applied for the determination of MIMO channel [36]. For a general MIMO system in Fig. 2.1, the capacity of MIMO channel can be determined as the maximum mutual information between $\mathbf{x}$ and $\mathbf{y}$, $I(\mathbf{x};\mathbf{y})$ as

$$C = \max I(\mathbf{x};\mathbf{y}), \tag{2.7}$$

and then the expression of MIMO capacity in AWGN channel becomes [23]

$$C = \log_2 \det(\mathbf{I}_{M_\mathrm{r}} + \frac{P}{M_\mathrm{t}\sigma^2}\mathbf{H}\mathbf{H}^H) \text{ [bps/Hz]}. \tag{2.8}$$

It is noted that this expression is for the case that transmit power is equally allocated to all antennas and CSI is unknown at Tx.

2.3 Introduction of MIMO relay networks

As introduced in Chapter 1, in some practical environments, relay nodes are necessary to help a pair of transceiver to transfer signals. In this section, we briefly introduce the technique of implementing relay nodes in the networks as well as the exploitation of MIMO technique in relay networks.

Figure 2.3 shows the chart of the implementation of relay nodes as well as the exploitation of MIMO in relay networks in various configurations. For basic configuration of wireless network, the network consists of one Tx and one Rx, each of which is equipped with single antenna as shown in Fig. 2.3a. If the transmission needs relay, the basic idea is to deploy a relay between Tx and Rx, as shown in Fig. 2.3b. In this case, two-hop relay network, or network with single relay node, is the most basic configuration of relay network. In this dissertation, we consider Decode-and-Forward (DF) scheme [37] as the most fundamental scheme in our research. In this scheme, source node transmit signal to relay node in the first timeslot, and then relay node decodes the received signal and regenerates the signal to transmit to destination node in the second timeslot. In addition, the DF scheme is extended to DF cooperative scheme where the destination node also utilizes the direct signal from the source node in the first timeslot to combine with the signal in the second timeslot to achieve diversity gain [38]- [40]. Since DF and DF cooperative can be achieved with single antenna configuration, we consider these two schemes as conventional schemes in this dissertation. The details of capacity calculation as well as the exploitation of MIMO in these two schemes will be described later in this chapter.

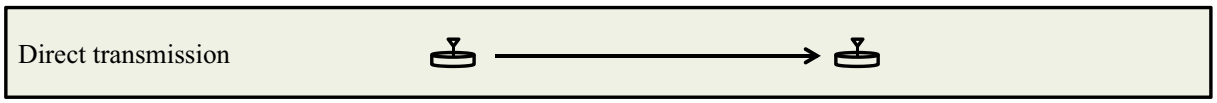

(a) Direct transmission.

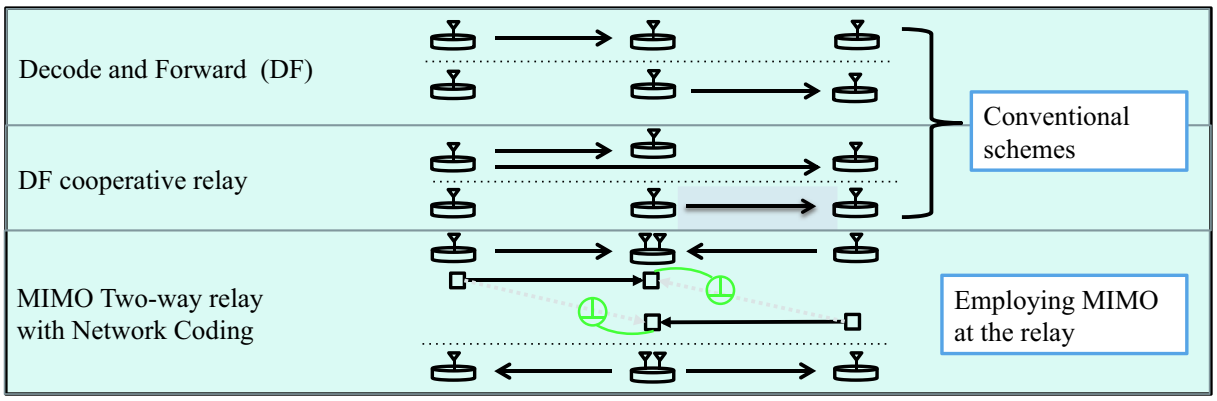

(b) Two-hop relay network.

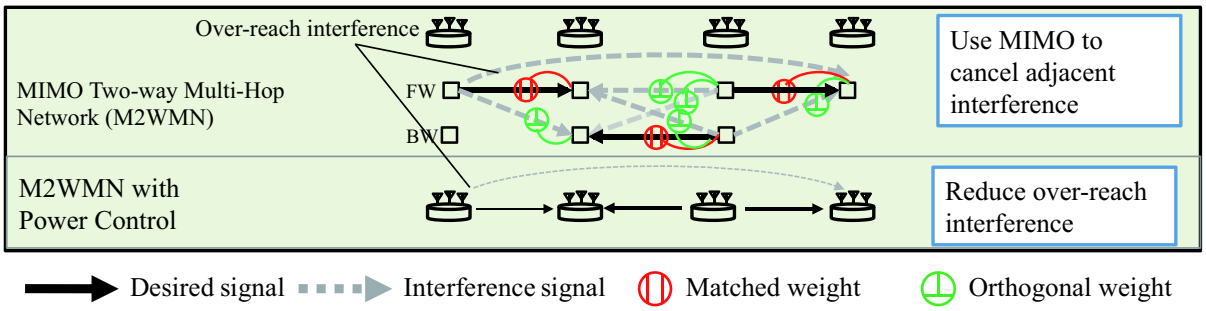

(c) Multi-hop relay network.

Figure 2.3 The chart of MIMO relaying schemes used in this dissertation.

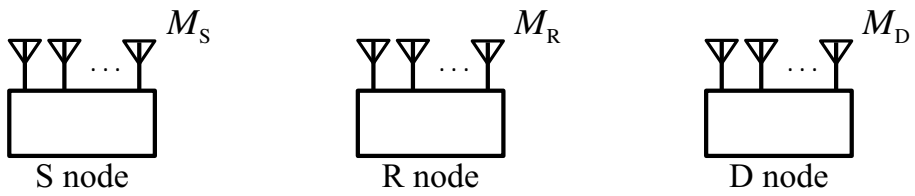

Figure 2.4 The system model of a basic two-hop MIMO relay network.

As mentioned, MIMO can be applied to increase the channel capacity of each transmission link. Recently, [27], [41] proposed two-way relay network with network coding scheme to enable bi-directional communications. This scheme is achieved by employing at least two antennas at the relay node as shown in Fig. 2.3b. Here, the increment of degree of freedom can be used to perform multiple access, where signal from source and destination can be simultaneously received at the relay node, and the interference can be eliminated by applying the orthogonal weight in the first timeslot. After that, the signal is combined by the mechanism of network coding and then broadcasted to source and destination nodes in the second timeslot. Here, the source and destination nodes use prior knowledge to decode the signal from the opposite side.

Until now, we consider the basic two-hop configuration. In some environments, the network needs more than two relay nodes to transfer the signal, so that the consideration of multi-hop relay networks is also necessary. In our consideration, we extend the MIMO two-way relaying scheme in the previous section to multi-hop configuration as shown in Fig. 2.3c. Owing to MIMO, each transceiver node determines the Tx-Rx weight by assigning orthogonal weight to eliminate the interference signal from the adjacent node and assigning parallel weight to desired signal [25]. Here, bi-directional communications in multi-hop networks can be achieved. However, the over-reach interference from far nodes still exists and has an effect to the network capacity. In order to reduce this effect, power control scheme is applied to adjust the Tx power of transmitter node as well as maximize the network capacity [42], [44]. The details of each relaying scheme as well as calculation method of network capacity are described in the rest of this chapter.

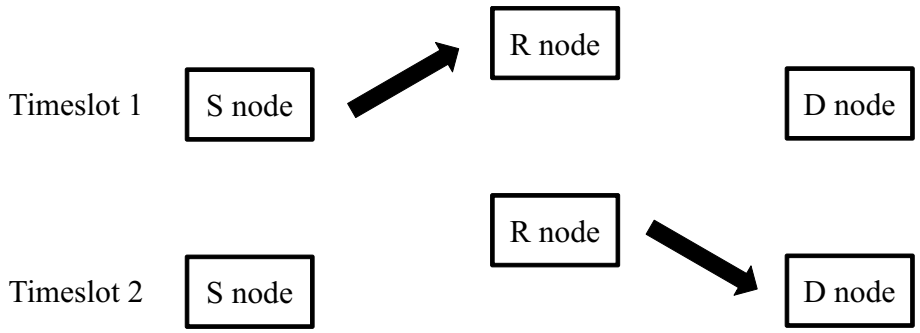

Figure 2.5 The network model of DF relaying scheme.

2.4 Relaying schemes for basic two-hop relay networks

Generally, a basic two-hop relay network consists of three transceiver nodes having a role of source, relay and destination which are denoted as S, R and D nodes respectively. The system model of the MIMO relay network is illustrated in Fig. 2.4. M_{S}, M_{R}, and M_{D} denote the number of antennas of S, R and D nodes respectively. $\mathbf{H}_{\mathrm{RS}} \in \mathcal{C}^{M_{\mathrm{R}} \times M_{\mathrm{S}}}$, $\mathbf{H}_{\mathrm{DR}} \in \mathcal{C}^{M_{\mathrm{D}} \times M_{\mathrm{R}}}$ and $\mathbf{H}_{\mathrm{DS}} \in \mathcal{C}^{M_{\mathrm{D}} \times M_{\mathrm{S}}}$ denote the channel matrices between S-R nodes, R-D nodes, and S-D nodes respectively. In the case that all nodes are equipped with single antenna, the complex channel response between S-R nodes, R-D nodes and S-D nodes are denoted by h_{RS}, h_{DR}, and h_{DS} respectively. Furthermore, P_{S}, P_{R} and P_{D} are defined as the transmit power of S, R, and D nodes respectively. The noise vectors at each node, i.e. $\mathbf{n}_{\mathrm{S}} \in \mathcal{C}^{M_{\mathrm{S}}}$, $\mathbf{n}_{\mathrm{R}} \in \mathcal{C}^{M_{\mathrm{R}}}$ and $\mathbf{n}_{\mathrm{D}} \in \mathcal{C}^{M_{\mathrm{D}}}$ are assumed to be complex AWGN with zero mean and covariance $\sigma^2\mathbf{I}_{M_{\mathrm{S}}}$, $\sigma^2\mathbf{I}_{M_{\mathrm{R}}}$ and $\sigma^2\mathbf{I}_{M_{\mathrm{D}}}$ for S, R, and D nodes respectively, where $\mathbf{I}_M$ denotes an $M \times M$ identity matrix.

2.4.1 Conventional relaying schemes

There are several relaying schemes proposed in previous research works, however, in this dissertation, we consider only two fundamental relaying schemes as conventional schemes for two-hop relay networks, i.e. Decode-and-Forward(DF) [37], and DF cooperative relay schemes [38]- [40].

2.4.1.1 Decode-and-Forward (DF)

The network model of DF scheme is shown in Fig. 2.5. As shown in this figure, R node decodes the message received from S node in the first timeslot and then regenerates signal to

transmit to D node in the second timeslot.

For single antenna configuration, the capacity of S-R and R-D links can be respectively calculated from Eq. (2.6) as

$$C_{\mathrm{RS}}^{\text{SISO-DF}} = \log_2(1+\frac{P_{\mathrm{S}}|h_{\mathrm{RS}}|^2}{\sigma^2}), \tag{2.9}$$

$$C_{\mathrm{DR}}^{\text{SISO-DF}} = \log_2(1+\frac{P_{\mathrm{R}}|h_{\mathrm{DR}}|^2}{\sigma^2}) \tag{2.10}$$

The end-to-end capacity can be determined by the capacity of the bottleneck link among two-hop links as

$$C_{\mathrm{E2E}}^{\text{SISO-DF}} = \frac{1}{2}\min(C_{\mathrm{RS}}^{\text{SISO-DF}}, C_{\mathrm{DR}}^{\text{SISO-DF}}), \tag{2.11}$$

Since the network needs two timeslots to carry the message from S node to D node, the end-to-end capacity has to be divided by two as shown in Eq. (2.11).

Similarly, the end-to-end capacity of DF scheme for MIMO configuration, where S, R and D nodes respectively are equipped with M_{S}, M_{R} and M_{D} antennas, can be determined as

$$C_{\mathrm{RS}}^{\text{MIMO-DF}} = \log_2 \det\left(\mathbf{I}_{M_{\mathrm{R}}} + \frac{P_{\mathrm{S}}}{M\sigma^2}\mathbf{H}_{\mathrm{RS}}\mathbf{H}_{\mathrm{RS}}^H\right), \tag{2.12}$$

$$C_{\mathrm{DR}}^{\text{MIMO-DF}} = \log_2 \det\left(\mathbf{I}_{M_{\mathrm{D}}} + \frac{P_{\mathrm{R}}}{M\sigma^2}\mathbf{H}_{\mathrm{DR}}\mathbf{H}_{\mathrm{DR}}^H\right), \tag{2.13}$$

$$C_{\mathrm{E2E}}^{\text{MIMO-DF}} = \frac{1}{2}\min(C_{\mathrm{RS}}^{\text{MIMO-DF}}, C_{\mathrm{DR}}^{\text{MIMO-DF}}), \tag{2.14}$$

where $M = \min(M_{\mathrm{S}}, M_{\mathrm{R}}, M_{\mathrm{D}})$ corresponds to the maximum number of streams the network can carry.

2.4.1.2 DF cooperative relay

This scheme is an extension of the simple DF scheme explained in the previous subsection. The diagram of this relaying scheme is illustrated in Fig. 2.6. In this scheme, S node transmits signal to R node while D node also receives the same signal in the first timeslot. In the next timeslot, D node receives the signal that is forwarded from R node. Here, D node receives the same signal in two timeslots so that cooperative diversity gain can be achieved.

For single antenna case, the capacity of S-R and R-D links can be obtain as

$$C_{\mathrm{RS}}^{\text{SISO-Co}} = \log_2(1+\frac{P_{\mathrm{S}}|h_{\mathrm{RS}}|^2}{\sigma^2}), \tag{2.15}$$

$$C_{\mathrm{DR}}^{\text{SISO-Co}} = \log_2(1+\frac{P_{\mathrm{R}}|h_{\mathrm{DR}}|^2}{\sigma^2}+\frac{P_{\mathrm{R}}|h_{\mathrm{DS}}|^2}{\sigma^2}). \tag{2.16}$$

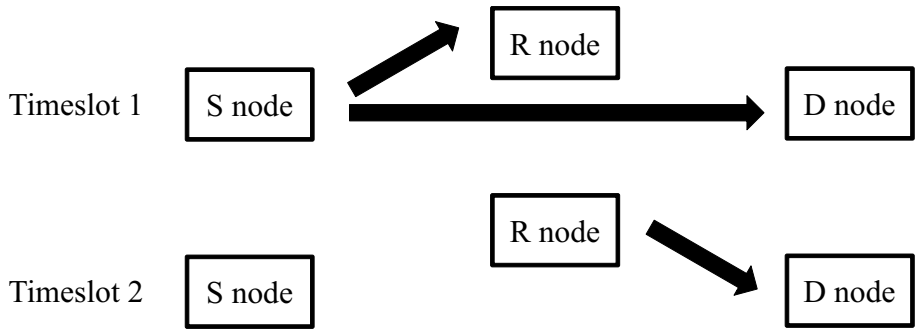

Figure 2.6 The network model of DF cooperative relaying scheme.

The last term of Eq. (2.16) is obtained from the priori knowledge of the direct S-D link in the first timeslot. Finally, the end-to-end capacity can be determined by the bottleneck link capacity as

$$C_{\mathrm{E2E}}^{\mathrm{SISO\text{-}Co}} = \frac{1}{2}\min(C_{\mathrm{RS}}^{\mathrm{SISO\text{-}Co}}, C_{\mathrm{DR}}^{\mathrm{SISO\text{-}Co}}). \tag{2.17}$$

Similarly, the end-to-end capacity of the network in MIMO configuration can be expressed by the following formulas,

$$C_{\mathrm{RS}}^{\mathrm{MIMO\text{-}Co}} = \log_2 \det\left(\mathbf{I}_{M_{\mathrm{R}}} + \frac{P_{\mathrm{S}}}{M\sigma^2}\mathbf{H}_{\mathrm{RS}}\mathbf{H}_{\mathrm{RS}}^{H}\right), \tag{2.18}$$

$$C_{\mathrm{DR}}^{\mathrm{MIMO\text{-}Co}} = \log_2 \det\left(\mathbf{I}_{M_{\mathrm{D}}} + \frac{P_{\mathrm{R}}}{M\sigma^2}\mathbf{H}_{\mathrm{DR}}\mathbf{H}_{\mathrm{DR}}^{H} + \frac{P_{\mathrm{S}}}{M\sigma^2}\mathbf{H}_{\mathrm{DS}}\mathbf{H}_{\mathrm{DS}}^{H}\right), \tag{2.19}$$

$$C_{\mathrm{E2E}}^{\mathrm{MIMO\text{-}Co}} = \frac{1}{2}\min(C_{\mathrm{RS}}^{\mathrm{MIMO\text{-}Co}}, C_{\mathrm{DR}}^{\mathrm{MIMO\text{-}Co}}), \tag{2.20}$$

where $M = \min(M_{\mathrm{S}}, M_{\mathrm{R}}, M_{\mathrm{D}})$ corresponds to the maximum number of streams the network can carry.

2.4.2 Two-way MIMO relay network scheme

In the previous subsection, the relay network transfers signal by the conventional relaying schemes which are originally designed for single antenna configuration, but MIMO is employed just to increase the link capacity. This subsection introduces the other way to utilize MIMO in relay networks. We first consider the relay network in single antenna configuration. In conventional relaying scheme, e.g. simple DF, if the network needs to transfer data in two directions- from S node to D node and from D node to S node, the network has to spend at

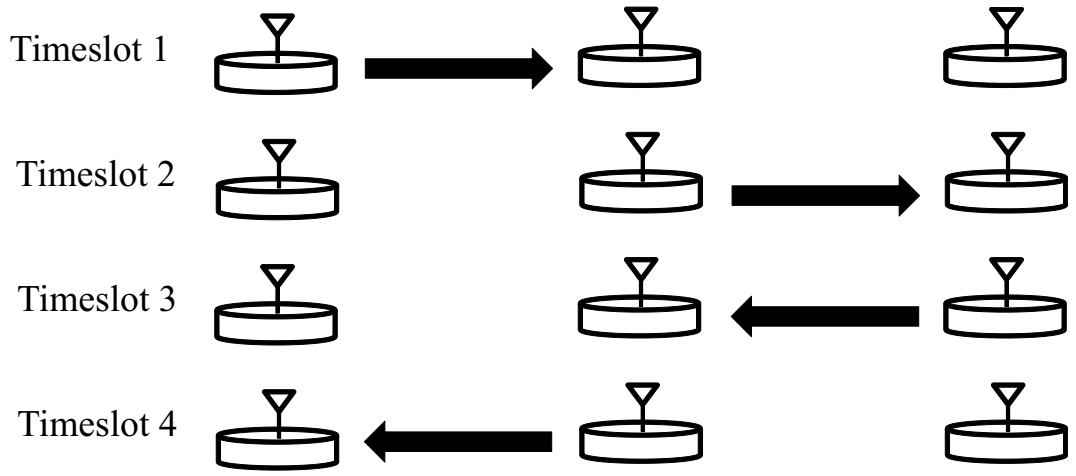

(a) Two-way communications with conventional scheme.

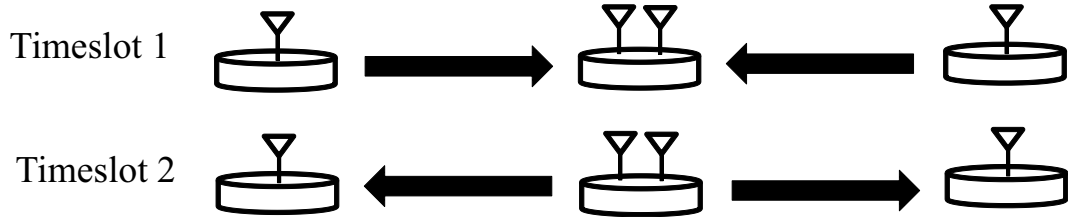

(b) Two-way communications with MIMO two-way scheme.

Figure 2.7 The comparison of conventional one-way and two-way relay networks.

least four timeslots as shown in Fig. 2.7a and this results in the reduction of time efficiency. In recent years, several works proposes to employ MIMO to allow the relay networks simultaneously transfer data in bi-direction by taking the advantage of spatial multiplexing, such that the required timeslots can be reduced as shown in Fig. 2.7b. There are two approaches to utilize MIMO to perform two-way relaying, i.e. network coding [27], [41] and beamforming [27]. The following describes the basic idea of two-way relaying schemes for two-hop relay networks in both approaches.

It is noted that the channel response matrices of R-S and D-R links are the transpose matrices of S-R and R-D links, $\mathbf{H}_{\mathrm{SR}} = \mathbf{H}_{\mathrm{RS}}^{T}$ and $\mathbf{H}_{\mathrm{RD}} = \mathbf{H}_{\mathrm{DR}}^{T}$, respectively.

2.4.2.1 Network coding approach

Figure 2.8 illustrates the concept of MIMO two-way relay network in network coding approach. The basic idea of network coding approach is that R node first receives the data messages x_{S} and x_{D} from S and D nodes at timeslot 1. Then, R node performs Exclusive-OR (XOR) based network coding to combine these two streams as $x_{\mathrm{R}} = x_{\mathrm{S}} \oplus x_{\mathrm{D}}$ and broadcasts this encoded message to S and D nodes at timeslot 2. Here, S and D nodes use their own prior knowledge to decode the desired messages as $x_{\mathrm{R}} \oplus x_{\mathrm{S}} = x_{\mathrm{D}}$ and $x_{\mathrm{R}} \oplus x_{\mathrm{D}} = x_{\mathrm{S}}$ respectively [41].

In order to enable the capability of two-way relay explained above, an additional antenna is needed at the R node. At the first timeslot, R node receives two signals from S and D nodes by using MIMO multiple access algorithm as shown in Fig. 2.8a. The received signal vector at R node can be expressed as

$$\begin{aligned} \mathbf{y}_{\mathrm{R}} &= [\mathbf{H}_{\mathrm{RS}}\ \mathbf{H}_{\mathrm{RD}}] \begin{bmatrix} x_{\mathrm{S}} \\ x_{\mathrm{D}} \end{bmatrix} + \mathbf{n}_{\mathrm{R}} && (2.21) \\ &= \mathbf{H}_{\mathrm{R}}\mathbf{x}_{\mathrm{SD}} + \mathbf{n}_{\mathrm{R}}, && (2.22) \end{aligned}$$

where $\mathbf{H}_{\mathrm{R}} = [\mathbf{H}_{\mathrm{RS}}\ \mathbf{H}_{\mathrm{RD}}]$ is the equivalent channel matrix at node R and $\mathbf{x}_{\mathrm{SD}} = [x_{\mathrm{S}}\ x_{\mathrm{D}}]^{T}$ is the vector of transmit signal elements from S and D nodes.

Then, R node determines the receive weight to estimate these receive signals. The simplest way is to exploit the ZF algorithm, so that the receive weight becomes $\mathbf{W}^{\mathrm{r}} = \mathbf{H}_{\mathrm{R}}(\mathbf{H}_{\mathrm{R}}^{H}\mathbf{H}_{\mathrm{R}})^{-1}$. After applying the weight to the received signal, the estimated signal vector becomes

$$\begin{aligned} \begin{bmatrix} \tilde{x}_{\mathrm{S}} \\ \tilde{x}_{\mathrm{D}} \end{bmatrix} &= \mathbf{W}^{\mathrm{r}H}\mathbf{H}_{\mathrm{R}}\mathbf{x}_{\mathrm{SD}} + \mathbf{W}^{\mathrm{r}H}\mathbf{n}_{\mathrm{R}} \\ &= \mathbf{x}_{\mathrm{SD}} + \mathbf{W}^{\mathrm{r}H}\mathbf{n}_{\mathrm{R}}, && (2.23) \end{aligned}$$

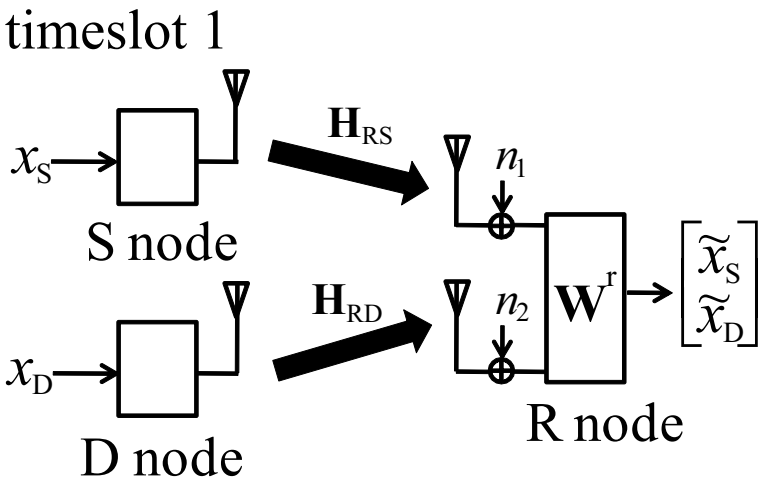

(a) MIMO multiple access in timeslot 1.

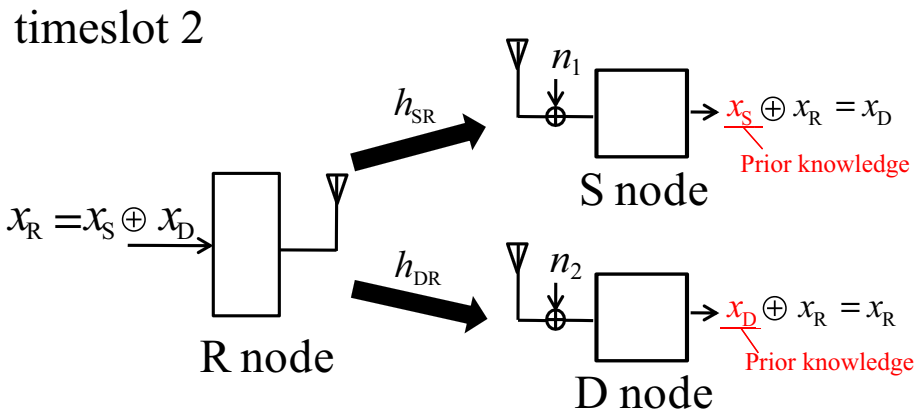

(b) Broadcast mode in timeslot 2.

Figure 2.8 The network model of MIMO relaying scheme in network coding approach.

where $\mathbf{W}^{\mathrm{r}H} = \left[\mathbf{w}_{\mathrm{RS}}^{\mathrm{r}H}\ \mathbf{w}_{\mathrm{RD}}^{\mathrm{r}H}\right]^T$. Hence, the capacity of S-R and D-R links for the first timeslot can be calculated as

$$C_{\mathrm{RS}} = \log_2\left(1 + \frac{P_{\mathrm{S}}}{\sigma^2}(\mathbf{w}_{\mathrm{RS}}^{rH}\mathbf{w}_{\mathrm{RS}}^{\mathrm{r}})^{-1}\right), \tag{2.24}$$

$$C_{\mathrm{RD}} = \log_2\left(1 + \frac{P_{\mathrm{S}}}{\sigma^2}(\mathbf{w}_{\mathrm{RD}}^{rH}\mathbf{w}_{\mathrm{RD}}^{\mathrm{r}})^{-1}\right). \tag{2.25}$$

Normally, at timeslot 2, only one antenna at R node is enough to broadcast the encoded signal to S and D nodes as shown in Fig. 2.8b. It is also possible to utilize an additional antenna to increase the performance such as performing transmitter diversity or applying Space-Time Block Code (STBC) [27]. However, to clarify the basic concept of two-way relay with network coding, we consider the system model where R node uses only one antenna in this section and the exploitation of multiple antennas would be described in later chapters. The receive signals of S and D nodes in timeslot 2 can be expressed as

$$\mathbf{y}_{\mathrm{S}} = h_{\mathrm{SR}}x_{\mathrm{R}} + n_{\mathrm{S}}, \tag{2.26}$$

$$\mathbf{y}_{\mathrm{D}} = h_{\mathrm{DR}}x_{\mathrm{R}} + n_{\mathrm{D}}, \tag{2.27}$$

where $x_{\mathrm{R}} = x_{\mathrm{S}} \oplus x_{\mathrm{D}}$ is the encoded message. After decoding the receive message, the capacity of R-S and R-D links can be concluded as

$$C_{\mathrm{SR}} = \log_2\left(1 + \frac{P_{\mathrm{R}}}{2\sigma^2}|h_{\mathrm{SR}}|^2\right), \tag{2.28}$$

$$C_{\mathrm{DR}} = \log_2\left(1 + \frac{P_{\mathrm{R}}}{2\sigma^2}|h_{\mathrm{DR}}|^2\right). \tag{2.29}$$

It is noted that since the transmit signal from R node contains 2 messages, the last terms in Eq. (2.28) and (2.29) are divided by 2.

From the capacity for each link obtained in (2.24), (2.25), (2.28) and (2.29), the capacity of forward and backward streams, C^{F} and C^{B}, can be respectively expressed as

$$C^{\mathrm{F}} = \min(C_{\mathrm{RS}}, C_{\mathrm{DR}}), \tag{2.30}$$

$$C^{\mathrm{B}} = \min(C_{\mathrm{SR}}, C_{\mathrm{RD}}). \tag{2.31}$$

Therefore, with two timeslots for two-way relay network in this case, the overall two-way capacity of this scenario C_{tw} can be concluded as

$$C_{\text{TW-NC}} = \frac{1}{2}(C^{\mathrm{F}} + C^{\mathrm{B}}). \tag{2.32}$$

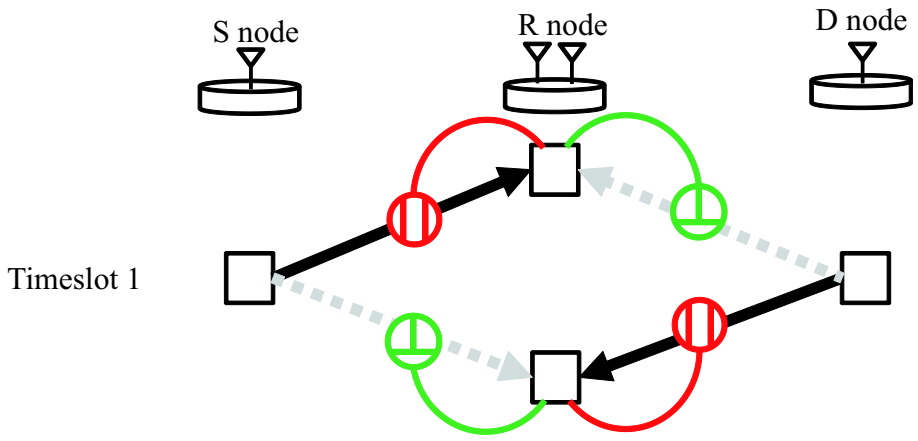

(a) MIMO multiple access in timeslot 1.

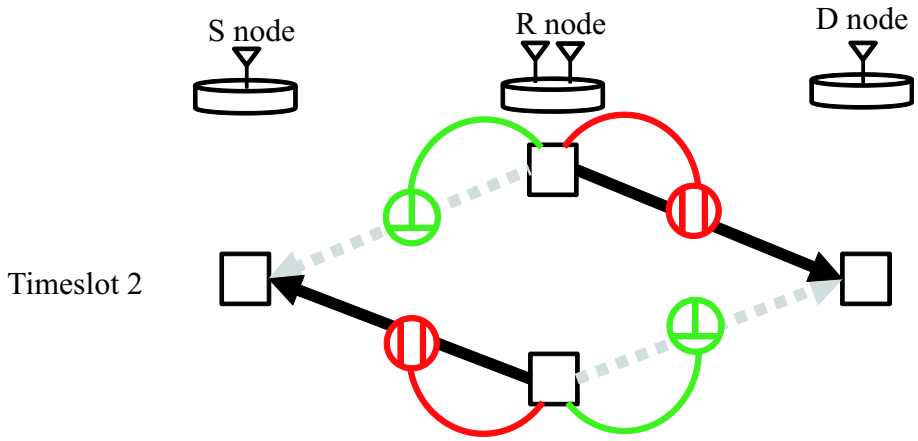

(b) MIMO broadcast in timeslot 2

Figure 2.9 The network model of MIMO relaying scheme in network coding approach.

2.4.2.2 Beamforming approach

In beamforming approach, the transmit data can be passed through the relay to its destination without XOR encoding. However, in this approach, CSI feedback is required to determine the precoding weight to perform MIMO broadcast in the second timeslot. The advantage of this approach can be seen when power control is involved in the multi-hop case. In this subsection, the basic concept of MIMO two-way relay in beamforming approach for two-hop relay network would be described.

Figure 2.9 illustrates the basic concept of MIMO two-way relay in beamforming approach. At the first timeslot, MIMO multiple access is performed similarly to the algorithm in network coding approach, but the detected signals are not combined. The capacity of S-R and D-R

links can also be determined by Eqs. (2.24) and (2.25) respectively.

At the second timeslot, MIMO broadcast is performed to transmit two signals to their corresponding destinations. Normally, MIMO broadcast is the reversed version of MIMO multiple access, so that pre-coding weight can be similarly determined by using ZF algorithm. Assumed that CSI of $\mathbf{H}_{\mathrm{SR}}$ and $\mathbf{H}_{\mathrm{DR}}$ is known at R node, the precoding weight is calculated $\mathbf{W}^{\mathrm{t}} = [\mathbf{W}^{\mathrm{tS}}\ \mathbf{W}^{\mathrm{tD}}]$, where $\mathbf{W}^{\mathrm{tS}} = (\mathbf{H}_{\mathrm{DR}}^{H})^{\perp}$ and $\mathbf{W}^{\mathrm{tD}} = (\mathbf{H}_{\mathrm{SR}}^{H})^{\perp}$ and $[.]^{\perp}$ denotes the orthogonal unit vector. Therefore, the receive vector where each element is the receive signal at S and D nodes can be expressed as

$$\begin{bmatrix} y_{\mathrm{S}} \\ y_{\mathrm{D}} \end{bmatrix} = [\mathbf{H}_{\mathrm{SR}}\ \mathbf{H}_{\mathrm{DR}}]\mathbf{W}^{\mathrm{t}} \begin{bmatrix} x_{\mathrm{D}} \\ x_{\mathrm{S}} \end{bmatrix} + \begin{bmatrix} n_{\mathrm{D}} \\ n_{\mathrm{S}} \end{bmatrix}, \tag{2.33}$$

$$= \begin{bmatrix} h_S^e & 0 \\ 0 & h_D^e \end{bmatrix} \mathbf{x}_{\mathrm{DS}} + \mathbf{n}_{\mathrm{DS}}. \tag{2.34}$$

Therefore, the capacity of R-S and R-D links can be concluded as

$$C_{\text{SR-BC}} = \log_2(1 + \frac{P_{\mathrm{R}}|h_S^e|^2}{\sigma^2}), \tag{2.35}$$

$$C_{\text{DR-BC}} = \log_2(1 + \frac{P_{\mathrm{R}}|h_D^e|^2}{\sigma^2}). \tag{2.36}$$

The forward flow, backward flow and end-to-end capacity can also be determined as

$$C^{\text{F-B}} = \min(C_{\mathrm{RS}}, C_{\text{DR-BC}}), \tag{2.37}$$

$$C^{\text{B-B}} = \min(C_{\text{SR-BC}}, C_{\mathrm{RD}}), \tag{2.38}$$

$$C_{\text{TW-B}} = \frac{1}{2}(C^{\text{F-B}} + C^{\text{B-B}}). \tag{2.39}$$

2.5 Relaying schemes for multi-hop relay networks

2.5.1 Conventional multi-hop relay networks

For the conventional multi-hop relay network, we apply the simple DF relaying scheme which basically performs in one-way manner. In this explanation, we consider a multi-hop network which contains 5 nodes of transceivers. Since the network contains several nodes, the main problem is co-channel interference in the multi-hop networks.

We first consider the case of single frequency channel. It is certain that interference from the adjacent node becomes a serious problem since it severely degrades throughput

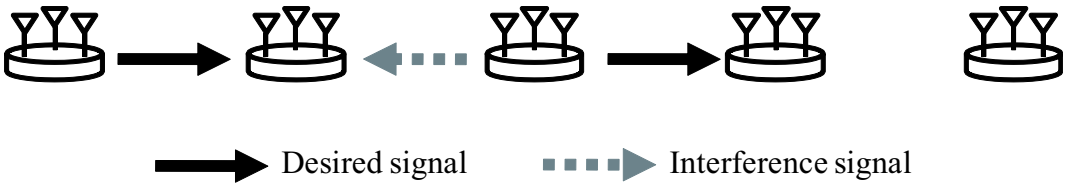

Figure 2.10 Interference problem in conventional multi-hop network.

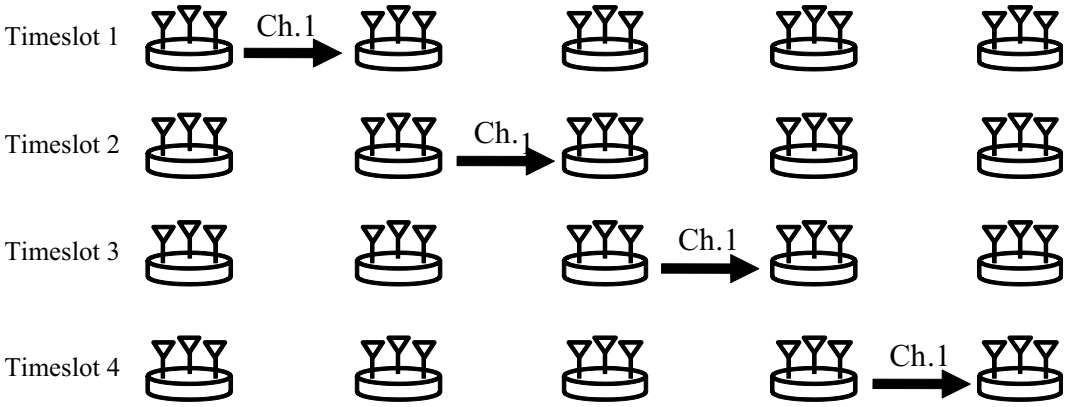

(a) Interference avoidance with time division.

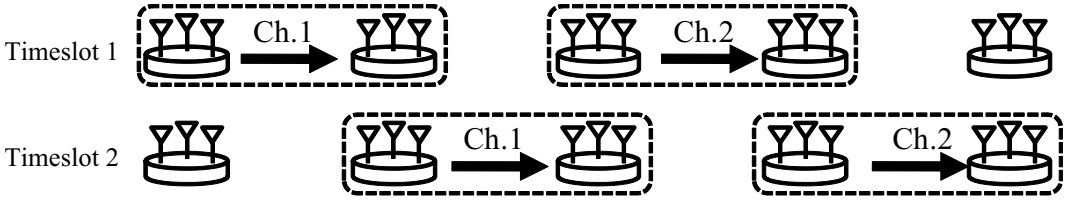

(b) Interference avoidance with dual frequency assignment.

Figure 2.11 Conventional multi-hop relaying scheme.

performance of the network as shown in Fig. 2.10. In order to avoid interference, the network has to spend at least 4 timeslots to carry the message from node 1 to node 5 as shown in Fig. 2.11a. This results in the degradation of time efficiency. The end-to-end capacity of this network can be expressed as

$$C_{\text{E2E-DF}} = \frac{1}{4}\min(C_{21}, C_{32}, C_{43}, C_{54}), \tag{2.40}$$

where C_{21}, C_{32}, C_{43}, and C_{54} correspond to link capacity from node 1 to 2, node 2 to 3, node 3 to 4 and node 4 to 5 respectively and can be calculated by using Shannon capacity formula described in Eq. (2.5). Here, Eq. (2.40) is divided by 4 since the network needs 4 timeslots.

On the other hand, we can avoid the interference by assigning different frequency channels among adjacent links as shown in Fig. 2.11b. Although the network can completely avoid co-channel interference and delay can be shortened, the usage of spectral resource becomes twice of single channel case. This results that the network needs 2 timeslots with 2 frequency channels to transfer the message, so that the end-to-end capacity reduces $2 \times 2 = 4$ times and the end-to-end capacity becomes the same as in Eq. (2.40).

2.5.2 MIMO Two-Way Multi-hop Relay Networks (M2WMNs)

In this scheme, we extend the concept of MIMO two-way relay network in beamforming approach explained in section 2.4.2.2 to apply in multi-hop relay networks. MIMO Two-Way Multi-hop Relay Networks (M2WMNs) [25] differs from the conventional scheme in two aspects. First, with MIMO broadcast and multiple access, M2WMN allows each Tx node to simultaneously transmit the forward (Fw) and backward (Bw) streams to its following and preceding nodes. Second, M2WMN provides adjacent node interference cancellation by joint Tx/Rx array processing.

The details of M2WMN are illustrated in Fig. 2.12. Each transceiver node is equipped with M-element MIMO antennas for adjacent node interference cancellation and Fw/Bw stream multiplexing. If we consider Fw/Bw streams separately, each Rx node n has two antenna weights, i.e. $\mathbf{w}_n^{\text{rF}}, \mathbf{w}_n^{\text{rB}} \in \mathcal{C}^M$ for Fw and Bw streams respectively. Similarly, each Tx node n has two Tx weights $\mathbf{w}_n^{\text{tF}}, \mathbf{w}_n^{\text{tB}} \in \mathcal{C}^M$ for Fw and Bw streams respectively. These Tx/Rx weights can be determined by using both linear and nonlinear MIMO algorithm [25]; but we focus on the linear ZF algorithm in this thesis to simplify our explanation. Since the Tx or Rx weight must cancel maximally two interference signals, each node requires at least $M = 3$ antennas.

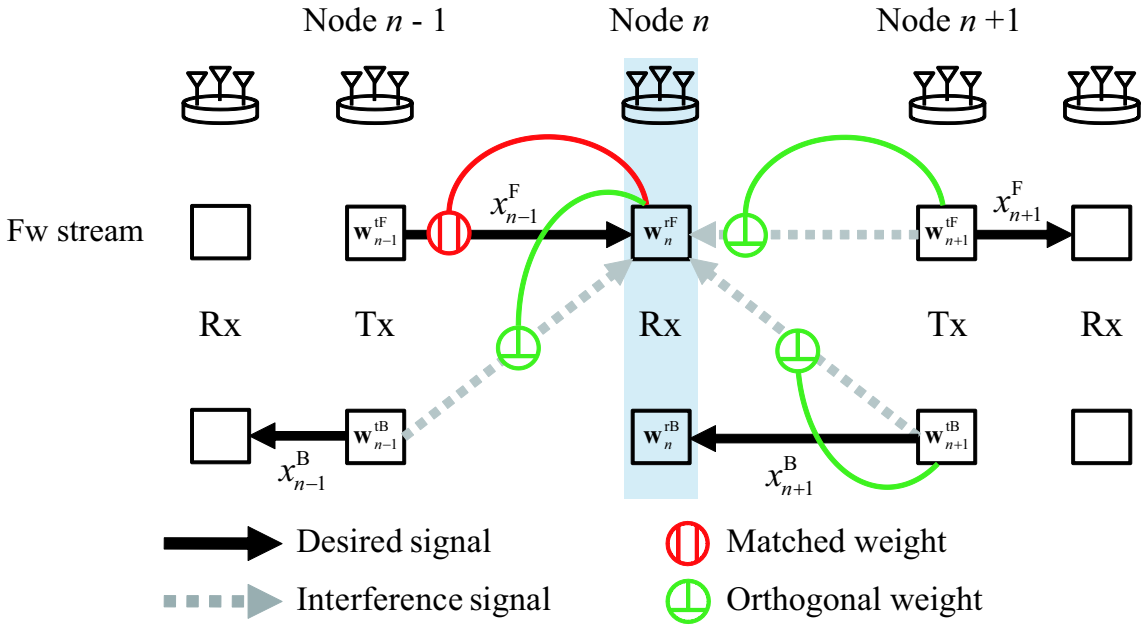

(a) Interference cancellation in the forward stream

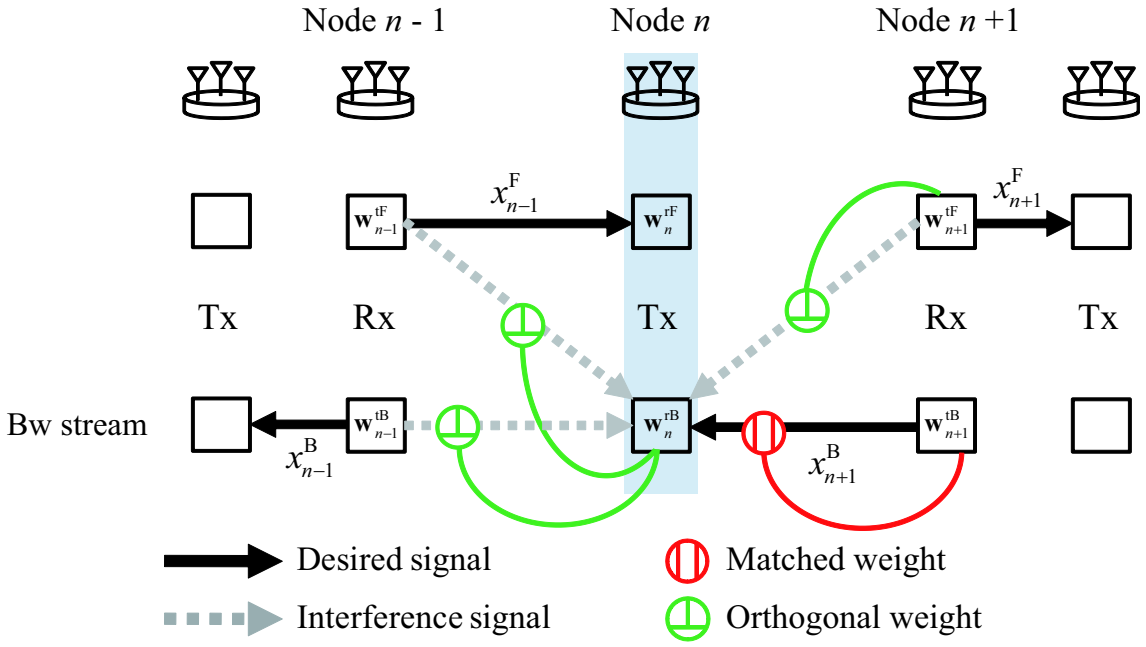

(b) Interference cancellation in the backward stream

Figure 2.12 Joint Tx/Rx linear interference cancellation in the forward and backward streams of Rx node n.

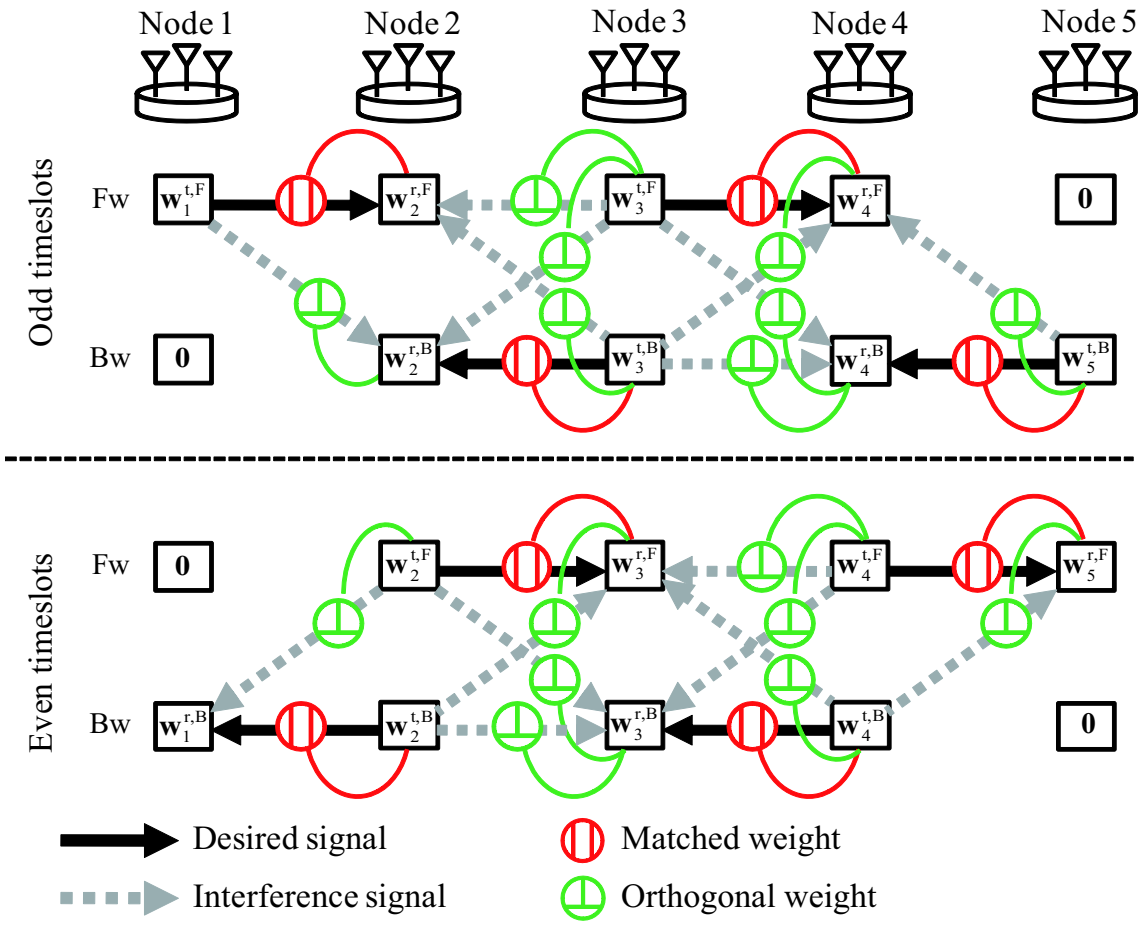

Figure 2.13 Flow multiplexing for MIMO two-way multi-hop network (Over-reach interference is not depicted).

Firstly, we consider the Fw stream of the n^{th} Rx node. As shown in Fig. 2.12a, x_{n-1}^{F} is the desired signal transferred from node $n-1$ while the other $x_{n-1}^{\text{B}}, s_{n+1}^{\text{F}}$, and x_{n+1}^{B} are adjacent node interference. Owing to 3-element array antenna at each node, only two interference signals can be cancelled. To overcome this limitation, three interference signals are cancelled by the combination of the antenna weight $\mathbf{w}_n^{\text{rF}}$ for interference signal from node $n-1$, and the Tx weights $\mathbf{w}_{n+1}^{\text{tF}}, \mathbf{w}_{n+1}^{\text{tB}}$ for two interference signals from node $n+1$, as shown in Fig. 2.12a. Similarly, in the Bw stream, the desired signal x_{n+1}^{B} is received at node n while the adjacent node interference signals, $x_{n-1}^{\text{F}}, x_{n-1}^{\text{B}}$, and x_{n+1}^{F}, are cancelled by the combination of Tx/Rx weights $\mathbf{w}_n^{\text{rB}}$ for two interference signals from node $n-1$, and $\mathbf{w}_{n+1}^{\text{tF}}$ for interference signal from node $n+1$, as shown in Fig. 2.12b.

Consequently, the Rx weights at node n can be calculated by using the previously determined Tx weights $\mathbf{w}_{n-1}^{\mathrm{tF}}$ and $\mathbf{w}_{n-1}^{\mathrm{tB}}$ at node $n-1$ as follows,

$$\mathbf{w}_n^{\mathrm{rF}} = \left[\left(\mathbf{H}_{n,(n-1)} \mathbf{w}_{n-1}^{\mathrm{tF}} \right)^{\parallel}, \left(\mathbf{H}_{n,(n-1)} \mathbf{w}_{n-1}^{\mathrm{tB}} \right)^{\perp} \right] \tag{2.41}$$

$$\mathbf{w}_n^{\mathrm{rB}} = \left[\left(\mathbf{H}_{n,(n-1)} \mathbf{w}_{n-1}^{\mathrm{tF}} \right)^{\perp}, \left(\mathbf{H}_{n,(n-1)} \mathbf{w}_{n-1}^{\mathrm{tB}} \right)^{\perp} \right], \tag{2.42}$$

where $\mathbf{H}_{n,(n-1)}$ is the channel matrix of the link between Tx node $n-1$ and Rx node n, $\left[\mathbf{x}^{\parallel}, \mathbf{y}^{\perp}\right]$ is a unit vector parallel to $\mathbf{x}$ but in orthogonal to the subspace of $\mathbf{y}$, and $\left[\mathbf{x}^{\perp}, \mathbf{y}^{\perp}\right]$ is a unit vector orthogonal to both $\mathbf{x}$ and $\mathbf{y}$.

Similarly, the Tx antenna weights of node $n+1$ are determined by:

$$\mathbf{w}_{n+1}^{\mathrm{tF}} = \left[\left((\mathbf{w}_n^{\mathrm{rF}})^H \mathbf{H}_{n,(n+1)} \right)^{\perp}, \left((\mathbf{w}_n^{\mathrm{rB}})^H \mathbf{H}_{n,(n+1)} \right)^{\perp} \right] \tag{2.43}$$

$$\mathbf{w}_{n+1}^{\mathrm{tB}} = \left[\left((\mathbf{w}_n^{\mathrm{rF}})^H \mathbf{H}_{n,(n+1)} \right)^{\perp}, \left((\mathbf{w}_n^{\mathrm{rB}})^H \mathbf{H}_{n,(n+1)} \right)^{\parallel} \right]. \tag{2.44}$$

It is noted that the end weights must satisfy $\mathbf{w}_1^{\mathrm{tB}} = \mathbf{w}_1^{\mathrm{rF}} = \mathbf{w}_5^{\mathrm{tF}} = \mathbf{w}_5^{\mathrm{rB}} = \mathbf{0}$. In practice, the Tx weight is initialized at the first node, and then the Tx/Rx weight calculation is performed from left to right by using (2.41)-(2.44).

By using the algorithm described above, M2WMN enables the network to perform simultaneous transmissions of forward and backward streams. As drawn in Fig. 2.13, all nodes in M2WMN switch their roles as Tx and Rx in the next timeslot, so that end-to-end bidirectional transmission can be achieved in two timeslots. Therefore, we distinguish between the set of Fw links and Bw links in odd numbered timeslots as $I_{\mathrm{o}} = I_{\mathrm{o}}^{\mathrm{F}} \cup I_{\mathrm{o}}^{\mathrm{B}}$, and in even numbered timeslots as $I_{\mathrm{e}} = I_{\mathrm{e}}^{\mathrm{F}} \cup I_{\mathrm{e}}^{\mathrm{B}}$. In our scenario where the network consists of 5 nodes, the set of Fw and Bw links in odd numbered timeslots are $I_{\mathrm{o}}^{\mathrm{F}} = \{1, 3\}$ and $I_{\mathrm{o}}^{\mathrm{B}} = \{2, 4\}$ respectively. For the even numbered timeslots, the set of Fw and Bw links are $I_{\mathrm{e}}^{\mathrm{F}} = \{2, 4\}$ and $I_{\mathrm{e}}^{\mathrm{B}} = \{1, 3\}$ respectively. For a specific link l, $\mathrm{T}(l)$ and $\mathrm{R}(l)$ respectively denote the corresponding Tx and Rx nodes of the link and p_l represents the transmit power for that link. Table 2.1 represents $\mathrm{T}(l)$ and $\mathrm{R}(l)$ of the corresponding link l.

Using these representations, the leakage channel gain between the Tx node $\mathrm{T}(k)$ of link k, and the Rx node $\mathrm{R}(l)$ of link l can be described by:

$$g_{l,k} = \mathbf{E}\left[\left| (\mathbf{w}_{\mathrm{R}(l)}^{\mathrm{r,dir}(l)})^H \mathbf{H}_{\mathrm{R}(l),\mathrm{T}(k)} \mathbf{w}_{\mathrm{T}(k)}^{\mathrm{t,dir}(k)} \right|^2 \right], \tag{2.45}$$

where $\mathrm{dir}(l)$ and $\mathrm{dir}(k)$ indicates the direction (Fw or Bw) of link l and link k respectively, and $\mathbf{H}_{\mathrm{R}(l),\mathrm{T}(k)}$ is the channel matrix of the link between $\mathrm{T}(k)$ and $\mathrm{R}(l)$. If $l = k$, g_{ll} denotes

Table 2.1 Tx and Rx node of their corresponding links.

Link index l		1	2	3	4
Odd timeslot	T(l)	1	3	3	5
	R(l)	2	2	4	4
Even timeslot	T(l)	2	2	4	4
	R(l)	1	3	3	5

the channel gain of the desired signal of link l, otherwise ($l \neq k$) g_{lk} represents the interference leakage level from link k to l.

Then the channel capacity of link l can be calculated by

$$C_l^{\mathrm{dir}(l)} = \log_2(1 + \gamma_l^{\mathrm{dir}(l)}), \tag{2.46}$$

$$\gamma_l^{\mathrm{dir}(l)} = \frac{p_l g_{l,l}}{\sum\limits_{l \neq k} p_k g_{l,k} + \sigma^2}, \tag{2.47}$$

where $\gamma_i^{\mathrm{dir}(i)}$ denotes the Signal to Interference plus Noise Ratio (SINR) of link l. In the case when power control is not applied, the transmit powers of all links are equally allocated.

By considering both directions of information flow, the average end-to-end capacity of M2WMN can be calculated by

$$C_{\text{E2E-M2WMN}} = \frac{1}{2}\left(C_{\text{E2E}}^{\mathrm{F}} + C_{\text{E2E}}^{\mathrm{B}}\right) [\text{bits/s/Hz}], \tag{2.48}$$

where $C_{\text{E2E}}^{\mathrm{F}} = \min\limits_{l \in I_{\mathrm{o}}^{\mathrm{F}} \cup I_{\mathrm{e}}^{\mathrm{F}}} C_l^{\mathrm{F}}$ and $C_{\text{E2E}}^{\mathrm{B}} = \min\limits_{l \in I_{\mathrm{o}}^{\mathrm{B}} \cup I_{\mathrm{e}}^{\mathrm{B}}} C_l^{\mathrm{B}}$ are respectively the end-to-end capacity of the Fw and Bw streams.

It is noted that we can also adopt the concept of MIMO Two-way relaying scheme in network coding approach to multi-hop networks. However, there is a difficulty to perform Tx power optimization to reduce the effect of overreach interference which will be described in the next subsection. Therefore, we do not consider the multi-hop relaying scheme in network coding in this thesis.

2.5.3 Power control for M2WMN

M2WMN can eliminate adjacent node interference and allow the network to communicate bi-directionally. However, the over-reach interference, drawn in Fig. 2.14, still limits the

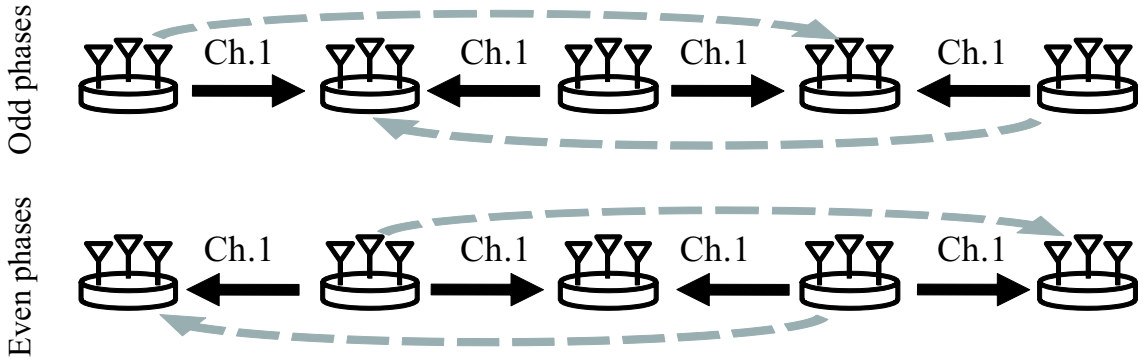

Figure 2.14 Over-reach interference in M2WMN.

network performance. By this reason, a power control algorithm is considered to optimize the transmission powers of each link in order to maximize SINR at the bottleneck link which is equivalent to the end-to-end capacity. The optimization problem is described as

$$\begin{aligned} &\underset{\mathbf{p}}{\text{maximize}} \quad \min_{l \in I_o^{\mathrm{F}} \cup I_o^{\mathrm{B}}} \overline{\gamma_l^{\mathrm{dir}(l)}} \\ &\text{subject to} \quad p_l + p_k \leq p_{\max} \forall l \neq k \text{ s.t. } T(l) = T(k), \end{aligned} \tag{2.49}$$

where $\overline{\gamma_l^{\mathrm{dir}(l)}}$ is the average SINR of link l in direction $\mathrm{dir}(l)$, the vector $\mathbf{p} = [p_1, ..., p_L]^T$ stacking the Tx powers of all the links is the optimization objective, and $p_{\max}$ is the allowable transmit power or power constraint of each node [42]. It is noted that the above optimization problem corresponds to the network in odd numbered timeslots. The optimization problem in even numbered timeslots can be determined.

The problem in Eq. (2.49) can be treated as a quasi-convex optimization problem and can be solved by using Geometric Programming [43]. However, this solution is a centralized method which assumes that a central controller has global knowledge of the channel leakage levels between Tx-Rx pairs to determine the optimal Tx powers of each link. It is obvious that the method is hard to implement in real scenarios. In this thesis, we apply an alternative distributed power control algorithm adapted from [44], whose details are described as follows.

Firstly, the notion of SINR metric in [44] is extended to derive the distributed power control algorithm suitable for Eq. (2.49). The SINR metric of link l at the iteration m is defined as:

$$S_l^{(i)} = \bar{\gamma}_l^{\mathrm{dir}(l)(i)} \frac{p_{\max}}{\mathbf{w}_{T(l)}^T \mathbf{p}^{(i)}} \tag{2.50}$$

where $\bar{\gamma}_l^{\mathrm{dir}(l)(i)}$ is the SINR of link l at the iteration i which can be computed from Eq. (2.47) and $\mathbf{w}_{T(l)} = [w_{T(l),1}, ..., w_{T(l),L}]$ denotes a linear constraint on power at node $T(l)$. Here, $w_{T(l),k} = 1$ when link k is an outgoing link from Tx node $T(l)$, otherwise $w_{T(l),k} = 0$. By sharing this single scalar parameter $S_l^{(i)}$, each Tx node can iteratively optimize the transmit power of its outgoing links. The power control algorithm is summarized as follows.

- Initialize the power allocation: $p_l^{(0)} = \frac{p_{\max}}{N_{T(l)}}$, where $N_{T(l)}$ is the number of outgoing links of node $T(l)$.
- Iterate until convergence:

  1. The SINR metric is individually computed at each node for all streams:

  $$S_l^{(i)} = \bar{\gamma}_l^{\mathrm{dir}(l)(i)} \frac{p_{\max}}{\mathbf{w}_{T(l)}^T \mathbf{p}^{(i)}}, l \in I_{\mathrm{o}}^{\mathrm{F}} \cup I_{\mathrm{o}}^{\mathrm{B}}$$

  2. The nodes share the SINR metric to determine the minimum SINR metric $S_{\min}^{(i)}$:

  $$S_{\min}^{(i)} = \min_l \ S_l^{(i)},$$

  3. Each transmit node independently updates its power for the next iteration $i+1$ as follows:

  $$p_l^{(i+1)} = p_l^{(i)} \frac{S_{\min}^{(i)}}{\bar{\gamma}_l^{\mathrm{dir}(l)(i)}}, l \in I_{\mathrm{o}}^{\mathrm{F}} \cup I_{\mathrm{o}}^{\mathrm{B}}.$$

In the above algorithm, the SINR metric $S_l^{(i)}$ can be interpreted as the increased SINR of link l at iteration i if its corresponding node's power level is scaled to the maximum $p_{\max}$ while the link's received interference power remains unchanged. This algorithm aims to achieve a uniform SINR for all links, so that we use the minimum SINR metric as a reference value for deciding which links need to increase or decrease their power. In order to share the minimum SINR metric, each node determines the minimum SINR metric locally against its neighbor nodes and then passes the new value through the network in two-way multi-hop manner. Through single parameter, the information of SINR metric can be shared among nodes at quite low level of coordination. The proof of convergence and optimality of this algorithm can be referred to [44].

Chapter 3

Design of two-hop MIMO relay network in a realistic shadowing environment

3.1 Motivation

In this chapter, we focus on the practical study of basic two-hop relay networks. Generally, shadow fading caused by obstacles between Tx and Rx in Non-Line-Of-Sight (NLOS) environments degrades the signal strength as well as data rate of wireless networks. As mentioned, relaying technique has an important role to deal with shadowing problem by allowing a relay node to forward signal from Tx to Rx which is obstructed by shadow fading [12]. Recently, Multiple-Input Multiple-Output (MIMO) or multiple antenna technique has been considered as a technique to improve wireless channel capacity [13]- [15]. Combining the benefit of these two techniques, recent studies also consider relay networks which employ MIMO technique [45]- [49].

So far, the studies of MIMO relay network are mostly based on theoretical channel models such as Rayleigh fading, which may be far from realistic [45]- [48]. The research of MIMO relay network based on practical measurements is necessary. Recently, a few practical studies have been reported in [28]- [30], [50]- [53]. [50]- [53] investigated the propagation characteristics of MIMO relay network in both NLOS and Line-Of-Sight (LOS) environment for channel modeling purpose. [28], [29] reported the impact of relay location on capacity performance. [29], [30] emphasized the necessity of relay node for capacity improvement in NLOS environment.

However, these papers have not investigated the following issues. [50]- [53] characterized MIMO relay channel, however, the studies did not clarify which condition of channel characteristic is good for MIMO relay networks to achieve high performance. Although [28], [29] investigated the impact of relay location, they did not concern which location is optimal to achieve the best performance and how to verify the location from the experiment results. Moreover, [30], [52] considered Amplified-and-Forward (AF) and DF relaying schemes which are the two most simplest relaying schemes widely used today. However, the other two relaying schemes introduced in Section 2.4, i.e. two-way relay employing network coding and DF cooperative relaying scheme have not been yet evaluated by experiments.

In this chapter, we present MIMO propagation measurements in an L-shaped corridor in 5 GHz band with three transceivers playing the rolls of a source, a relay and a destination node. Each transceiver is equipped with four antennas and utilizes the hardware developed in [54]. The experiments cover two types of environment. In the first one, the source and the destination nodes are located in different arms of the corridor, while in the second one, the nodes are located at a same arm of the corridor. The first one corresponds to an NLOS environment with strong shadowing effect due to the shape of the corridor. The latter one corresponds to a LOS environment where shadowing effect can be neglected. Relay node is placed in various locations between the source and destination nodes along the corridor. Channel matrices among nodes are measured. Based on the measured channels, the efficiency of various relaying schemes is evaluated in both NLOS and LOS environment cases.

By using measurement data, this chapter mainly investigates the two following problems: 1) Where is the best relay location and what is a good condition for MIMO relay channel that makes the network achieve its best performance? 2) Among three fundamental relaying schemes, which one is the most efficient in the real shadowing environment? In addition, we investigate the propagation characteristics of the MIMO relay network in both large-scale and small-scale distance ranges. Also, we propose a novel Relay Placement Estimation (RPE) scheme in order to estimate the best location for relay node. The novel scheme is established by determining the quality of the bottleneck link in relay networks.

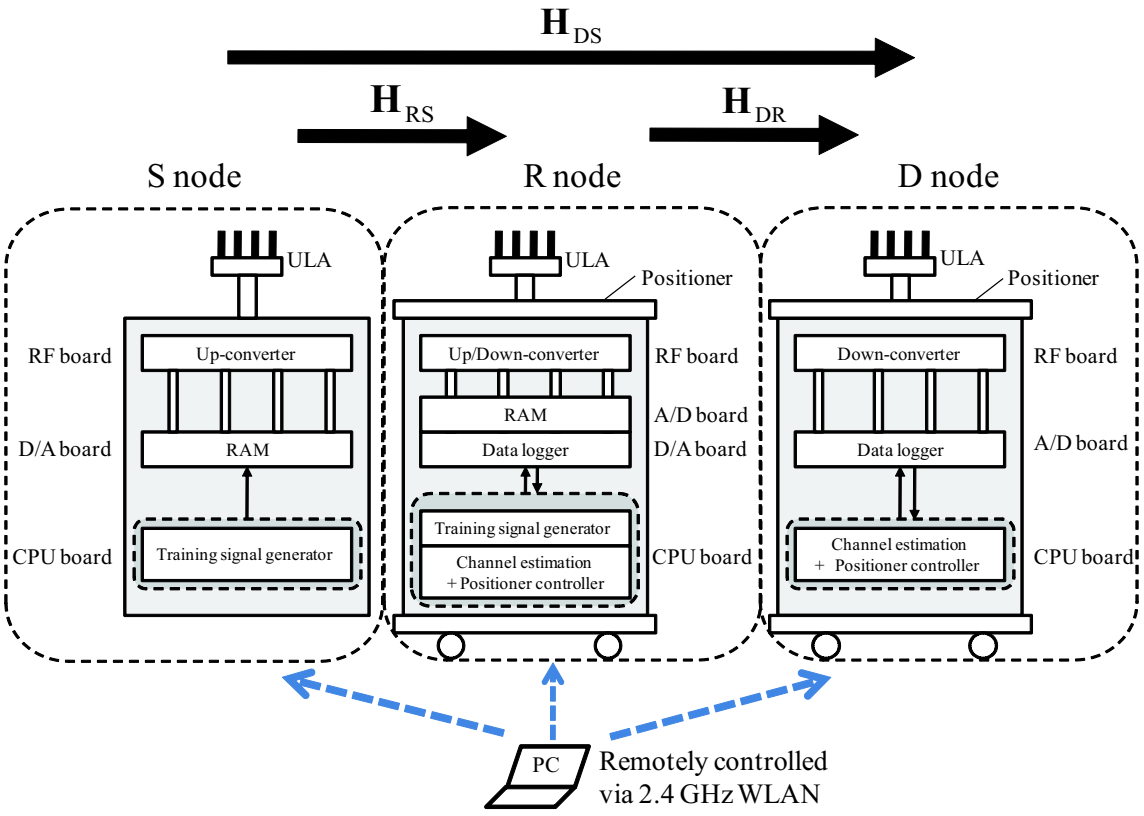

Figure 3.1 Block diagram of MIMO-OFDM relay measurement system.

3.2 MIMO relay channel measurement

3.2.1 Measurement hardware

In this chapter, we consider the general two-hop MIMO relay network model described in Section 2.4. For the measurement experiment, three MIMO transceivers developed in [54] are utilized to measure the channel matrices $\mathbf{H}_{\mathrm{RS}}$, $\mathbf{H}_{\mathrm{DR}}$, and $\mathbf{H}_{\mathrm{DS}}$ by implementing MIMO-OFDM relay measurement firmware on the transceivers. Figure 3.1 also shows the block diagram of the measurement system and Table 3.1 shows the system parameters.

At Tx side (S and R nodes), training signals are generated from the memory tables implemented on the FPGAs of the D/A board. These training signals contain 64 OFDM symbols which are modified from IEEE 802.11a preamble to be orthogonal between antenna elements. These baseband signals are up-converted to 5.06GHz and transmitted from the 4-element Uniform Linear Array (ULA).

Table 3.1 Parameters of measurement system.

MIMO configuration	4(S) 4(R) 4(D)
Antenna configuration	A half wave length spacing ULA
Center frequency	5.06 GHz
System bandwidth	20 MHz
Transmit power per node	0 dBm
Training signal	Extended IEEE 802.11a OFDM
Training signal length	64 OFDM symbols
Sampling frequency	80 MHz
Measurement area	36 × 36 cm (1.8 cm step)

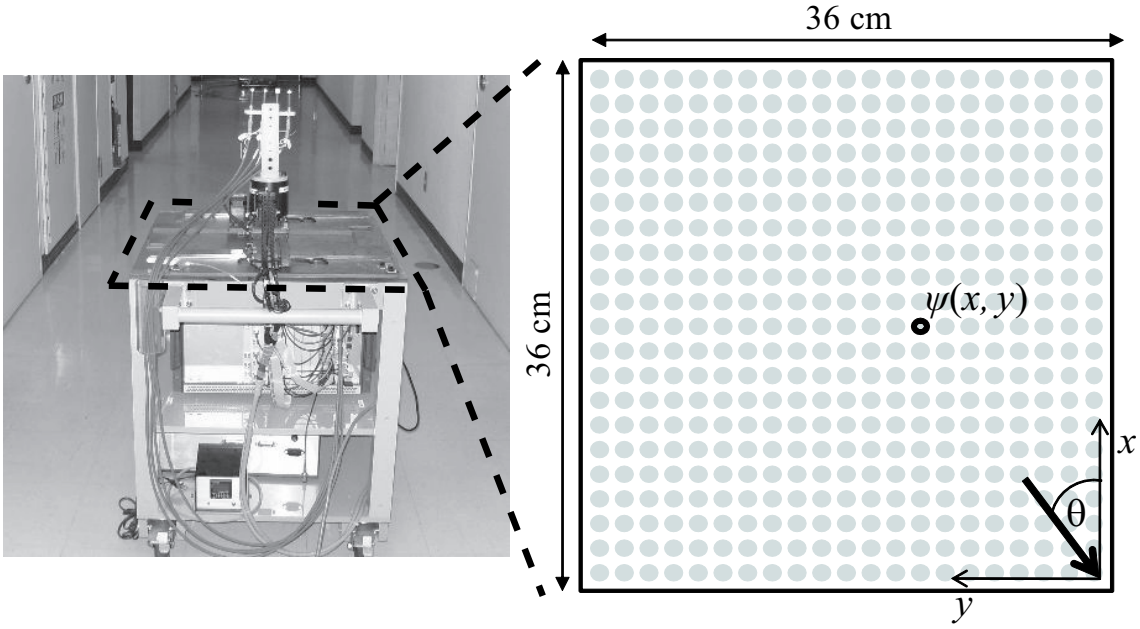

Figure 3.2 Measurement equipments and the coordinate of the positioner.

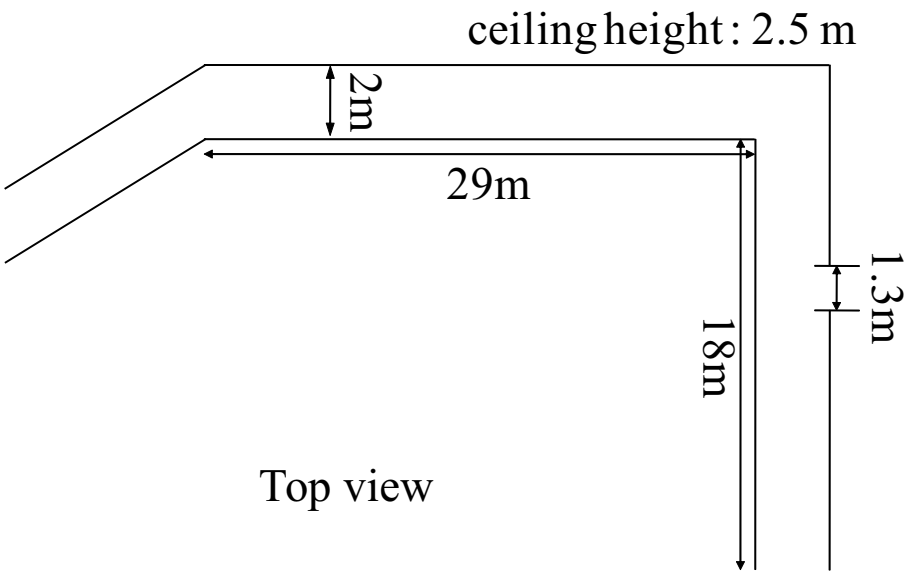

Figure 3.3 The L-shaped corridor environment.

At Rx side (R and D nodes), the RF signals received by 4-element ULA are down-converted and sampled in the A/D board. Frame synchronization timing is extracted by utilizing the OFDM preamble symbol. Afterward, an off-line channel estimation is performed on the synchronized received signals. Moreover, 4-element array antenna separated by half wavelength is equipped on a moving arm of a positioner such that the receiver can obtain multiple spatial samples of MIMO channel at each receiver location. At last, a MIMO channel matrix $\mathbf{H}_{\{.\}}(k,\psi) \in \mathcal{C}^{M_\mathrm{r}\times M_\mathrm{t}}$ is obtained after calibration process is performed to compensate for cable loss and transceiver gains. Here, M_t and M_r are the number of antennas of the transmitter and the receiver respectively, k is the subcarrier index, and $\psi\,(x,y)$ is the position index on the positioner as depicted in Fig. 3.2. Therefore, measurement data of 52 subcarriers in 441 different local positions with 1.8cm step within a $36 \times 36\mathrm{cm}^2$ area on the positioner are captured. During the experiment, all equipments are remotely controlled by a notebook PC via 2.4GHz WLAN.

3.2.2 Measurement environment

The experiment is conducted in an L-shaped corridor of a concrete structure building in the university campus. Figure 3.3 illustrates the experimental environment containing two straight corridor arms with 2-meter width, 2.5-meter height and the length of 18 m and 29 m.

Along the wall of the corridor, there are some room doors and there is also an opened-wall fire exit in the 18 m corridor arm.

In order to observe the effect of shadowing, the experimental environment is divided into two cases i.e. the L-shaped Corridor case and the Straight Corridor case, as shown in Figs. 3.4a and 3.4b respectively. The L-shaped Corridor case corresponds to an NLOS environment containing strong shadowing effect while the Straight Corridor case corresponds to a LOS environment where shadowing effect is negligible.

Since the experiment is aimed to determine the appropriate location of the relay, the locations for S, R and D nodes in the experiment are designed for both cases as follows. In the L-shaped corridor case, S and D nodes are located at the different corridor arms with the separated distance of d and have equal distance from the corner of the L-shaped corridor, as shown in Fig. 3.4a. The experiment is started with the channel measurement in the L-shaped Corridor environment to find the maximum distance between S and D nodes, d, which makes the channel estimation errors at the receiver lower than 1%. In this experiment, we found that $d = 17.67$m. The location for relay is designed by assigning relay location 0 to the location at the corner of the L-shaped corridor; -1, -2, -3, and -4 to the relay locations in the arm containing S node; and 1, 2, 3 and 4 to the relay locations in the arm containing D node, as shown in Fig. 3.4a. In the Straight Corridor case, S and D nodes are located in a same corridor arm and are separated by the same calculated distance d, as shown in Fig. 3.4b. The relay location 0 is assigned to the relay location with similar distance from S node as in the L-shaped corridor case. The other relay locations are assigned similarly as in L-shaped Corridor case with respect to the new origin location 0.

For both experiments, the measurement is performed in the following procedure. Firstly, R node is located at relay location of -4. Then, S node transmits signal for R and D node to obtain $\mathbf{H}_{\mathrm{RS}}$ and $\mathbf{H}_{\mathrm{DS}}$. Next, S node stops transmission and R node transmits signal such for D node to obtain $\mathbf{H}_{\mathrm{DR}}$. Then, R node stops the transmission and is moved to the next relay location, and the measurement is repeated with the same procedure. The measurement procedure is concluded in the flowchart illustrated in Fig. 3.5.

3.3 Propagation characteristic analysis

By using measurement data, this section investigates the propagation characteristics in the L-shaped corridor environment for MIMO relay network. The analysis covers two main following

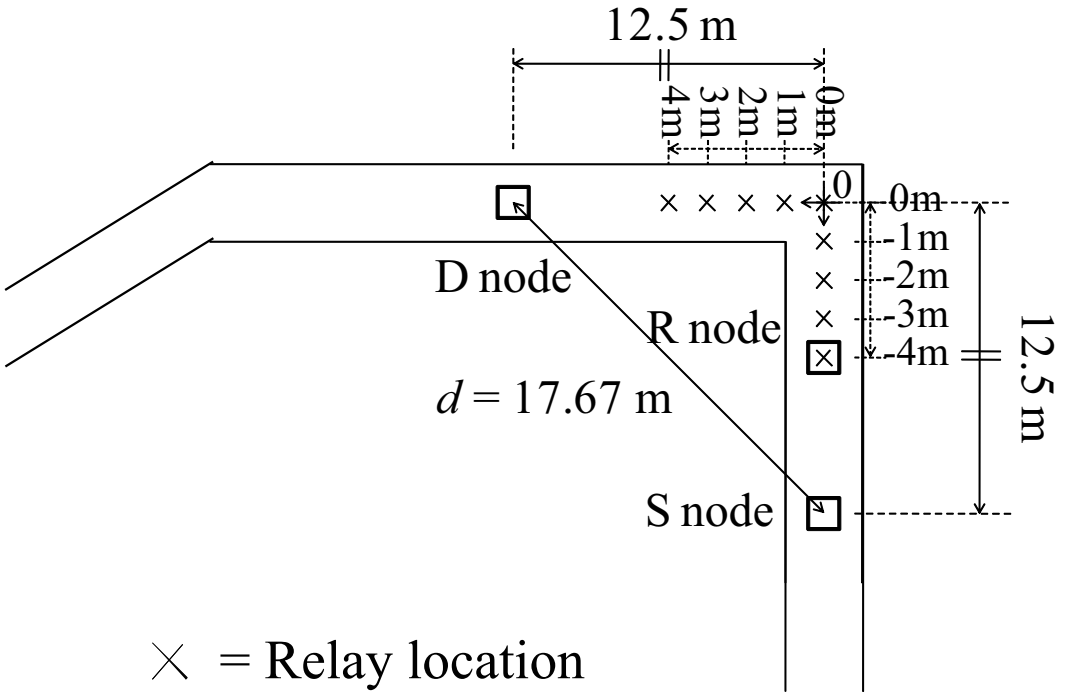

(a) L-shaped Corridor diagram.

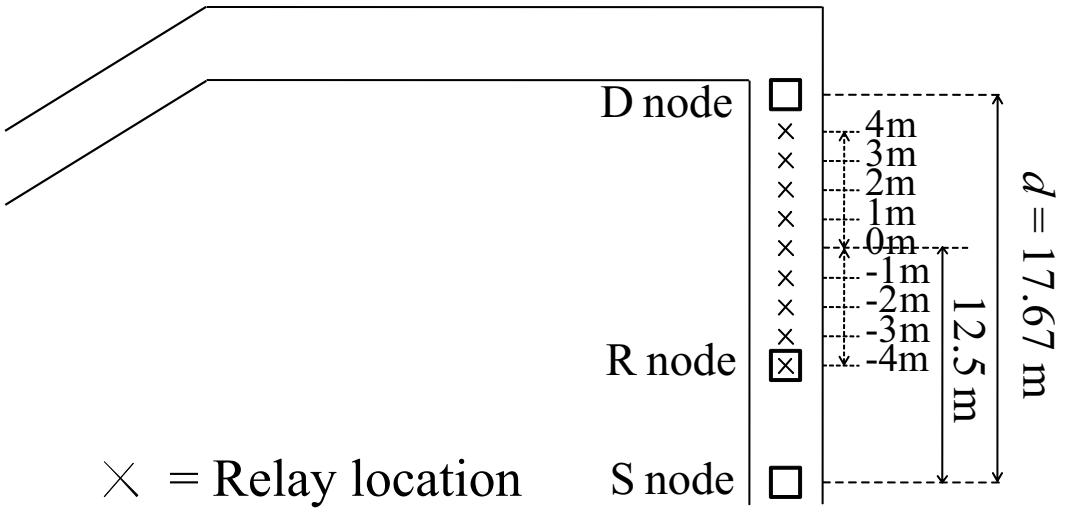

(b) Straight Corridor diagram.

Figure 3.4 The layout of locations for S, R and D nodes.

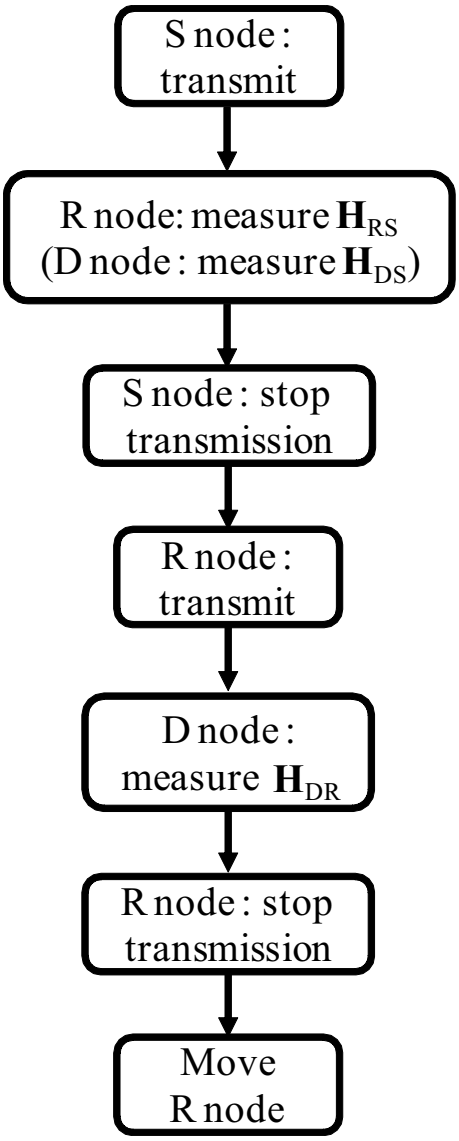

Figure 3.5 The flowchart of measurement procedure.

perspectives of radio propagations.

- **Large-scale propagation:** The study mainly observes the received signal strength varying in large-scale range of distance. In this analysis, the large-scale propagation characteristic is represented by pathloss between the Tx and the Rx. In addition, shadowing effect when the Tx and the Rx are located in different arms of the L-shaped corridor can also be observed in this large-scale analysis.

- **Small-scale propagation:** The study mainly observes the statistics of the channel in small-scale local areas. The analysis in small-scale areas contain analyses of spatial correlations and angular profiles which describe the characteristics of multi-path signals. In this paper, Ψ is denoted as a local area which is assumed to satisfy the following two conditions.

  a) A 12×12 cm^2 area is defined as a local area small enough such that power variation of each path does not exceed 1dB to satisfy the condition of wide sense stationary (WSS) approximately [55]- [57].

  b) The ergodic variation of signals in frequency domain is assumed to be sufficiently small to support averaging in frequency domain. This assumption is considered based on log-distance pathloss equation in free space [12], $P_{\mathrm{L}} = 20\log(f)+20\log(d)+\text{constant}$, where P_{L}, f and d denote pathloss, frequency, and distance between Tx and Rx respectively. With a bandwidth of 20 MHz for the central frequency of 5.06 GHz and distance within local area of 12 cm, pathloss variation over frequency domain of the experiment does not exceed 1dB. Therefore, the variation in frequency domain is neglected in this paper.

3.3.1 Pathloss

Pathloss is calculated from the link between the first antenna of the Tx and the Rx, $P_{\mathrm{L}}(k,\psi) = \mid h^{11}_{\{.\}}(k,\psi) \mid^2$. By averaging the pathloss over all subcarriers k at each local position of the positioner, the distributions of the pathloss of the signal transmitted from S to R and D nodes with respect to the locations of the positioner are illustrated in Figs. 3.6a and 3.6b. Furthermore, in order to find the tendency of pathloss for S-R and R-D links with respect to relay locations, pathloss averaged over all local positions ψ at each location are plotted on the graph shown in Fig. 3.7.

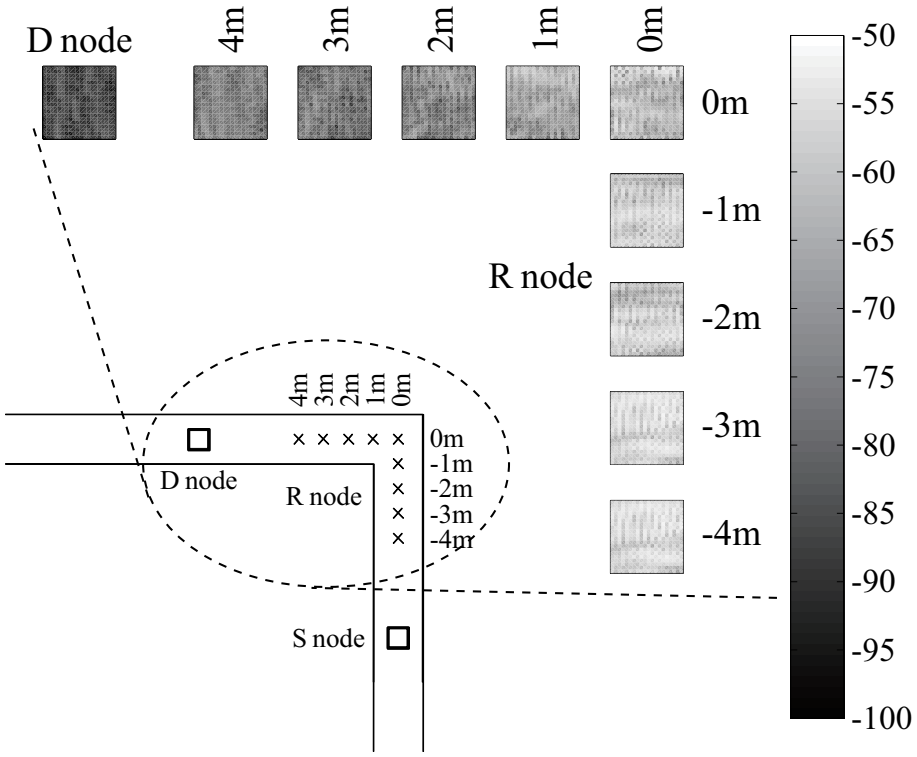

(a) L-shaped Corridor case.

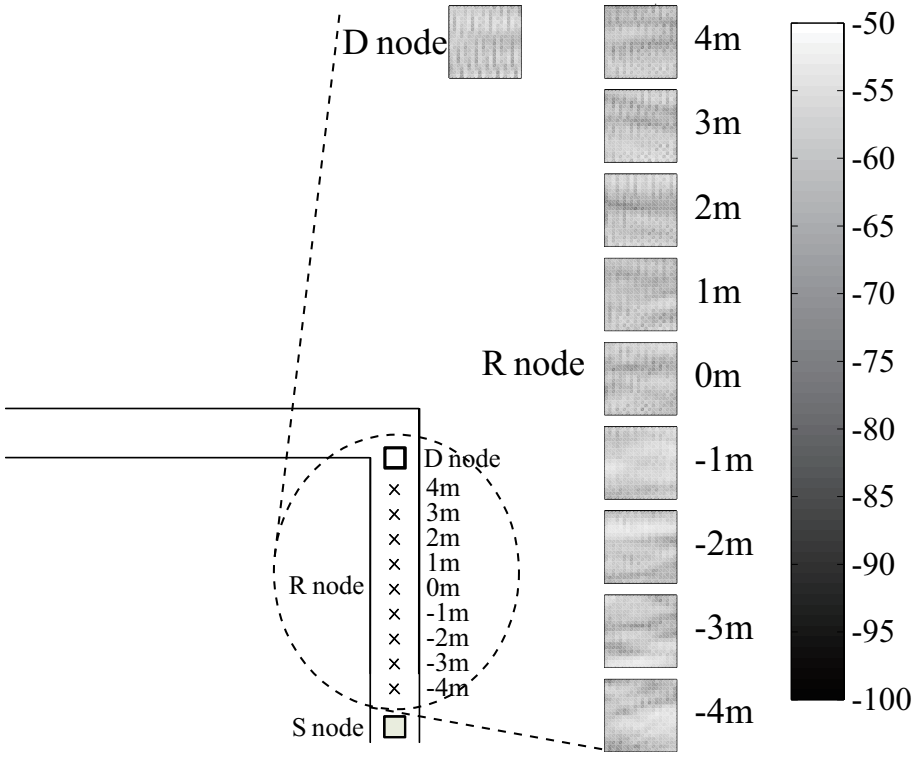

(b) Straight Corridor case.

Figure 3.6 Distribution of pathloss over positioner at each receiver location.

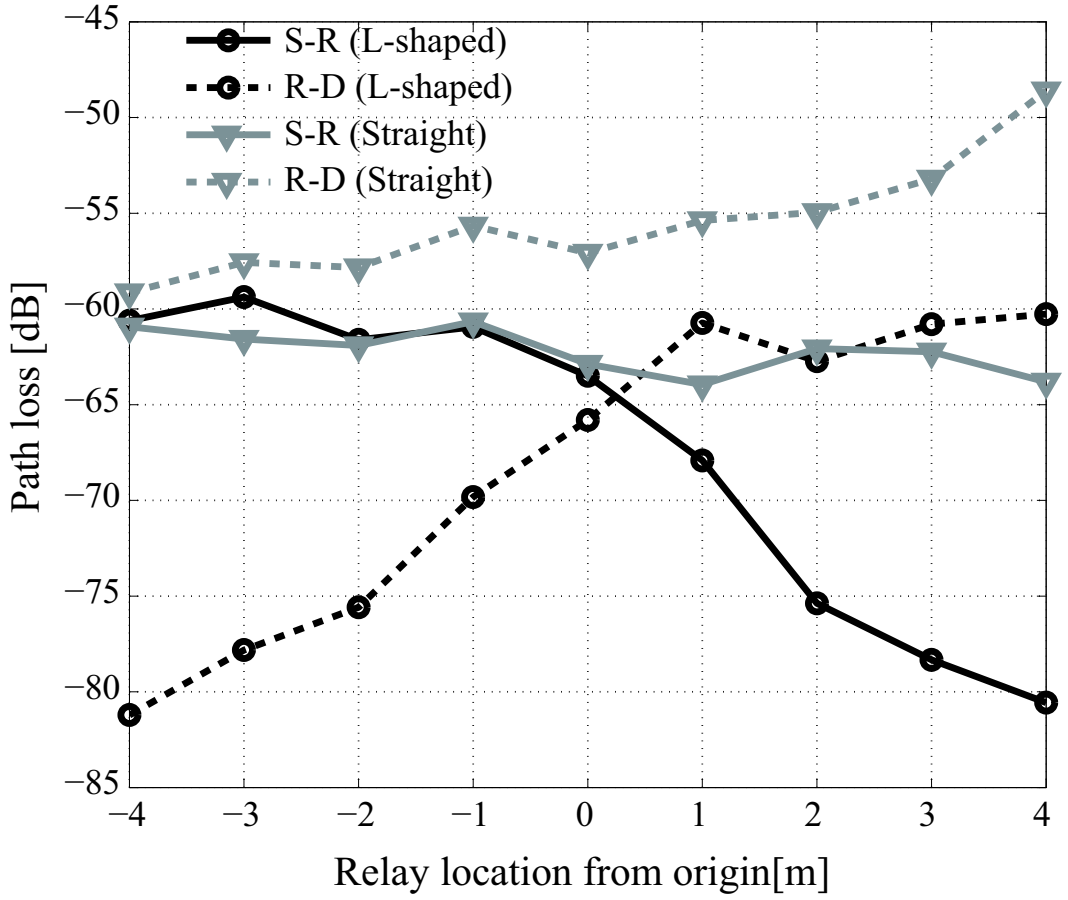

Figure 3.7 Pathloss characteristic comparison.

In the L-shaped Corridor, when R node is located in the same arm of the corridor containing S node, the pathloss of the S-R link is almost at a same level. This similar tendency can be seen in the case of Straight Corridor. However, when R node is located at the other arm, the decrease of the received signal strength can be obviously seen. This result shows the effect of shadowing that degrades the signal strength in the propagation path. Moreover, pathloss characteristics of R-D link also confirm the effect of shadowing when R and D nodes are located in different arms of the L-shaped corridor. Note that the increasing tendency of pathloss of R-D link in the Straight Corridor case is due to asymmetric relay locations with respect to the middle point between S and D nodes, which makes the distance between Tx and Rx closer than that in S-R link.

3.3.2 Spatial correlation

In this part, the spatial correlations between adjacent antenna elements at the Tx side and the Rx side of the propagation channels in L-shaped Corridor environment are investigated. For each relay location, the calculation of spatial correlation coefficient is performed within each local area of the positioner. The correlation coefficient for each local area Ψ at Tx side denoted as $\rho_{t,\Psi}$, and at Rx side denoted as $\rho_{r,\Psi}$, are calculated by the following formulas.

$$\mathbf{R}_{\{.\}\mathrm{t}}(k,\psi) = \mathbf{H}^{H}_{\{.\}}(k,\psi)\mathbf{H}_{\{.\}}(k,\psi)$$
$$\mathbf{R}_{\{.\}\mathrm{r}}(k,\psi) = \mathbf{H}_{\{.\}}(k,\psi)\mathbf{H}^{H}_{\{.\}}(k,\psi)$$

$$\rho_{\{.\}\mathrm{t},\Psi} = \frac{1}{M_{\mathrm{f}}(M_{\mathrm{t}}-1)} \sum_{k=1}^{M_{\mathrm{f}}} \sum_{\substack{i=1 \\ j=i+1}}^{M_{\mathrm{t}}-1} \left| \mathop{\mathrm{E}}_{\psi\in\Psi} \left[\frac{r_{\{.\}\mathrm{t}i,j}(k,\psi)}{\sqrt{r_{\{.\}\mathrm{t}i,i}(k,\psi)}\sqrt{r_{\{.\}\mathrm{t}j,j}(k,\psi)}} \right] \right|$$
$$\rho_{\{.\}\mathrm{r},\Psi} = \frac{1}{M_{\mathrm{f}}(M_{\mathrm{r}}-1)} \sum_{k=1}^{M_{\mathrm{f}}} \sum_{\substack{i=1 \\ j=i+1}}^{M_{\mathrm{r}}-1} \left| \mathop{\mathrm{E}}_{\psi\in\Psi} \left[\frac{r_{\{.\}\mathrm{r}i,j}(k,\psi)}{\sqrt{r_{\{.\}\mathrm{r}i,i}(k,\psi)}\sqrt{r_{\{.\}\mathrm{r}j,j}(k,\psi)}} \right] \right|,$$

where $r_{\{.\}\mathrm{t}i,j}(k,\psi)$ and $r_{\{.\}\mathrm{r}i,j}(k,\psi)$ denote the i^{th} row and j^{th} column element of the matrices $\mathbf{R}_{\{.\}\mathrm{t}}(k,\psi)$ and $\mathbf{R}_{\{.\}\mathrm{r}}(k,\psi)$ respectively.

Figures 3.8a, and 3.8b respectively show the spatial correlation coefficient distributions at the source and the relay side for S-R link with respect to relay locations. Similarly, Figs. 3.8c and 3.8d show the spatial correlation coefficient distributions at the relay and the destination side for R-D link respectively.

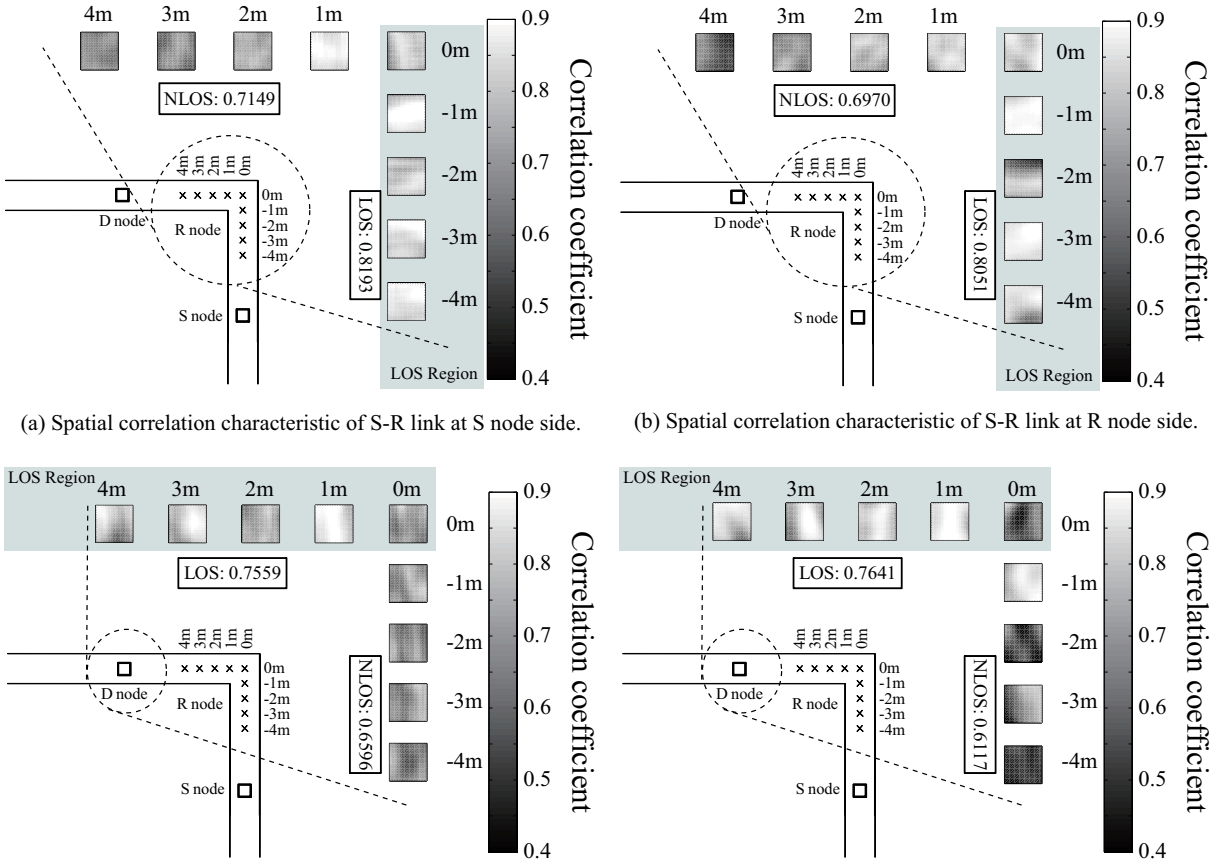

(a) Spatial correlation characteristic of S-R link at S node side.

(b) Spatial correlation characteristic of S-R link at R node side.

(c) Spatial correlation characteristic of R-D link at R node side.

(d) Spatial correlation characteristic of R-D link at D node side.

Figure 3.8 Spatial correlation characteristics in L-shaped Corridor environment.

As illustrated in the figures, the analysis is separated into two regions by receiver locations. LOS region is defined as the area where Tx and Rx are located in the same arm of the corridor, while NLOS is defined as the area when Tx and Rx are located in different arms of the corridor. Hence, for the L-shaped corridor case, LOS region corresponds to the area when R node is located at relay locations -4, -3, -2, -1 and 0 for S-R link and at relay locations 0, 1, 2, 3 and 4 for R-D link. On the other hand, NLOS region corresponds to the area where R node is located at relay locations 1, 2, 3 and 4 for S-R link, and at relay locations -4, -3, -2 and -1 for R-D link.

To facilitate the analysis, the average values of correlation coefficient of all local areas in each region are observed. The region averaged values in each region for both S-R and R-D links are described in Fig. 3.8. The results show that the average coefficients of LOS regions are larger than those of NLOS regions. This implies that multipath effect is more obvious at both Tx and Rx side in NLOS regions.

In addition, for S-R link, the correlation coefficients are remarkably high at relay location 1 compared to the rest of relay locations in NLOS region. This can be explained by the effect of the dominant reflected signal from the wall facing to the array antenna at S node. Also, the correlation coefficients are obviously high at relay location -1 for R-D link in NLOS region. This can also be explained by the dominant incoming diffracted signal at the corner of L-shaped corridor. These effects will be clarified in angular profile analysis described in the next section.

3.3.3 Angular profile

Angular profile is investigated in order to observe the direction of multipath signals at all receiver locations in the relay network. The incoming angle θ is defined as an angle between the x axis and the considered direction of the incoming signal as shown in Fig. 3.2. In this analysis, the local area Ψ at the center of the positioner is chosen as a representative area to find the angular profile at each receiver location. The envelope of the incoming signal in direction θ at subcarrier k is given as

$$\mu_{\{.\}k}(\theta, \Psi) = \int_{x-\frac{\Delta x}{2}}^{x+\frac{\Delta x}{2}} \int_{y-\frac{\Delta y}{2}}^{y+\frac{\Delta y}{2}} H_{\{.\}11k}(x, y) e^{-j\omega(x,y,\theta)} dy dx, \tag{3.1}$$

where $\omega(x, y, \theta) = \frac{2\pi}{\lambda}(x\cos\theta + y\sin\theta)$ is the wave number, λ is the wavelength, and Δx and Δy are the length of a local area in x and y axis of the positioner respectively. The angular profile of a local area Ψ is derived by averaging the incoming signal power over all subcarriers as

$$P_{\{.\}}(\theta, \Psi) = \frac{1}{M_{\mathrm{f}}} \sum_{k=1}^{M_{\mathrm{f}}} |\mu_{\{.\}k}(\theta, \Psi)|^2. \tag{3.2}$$

The calculation results of angular profiles for each relay location of S-R and R-D links in the L-shaped Corridor case are plotted in Figs. 3.9a and 3.9b respectively.

In LOS region of the S-R link, two main lobes in opposite directions can be obviously seen in Fig. 3.9a. The results show that multipath signals come from two main directions consisting of the direct wave between the Tx and the Rx, and the reflected wave from the wall behind the Rx. Furthermore, from the shape of angular profile of S-R link at location 1 in Fig. 3.9a, it can be implied that the direction of most of multipath signals are from the reflected wave from the wall existing in the opposite side of the Tx. Due to this dominant direction of multipaths, the correlation of this location is higher than the rest locations in NLOS region [58].

Similarly, for the R-D link, the results show that the signals in NLOS region are weaker than those in LOS region due to shadowing. Furthermore, the dominant direction of multipath signals coming from the edge of the L-shaped corridor can be observed. This can be explained by the fact that since Tx at location -1 in 3.9b stays closer to the edge of the corridor rather than Tx at other locations in NLOS region, incident signals diffracted at the edge of corridor from the Tx is strong and dominates the direction of incoming signal at the Rx. Due to the dominant direction of multipath signals, the spatial correlation at this location is higher than the rest ones in NLOS region.

3.4 Relay network schemes and analysis method

In this section, we use the experiment data to analyze the network capacity with various relaying schemes. To facilitate our analysis and also to observe the effect of multiple antennas, the analysis is divided into two scenarios with different antenna configurations which are called 222 and 242 MIMO scenarios, as shown in Fig. 3.10. In 222 MIMO scenario, all nodes in the network are equipped with two antennas, while in 242 MIMO scenario, the number of antennas of S, R and D nodes are 2, 4 and 2 antennas respectively. In this analysis, the

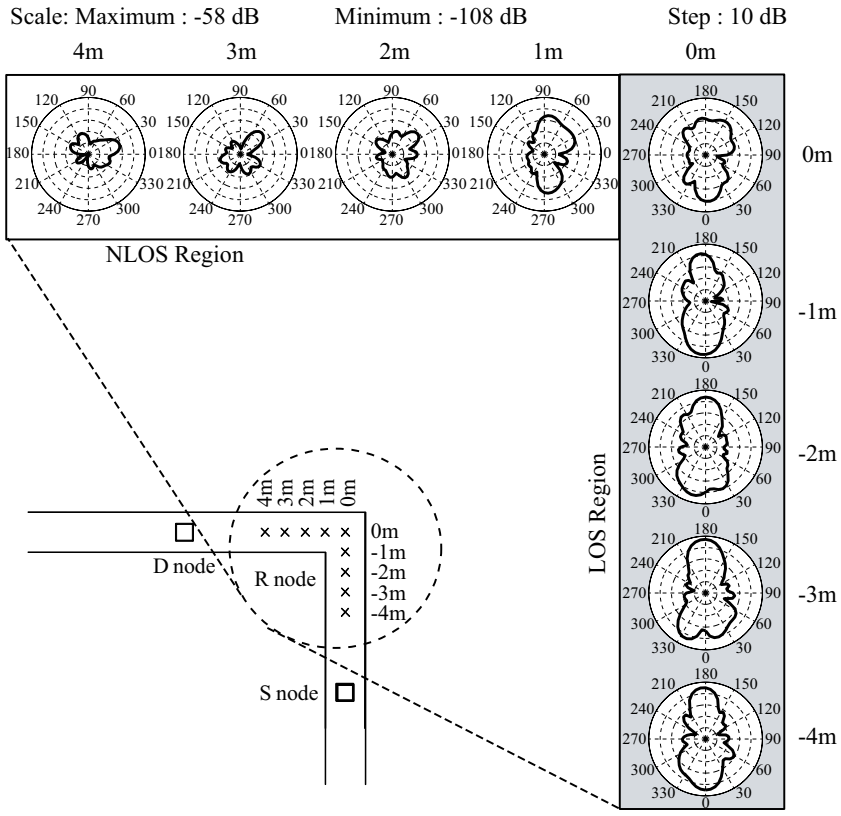

(a) S-R link.

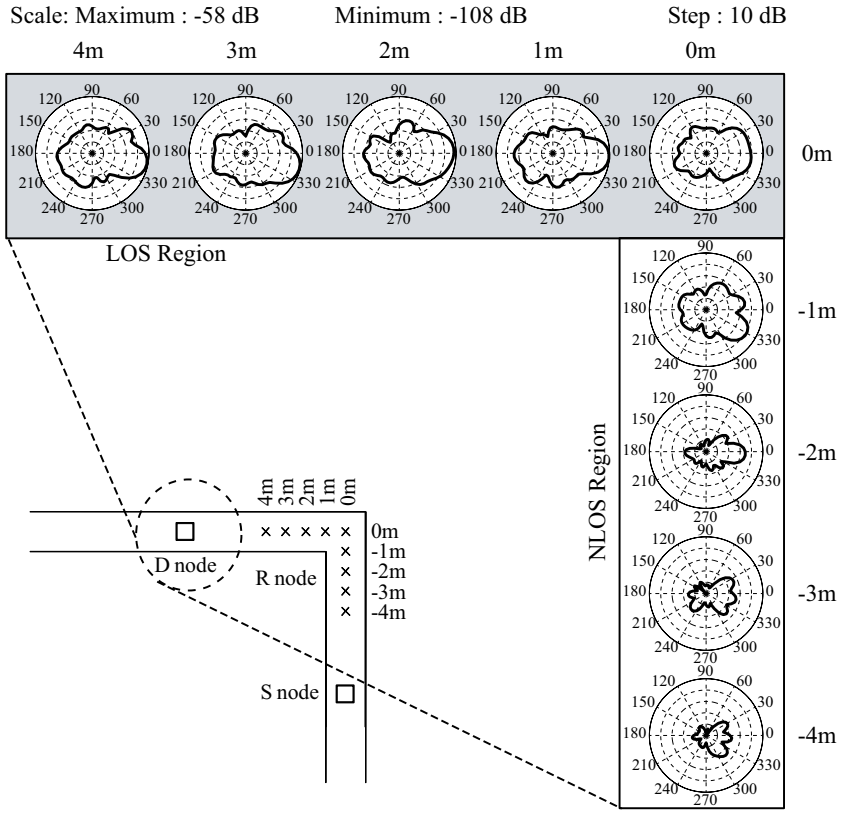

(b) R-D link.

Figure 3.9 Angular profile.

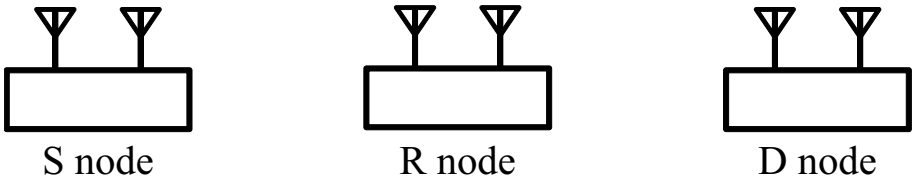

(a) 222 MIMO scenario.

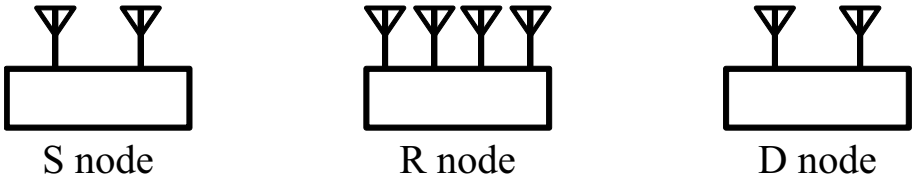

(b) 242 MIMO scenario.

Figure 3.10 Antenna configurations for capacity analysis.

measurement data of the first two antennas among four equipped antennas are used for the node with two-antenna configuration.

For the rest of this section, the capacity of the network for each relaying scheme is calculated by the following procedure. Firstly, the capacity for each link in subcarrier k at position ψ, $C_{\psi}^{\{.\}}(k)$, can be calculated by using the measured channel matrix $\mathbf{H}_{\{.\}}(k,\psi)$ as,

$$\bar{C}_{\psi}^{\{.\}}(k) = f(\mathbf{H}_{\{.\}}(k,\psi)). \tag{3.3}$$

The calculation function of $f(.)$ depends on the corresponding relaying scheme which will be described later. Then, we obtain the capacity at each position ψ by averaging $C_{\psi}^{\{.\}}(k)$ over all subcarriers as

$$\bar{C}_{\psi}^{\{.\}} = \frac{1}{M_{\mathrm{f}}} \sum_{k=1}^{M_{\mathrm{f}}} C_{\psi}^{\{.\}}(k). \tag{3.4}$$

Next, the capacity of 2-hop network of specific scheme $< . >$ at position ψ_1 and ψ_2 of relay and destination is concluded as

$$\bar{C}_{\psi_1,\psi_2}^{<.>} = g(\bar{C}_{\psi_1}^{\mathrm{RS}}, \bar{C}_{\psi_2}^{\mathrm{DR}}), \tag{3.5}$$

where $\bar{C}_{\psi_1}^{\mathrm{RS}}$ and $\bar{C}_{\psi_2}^{\mathrm{DR}}$ are the average capacity of S-R and R-D links at position ψ_1 and ψ_2 respectively. The function $g(.)$ also depends on each relaying scheme which will be describe later. Finally, the average capacity given by averaging over all samples, $\bar{C}_{\psi_1,\psi_2}^{<.>}$, for all link

pairs is given by

$$\tilde{C}^{<\cdot>} = \mathrm{E}_{\psi_1,\psi_2}\left[\bar{C}^{<\cdot>}_{\psi_1,\psi_2}\right]. \tag{3.6}$$

Recently, there are several relaying schemes which have been proposed for MIMO two-hop relay networks. In this thesis, we consider three most fundamental relaying networks, i.e. Decode-and-Forward (DF) relaying, DF cooperative relaying and MIMO two-way relaying with network coding schemes. For the first two schemes, we consider them as the conventional schemes as described in Section 2.4.1. For MIMO two-way relaying scheme, we consider only network coding approach since it is the simplest way to perform bi-directional communication without the necessity of channel knowledge at transmitter side. In addition, we assume that all Rxs are assumed to know perfect channel state information (CSI).

The following describes the realization of these three relaying schemes in different antenna configurations to obtain the best performance.

3.4.1 Decode-and-Forward (DF)

The fundamental of this scheme is described in Section 2.4.1.1. This scheme is considered as the simplest way of one-way relaying communication where the relay just decodes the receive signal and then regenerates the signal to forward to the destination node. For the end-to-end capacity performance, we recall the formulae in Eqs. (2.9)-(2.11) and rewrite them as,

$$C^{\mathrm{RS}}_{\psi_1}(k) = \log_2 \det[\mathbf{I}_{M_\mathrm{R}} + \frac{P_\mathrm{S}}{M\sigma^2}\mathbf{H}_{\mathrm{RS}}\mathbf{H}^H_{\mathrm{RS}}] \tag{3.7}$$

$$C^{\mathrm{DR}}_{\psi_2}(k) = \log_2 \det[\mathbf{I}_{M_\mathrm{D}} + \frac{P_\mathrm{R}}{M\sigma^2}\mathbf{H}_{\mathrm{DR}}\mathbf{H}^H_{\mathrm{DR}}] \tag{3.8}$$

$$\bar{C}^{\mathrm{DF}}_{\psi_1,\psi_2} = \frac{1}{2}\min(\bar{C}^{\mathrm{RS}}_{\psi_1}, \bar{C}^{\mathrm{DR}}_{\psi_2}), \tag{3.9}$$

where $M = \min(M_\mathrm{S}, M_\mathrm{R}, M_\mathrm{D})$.

3.4.2 DF cooperative relay

As described in Section 2.4.1.2, this scheme is the extension of the regular DF where the destination node utilize the prior knowledge in the first timeslot to obtain diversity gain. Again, we recall the formulae of end-to-end capacity performance in Eqs. (2.18)-(2.20) and

rewrite them as,

$$C_{\psi_1}^{\mathrm{RS}}(k) = \log_2 \det\ [\mathbf{I}_{M_\mathrm{R}} + \frac{P_\mathrm{S}}{M\sigma^2}\mathbf{H}_{\mathrm{RS}}\mathbf{H}_{\mathrm{RS}}^H] \tag{3.10}$$

$$C_{\psi_2}^{\mathrm{DR}}(k) = \log_2 \det[\mathbf{I}_{M_\mathrm{D}} + \frac{P_\mathrm{S}}{M\sigma^2}\mathbf{H}_{\mathrm{DS}}\mathbf{H}_{\mathrm{DS}}^H + \frac{P_\mathrm{R}}{M\sigma^2}\mathbf{H}_{\mathrm{DR}}\mathbf{H}_{\mathrm{DR}}^H]$$

$$\bar{C}_{\psi_1,\psi_2}^{\mathrm{DFCo}} = \frac{1}{2}\min(\bar{C}_{\psi_1}^{\mathrm{RS}}, \bar{C}_{\psi_2}^{\mathrm{DR}}), \tag{3.11}$$

where $M = \min(M_\mathrm{S}, M_\mathrm{R}, M_\mathrm{D})$.

3.4.3 Two-way relay with network coding

For two-way relaying scheme employing network coding, we apply the fundamental concept described in Section 2.4.2.1 to the considering 222 and 242 MIMO antenna configurations. Basically, R node receives two different signals from S and D nodes by using MIMO multiple access algorithm in the first timeslot, and then R node performs network coding to combine these two signals to broadcast to S and D which decodes its desired signal with the prior knowledge in the second timeslot.

Since the number of antennas at R node is different in two scenarios, the algorithm of transmission and detection in the network has to be separately considered. In this analysis, we also apply STBC and ZF method for network coding with MIMO scheme proposed in [27] to allow the network perform its best to achieve diversity performance in each antenna configuration. The details are described as follows.

3.4.3.1 222 MIMO scenario

The diagram of two-way MIMO relaying in 222 MIMO scenario is illustrated in Fig. 3.11. Since R node has two antennas in this scenario, it can simultaneously receive two different streams. Thus, two single streams can be sent from S and D nodes. Here, the transmission of single stream with two antennas is performed by applying STBC algorithm to obtain full diversity gain. At S node, over the first symbol period, two different symbols $x_\mathrm{S}(1)$ and $x_\mathrm{S}(2)$ of transmit signal x_S are simultaneously transmitted over antenna 1 and 2, respectively. Over the next symbol period, $x_\mathrm{S}^*(2)$ and $-x_\mathrm{S}^*(1)$ are transmitted similarly. The transmit signal at D node is also similarly considered. Here, the transmit signal matrix of S-R and D-R links

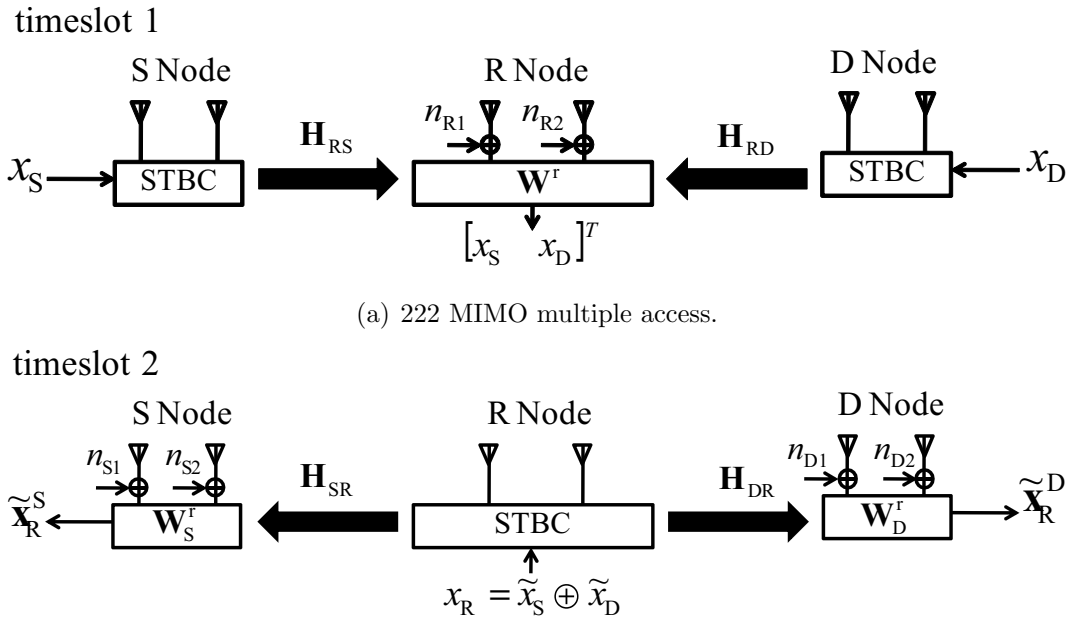

(a) 222 MIMO multiple access.

(b) 222 MIMO broadcast.

Figure 3.11 Two-way relay network with network coding in 222 MIMO scenario.

become

$$\mathbf{x}_S^{\text{STBC}} = \begin{bmatrix} x_{S(1)} & x_{S(2)} \\ x_{S(2)}^* & -x_{S(1)}^* \end{bmatrix}, \tag{3.12}$$

$$\mathbf{x}_D^{\text{STBC}} = \begin{bmatrix} x_{D(1)} & x_{D(2)} \\ x_{D(2)}^* & -x_{D(1)}^* \end{bmatrix}, \tag{3.13}$$

respectively.

Hence, the equivalent channel matrix of S-R and D-R links respectively become

$$\mathbf{H}_{RS}^{\text{STBC}} = \begin{bmatrix} h_{RS}^{11} & -(h_{RS}^{12})^* & h_{RS}^{21} & -(h_{RS}^{22})^* \\ h_{RS}^{12} & (h_{RS}^{11})^* & h_{RS}^{22} & (h_{RS}^{21})^* \end{bmatrix}^T, \tag{3.14}$$

$$\mathbf{H}_{RD}^{\text{STBC}} = \begin{bmatrix} h_{RD}^{11} & -(h_{RD}^{12})^* & h_{RD}^{21} & -(h_{RD}^{22})^* \\ h_{RD}^{12} & (h_{RD}^{11})^* & h_{RD}^{22} & (h_{RD}^{21})^* \end{bmatrix}^T, \tag{3.15}$$

where h_{XY}^{ab} is a channel response of transmission from Tx antenna b at Y node to Rx antenna a at X node, and the notation $[.]^*$ refers to conjugate operation.

The received signal vector can be expressed as

$$\mathbf{y} = \mathbf{H}_R \mathbf{x}_{SD} + \mathbf{n}_R, \tag{3.16}$$

where $\mathbf{H}_{\mathrm{R}} = \left[\mathbf{H}_{\mathrm{RS}}^{\mathrm{STBC}}\ \mathbf{H}_{\mathrm{RD}}^{\mathrm{STBC}}\right]$ and $\mathbf{x}_{\mathrm{SD}} = [x_{\mathrm{S}}(1)\ x_{\mathrm{S}}(2)\ x_{\mathrm{D}}(1)\ x_{\mathrm{D}}(2)]^T$.

The detection of data streams can be performed at R node by applying ZF weight which is defined as

$$\mathbf{W}^{\mathrm{r}} = \mathbf{H}_{\mathrm{R}}(\mathbf{H}_{\mathrm{R}}^H\mathbf{H}_{\mathrm{R}})^{-1}. \tag{3.17}$$

After applying the weight to the received signal, the estimated signal vector becomes

$$\begin{aligned}\tilde{\mathbf{x}}_{\mathrm{SD}} &= \mathbf{W}^{\mathrm{r}H}\mathbf{H}_{\mathrm{R}}\mathbf{x}_{\mathrm{SD}} + \mathbf{W}^{\mathrm{r}H}\mathbf{n}_{\mathrm{R}} \\ &= \mathbf{x}_{\mathrm{SD}} + \mathbf{W}^{\mathrm{r}H}\mathbf{n}_{\mathrm{R}},\end{aligned} \tag{3.18}$$

where $\tilde{\mathbf{x}}_{\mathrm{SD}} = [\tilde{x}_{\mathrm{S}}(1)\ \tilde{x}_{\mathrm{S}}(2)\ \tilde{x}_{\mathrm{D}}(1)\ \tilde{x}_{\mathrm{D}}(2)]$, and $\mathbf{W}^{\mathrm{r}H} = \left[\mathbf{w}_{\mathrm{RS}}^{\mathrm{r}H}\ \mathbf{w}_{\mathrm{RD}}^{\mathrm{r}H}\right]^T$.

Hence, the capacity of S-R and D-R links can be calculated as

$$C_{\psi_1}^{\mathrm{RS}}(k) = \frac{1}{2}\log_2\det[\mathbf{I}_{M_{\mathrm{S}}} + \frac{P_{\mathrm{S}}}{M_{\mathrm{S}}\sigma^2}(\mathbf{w}_{\mathrm{RS}}^{rH}\mathbf{w}_{\mathrm{RS}}^{\mathrm{r}})^{-1}] \tag{3.19}$$

$$C_{\psi_1}^{\mathrm{RD}}(k) = \frac{1}{2}\log_2\det[\mathbf{I}_{M_{\mathrm{D}}} + \frac{P_{\mathrm{D}}}{M_{\mathrm{D}}\sigma^2}(\mathbf{w}_{\mathrm{RD}}^{rH}\mathbf{w}_{\mathrm{RD}}^{\mathrm{r}})^{-1}]. \tag{3.20}$$

For the next timeslot, the estimated symbol from S and D nodes are combined into one transmit signal, x_{R}, and then broadcast to S and D nodes. Since R node can broadcast the network coded signal with multiple antennas, STBC is also employed in this timeslot. Hence, the transmit signal matrix can be obtained as same as in Eq. (3.15). Hence,the channel matrix of R-S and R-D respectively become

$$\mathbf{H}_{\mathrm{SR}}^{\mathrm{STBC}} = \begin{bmatrix} h_{\mathrm{SR}}^{11} & -(h_{\mathrm{SR}}^{12})^* & h_{\mathrm{SR}}^{21} & -(h_{\mathrm{SR}}^{22})^* \\ h_{\mathrm{SR}}^{12} & (h_{\mathrm{SR}}^{11})^* & h_{\mathrm{SR}}^{22} & (h_{\mathrm{SR}}^{21})^* \end{bmatrix}^T, \tag{3.21}$$

$$\mathbf{H}_{\mathrm{SR}}^{\mathrm{STBC}} = \begin{bmatrix} h_{\mathrm{DR}}^{11} & -(h_{\mathrm{DR}}^{12})^* & h_{\mathrm{DR}}^{21} & -(h_{\mathrm{DR}}^{22})^* \\ h_{\mathrm{DR}}^{12} & (h_{\mathrm{DR}}^{11})^* & h_{\mathrm{DR}}^{22} & (h_{\mathrm{DR}}^{21})^* \end{bmatrix}^T. \tag{3.22}$$

The receive weight for S and D nodes with STBC coding can be determined as

$$\mathbf{W}_{\mathrm{S}}^{\mathrm{r}} = \mathbf{H}_{\mathrm{SR}}^{\mathrm{STBC}}(\mathbf{H}_{\mathrm{SR}}^{\mathrm{STBC}H}\mathbf{H}_{\mathrm{SR}}^{\mathrm{STBC}})^{-1}, \tag{3.23}$$

$$\mathbf{W}_{\mathrm{D}}^{\mathrm{r}} = \mathbf{H}_{\mathrm{DR}}^{\mathrm{STBC}}(\mathbf{H}_{\mathrm{DR}}^{\mathrm{STBC}H}\mathbf{H}_{\mathrm{DR}}^{\mathrm{STBC}})^{-1}, \tag{3.24}$$

respectively.

After applying the weight to the received signal, the estimated signal at S and D nodes become

$$\tilde{\mathbf{x}}_{\mathrm{R}}^{\mathrm{S}} = \mathbf{x}_{\mathrm{R}} + \mathbf{W}_{\mathrm{S}}^{\mathrm{r}H}\mathbf{n}_{\mathrm{S}}, \tag{3.25}$$

$$\tilde{\mathbf{x}}_{\mathrm{R}}^{\mathrm{D}} = \mathbf{x}_{\mathrm{D}} + \mathbf{W}_{\mathrm{D}}^{\mathrm{r}H}\mathbf{n}_{\mathrm{D}}, \tag{3.26}$$

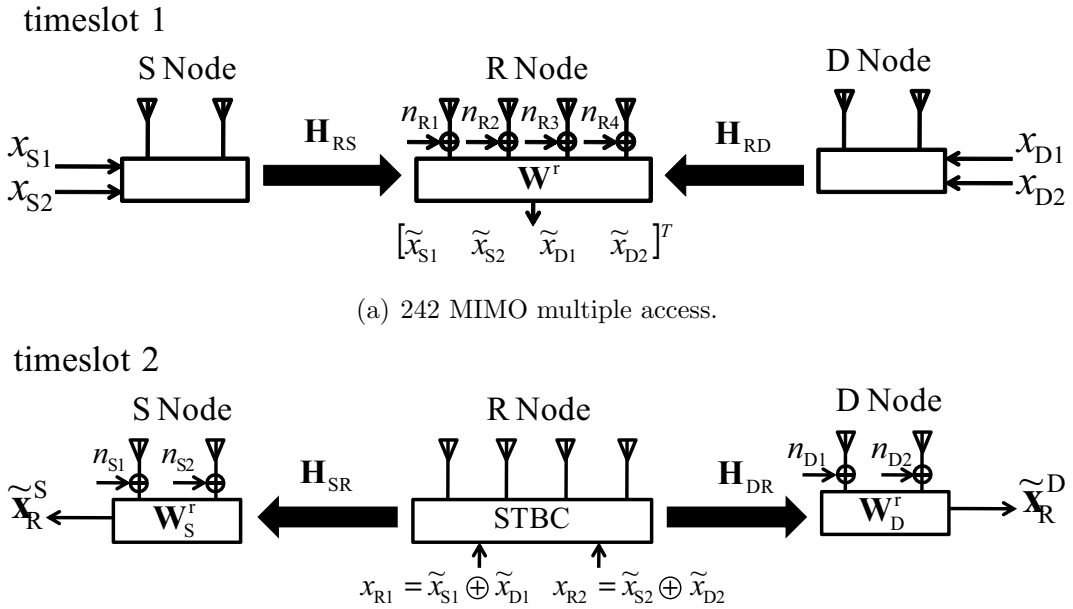

(a) 242 MIMO multiple access.

(b) 242 MIMO broadcast.

Figure 3.12 Two-way relay network with network coding in 242 MIMO scenario.

respectively.

Hence, the capacities of R-S and R-D links can be calculated as

$$C_{\psi_1}^{\mathrm{SR}}(k) = \frac{1}{2}\log_2 \det[\mathbf{I}_{M_\mathrm{R}} + \frac{P_\mathrm{R}}{2M_\mathrm{R}\sigma^2}(\mathbf{W}_\mathrm{S}^{\mathrm{r}H}\mathbf{W}_\mathrm{S}^{\mathrm{r}})^{-1}], \tag{3.27}$$

$$C_{\psi_1}^{\mathrm{DR}}(k) = \frac{1}{2}\log_2 \det[\mathbf{I}_{M_\mathrm{R}} + \frac{P_\mathrm{R}}{2M_\mathrm{R}\sigma^2}(\mathbf{W}_\mathrm{D}^{\mathrm{r}H}\mathbf{W}_\mathrm{D}^{\mathrm{r}})^{-1}], \tag{3.28}$$

respectively.

The average capacity of forward flow, backward flow and the whole two-way relay network can be concluded as the following formulas respectively.

$$\bar{C}_{\psi_1,\psi_2}^{\mathrm{F,tw2}} = \min(\bar{C}_{\psi_1}^{\mathrm{RS}}, \bar{C}_{\psi_2}^{\mathrm{DR}}), \tag{3.29}$$

$$\bar{C}_{\psi_1,\psi_2}^{\mathrm{B,tw2}} = \min(\bar{C}_{\psi_1}^{\mathrm{SR}}, \bar{C}_{\psi_2}^{\mathrm{RD}}), \tag{3.30}$$

$$\bar{C}_{\psi_1,\psi_2}^{\mathrm{tw2}} = \frac{1}{2}(\bar{C}_{\psi_1,\psi_2}^{\mathrm{F,tw2}} + \bar{C}_{\psi_1,\psi_2}^{\mathrm{B,tw2}}). \tag{3.31}$$

3.4.3.2 242 MIMO scenario

In this scenario, R node is equipped with four antennas, so it can obtain maximally four different streams. In the first timeslot, or MIMO multiple access mode, two different signal streams

can be simultaneously sent at both S and D nodes. Figure 3.12a illustrates the network diagram for MIMO multiple access in timeslot 1. The equivalent channel of received signal at R node can be expressed as $\mathbf{H}_{\mathrm{R}} = [\mathbf{H}_{\mathrm{RS}}\ \mathbf{H}_{\mathrm{RD}}]$ and the receive weight can be determined as $\mathbf{W}^{\mathrm{r}} = \mathbf{H}_{\mathrm{R}}(\mathbf{H}_{\mathrm{R}}^{H}\mathbf{H}_{\mathrm{R}})^{-1}$, where $\mathbf{W}^{\mathrm{r}H} = \left[\mathbf{w}_{\mathrm{RS}}^{\mathrm{r}H}\ \mathbf{w}_{\mathrm{RD}}^{\mathrm{r}H}\right]^{T}$.

After applying the weight to the received signal, the estimated signal vector becomes

$$\begin{aligned}\tilde{x}_{\mathrm{SD}} &= \mathbf{W}^{\mathrm{r}H}\mathbf{H}_{\mathrm{R}}\mathbf{x}_{\mathrm{SD}} + \mathbf{W}^{\mathrm{r}H}\mathbf{n}_{\mathrm{R}} \\ &= \mathbf{x}_{\mathrm{SD}} + \mathbf{W}^{\mathrm{r}H}\mathbf{n}_{\mathrm{R}},\end{aligned} \tag{3.32}$$

where $\tilde{x}_{\mathrm{SD}} = \left[\tilde{\mathbf{x}}_{\mathrm{S}}^{T}\ \tilde{\mathbf{x}}_{\mathrm{D}}^{T}\right]^{T} = [\tilde{x}_{\mathrm{S1}}\ \tilde{x}_{\mathrm{S2}}\ \tilde{x}_{\mathrm{D1}}\ \tilde{x}_{\mathrm{D2}}]^{T}$, and $\mathbf{W}^{\mathrm{r}H} = \left[\mathbf{w}_{\mathrm{RS}}^{\mathrm{r}H}\ \mathbf{w}_{\mathrm{RD}}^{\mathrm{r}H}\right]^{T}$.

Therefore, the capacities of S-R and D-R links can be calculated as

$$C_{\psi_1}^{\mathrm{RS}}(k) = \log_2 \det[\mathbf{I}_{M_{\mathrm{S}}} + \frac{P_{\mathrm{S}}}{M_{\mathrm{S}}\sigma^2}(\mathbf{w}_{\mathrm{RS}}^{rH}\mathbf{w}_{\mathrm{RS}}^{\mathrm{r}})^{-1}], \tag{3.33}$$

$$C_{\psi_1}^{\mathrm{RD}}(k) = \log_2 \det[\mathbf{I}_{M_{\mathrm{S}}} + \frac{P_{\mathrm{S}}}{M_{\mathrm{S}}\sigma^2}(\mathbf{w}_{\mathrm{RD}}^{rH}\mathbf{w}_{\mathrm{RS}}^{\mathrm{r}})^{-1}] \tag{3.34}$$

respectively.

For the next timeslot, the diagram is shown in Fig. 3.12b. In this timeslot, each two messages from S and D nodes are combined to be two transmit signal streams, x_{R1} and x_{R2}. With four antennas at R node, STBC can also be applied in this broadcast mode. In the first symbol period, antenna 1 and 2 are used for transmitting different symbols $x_{\mathrm{R1(1)}}$ and $x_{\mathrm{R1(2)}}$ of the transmit signal x_{R1} and antenna 3 and 4 are used for transmitting different symbols $x_{\mathrm{R2(1)}}$ and $x_{\mathrm{R2(2)}}$ of the transmit signal x_{R2} respectively. In the next symbol period, the transmit symbols are $-x_{\mathrm{R1(2)}}^{*}$, $x_{\mathrm{R1(1)}}^{*}$, $-x_{\mathrm{R2(2)}}^{*}$ and $x_{\mathrm{R2(1)}}^{*}$ at antenna 1, 2, 3 and 4 respectively. Then, the channel matrices of R-S and R-D links can be concluded as

$$\mathbf{H}_{\mathrm{SR}}^{\mathrm{STBC}} = \begin{bmatrix} h_{\mathrm{SR}}^{11} & h_{\mathrm{SR}}^{12} & h_{\mathrm{SR}}^{13} & h_{\mathrm{SR}}^{14} \\ -(h_{\mathrm{SR}}^{12})^{*} & (h_{\mathrm{SR}}^{11})^{*} & -(h_{\mathrm{SR}}^{14})^{*} & (h_{\mathrm{SR}}^{13})^{*} \\ h_{\mathrm{SR}}^{21} & h_{\mathrm{SR}}^{22} & h_{\mathrm{SR}}^{23} & h_{\mathrm{SR}}^{24} \\ -(h_{\mathrm{SR}}^{22})^{*} & (h_{\mathrm{SR}}^{21})^{*} & -(h_{\mathrm{SR}}^{24})^{*} & (h_{\mathrm{SR}}^{23})^{*} \end{bmatrix}, \tag{3.35}$$

$$\mathbf{H}_{\mathrm{DR}}^{\mathrm{STBC}} = \begin{bmatrix} h_{\mathrm{DR}}^{11} & h_{\mathrm{DR}}^{12} & h_{\mathrm{DR}}^{13} & h_{\mathrm{DR}}^{14} \\ -(h_{\mathrm{DR}}^{12})^{*} & (h_{\mathrm{DR}}^{11})^{*} & -(h_{\mathrm{DR}}^{14})^{*} & (h_{\mathrm{DR}}^{13})^{*} \\ h_{\mathrm{DR}}^{21} & h_{\mathrm{DR}}^{22} & h_{\mathrm{DR}}^{23} & h_{\mathrm{DR}}^{24} \\ -(h_{\mathrm{DR}}^{22})^{*} & (h_{\mathrm{DR}}^{21})^{*} & -(h_{\mathrm{DR}}^{24})^{*} & (h_{\mathrm{DR}}^{23})^{*} \end{bmatrix}, \tag{3.36}$$

respectively.

The ZF receive weight and the estimated signal can be obtained as similar as in the broadcast mode with STBC in 222 scenario. Therefore, the capacities of R-S and R-D links can be concluded as

$$C_{\psi_1}^{\mathrm{SR}}(k) = \frac{1}{2}\log_2 \det[\mathbf{I}_{M_\mathrm{R}} + \frac{P_\mathrm{R}}{2M_\mathrm{R}\sigma^2}(\mathbf{W}_\mathrm{S}^{\mathrm{r}H}\mathbf{W}_\mathrm{S}^{\mathrm{r}})^{-1}], \tag{3.37}$$

$$C_{\psi_1}^{\mathrm{DR}}(k) = \frac{1}{2}\log_2 \det[\mathbf{I}_{M_\mathrm{R}} + \frac{P_\mathrm{R}}{2M_\mathrm{R}\sigma^2}(\mathbf{W}_\mathrm{D}^{\mathrm{r}H}\mathbf{W}_\mathrm{D}^{\mathrm{r}})^{-1}], \tag{3.38}$$

respectively.

The average capacity of forward flow, backward flow and the whole two-way relay network can be concluded as the following formulae respectively.

$$\bar{C}_{\psi_1,\psi_2}^{\mathrm{F,tw4}} = \min(\bar{C}_{\psi_1}^{\mathrm{RS}}, \bar{C}_{\psi_2}^{\mathrm{DR}}), \tag{3.39}$$

$$\bar{C}_{\psi_1,\psi_2}^{\mathrm{B,tw4}} = \min(\bar{C}_{\psi_1}^{\mathrm{SR}}, \bar{C}_{\psi_2}^{\mathrm{RD}}), \tag{3.40}$$

$$\bar{C}_{\psi_1,\psi_2}^{\mathrm{tw4}} = \frac{1}{2}(\bar{C}_{\psi_1,\psi_2}^{\mathrm{F,tw4}} + \bar{C}_{\psi_1,\psi_2}^{\mathrm{B,tw4}}). \tag{3.41}$$

3.5 Results of capacity analysis

First of all, we consider the capacity of the direct S-D link in both L-shaped Corridor and Straight Corridor case, shown in Fig. 3.13. The results show that the capacity of the direct link in non-shadowing environment is obviously higher than that in shadowing environment. This reconfirmed the fact that shadowing has an effect on the network performance.

Moreover, the results also show that the network performance is improved by applying relay technique in the L-shaped Corridor case, as shown in Figs. 3.13a and 3.13c. On the other hand, relaying technique does not improve the capacity of relay network in Straight Corridor case, as shown in Figs. 3.13b and 3.13d. The reason is that relaying requires twice the time to transmit signal from S to D node as that of the direct communication which uses only one timeslot. It can be implied that relaying is not necessary for the case of LOS environment.

In addition, for the L-shaped Corridor case, the results in Figs. 3.13a and 3.13c show that the network can achieve the best performance when the relay is located at relay location 0 corresponding to the corner of the L-shaped Corridor. The reason is that R node can receive signal from S and D nodes directly without signal strength degradation by shadowing.

Furthermore, the results also show that the network can achieve the best performance by applying two-way relay with network coding. The reason is that the technique can reduce

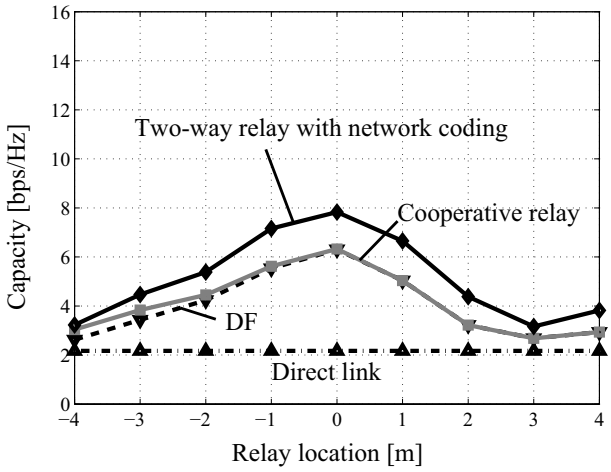

(a) 222 MIMO in L-shaped Corridor case.

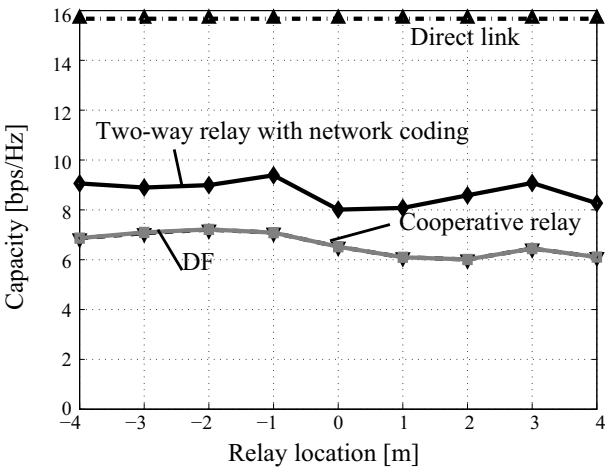

(b) 222 MIMO in Straight Corridor case.

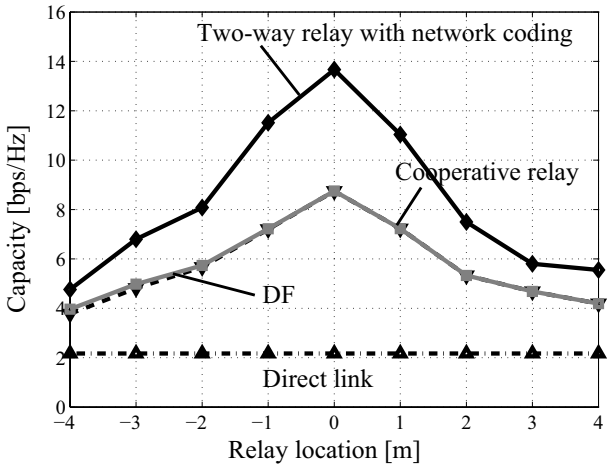

(c) 242 MIMO in L-shaped Corridor case.

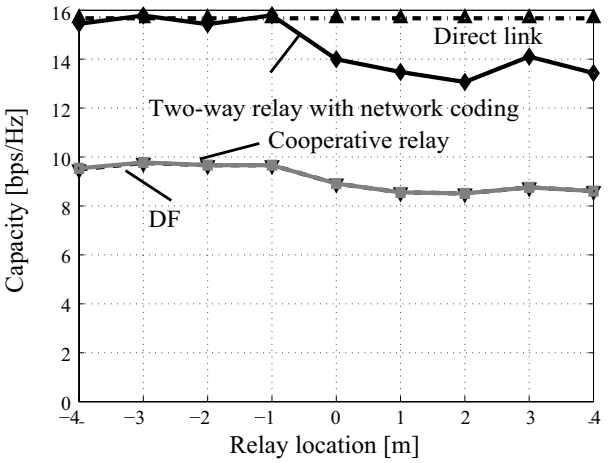

(d) 242 MIMO in Straight Corridor case.

Figure 3.13 Capacity characteristics.

the number of required timeslots for transferring message bi-directionally. Interestingly, the capacity improvement is more obvious when the number of antennas at relay node is higher. This is because the network in 242 MIMO scenario can transfer data as almost twice as that of 222 MIMO scenario.

Finally, it can be seen that the capacity of DF cooperative relaying scheme does not significantly improve the performance of the conventional DF scheme as depicted in Figs. 3.13a and 3.13c. The reason is that the direct signal S-D link cannot properly cooperate with relay link due to signal strength degradation caused by shadowing. In other words, cooperative relaying scheme is not effective in strong shadowing environment.

3.6 Relay Placement Estimation (RPE) scheme

The previous section shows that the optimum relay location is at the corner of the L-shaped corridor in terms of network capacity. This section introduces the novel placement estimation scheme for two-hop MIMO relay networks.

In order to predict the optimum relay location, our RPE scheme is proposed by the following formulae.

$$\mathbf{R}_{\mathrm{RS},l} = \underset{k,\psi}{\mathrm{E}}[\mathbf{H}_{\mathrm{RS},l}(k,\psi)\mathbf{H}^{H}_{\mathrm{RS},l}(k,\psi)] \tag{3.42}$$

$$\mathbf{R}_{\mathrm{DR},l} = \underset{k,\psi}{\mathrm{E}}[\mathbf{H}_{\mathrm{DR},l}(k,\psi)\mathbf{H}^{H}_{\mathrm{DR},l}(k,\psi)] \tag{3.43}$$

$$\delta_l = \min(\det(\mathbf{R}_{\mathrm{RS},l}), \det(\mathbf{R}_{\mathrm{DR},l})) \tag{3.44}$$

$$l_{\mathrm{opt}} = \arg\max_{l\in L} \delta_l, \tag{3.45}$$

where $\mathbf{H}_{\mathrm{RS},l}(k,\psi)$ and $\mathbf{H}_{\mathrm{DR},l}(k,\psi)$ respectively denote the channel matrix of S-R and R-D links at subchannel k and position ψ for relay location $l \in L$, $L = \{-4,-3,...,3,4\}$ denotes the set of relay location candidates, $\mathbf{R}_{\mathrm{RS},l}$ and $\mathbf{R}_{\mathrm{DR},l}$ represent the correlation matrix of S-R and R-D links for location l, δ_l denotes the RPE value of relay location l, and l_{opt} is the optimum relay location.

In the proposed RPE scheme, the determinant of the correlation matrix of each link indicates the quality of MIMO link which depends on link gain and spatial correlation characteristics. In Eq. (3.44), the RPE value δ_l of relay location l is obtained from the determinant value of the link which has worse quality. In other words, this value characterizes the bottleneck link at each relay location. Then, the optimum relay location l_{opt} can be determined in

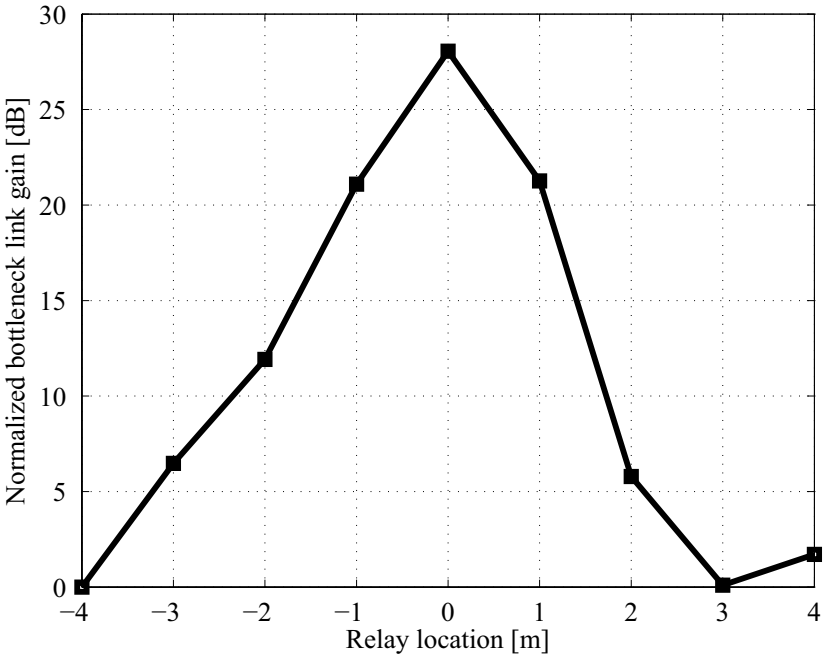

Figure 3.14 Estimation result by using the proposed RPE.

Eq. (3.45) as the location with the highest bottleneck link quality. Since the previous section mainly discussed the capacity with two antenna configuration, the consideration of RPE is also based on 2x2 MIMO configuration.

By applying the RPE scheme to the experiment data in the L-shaped Corridor case, the calculation result of δ_l at each relay location is plotted in Fig. 3.14. In this figure, the value of δ_l is normalized such that $\min_{l \in L}(\delta_l)$ corresponds to the value of 0 dB. From this figure, it can be observed that $l_{\text{opt}} = 0$ which means that the relay location 0 is predicted as the optimal relay location for the case of the L-shaped Corridor. This result agrees well with the conclusion from the capacity analysis, which validates the effectiveness of the proposed RPE scheme.

3.7 Chapter summary

This chapter conducted the basic study of two-hop MIMO relay networks via a propagation measurement experiment in an L-shaped corridor where strong shadowing effect degrades the signal strength of the direct link. Based on the measurement data, the large-scale and small-scale propagation characteristics in the L-shaped corridor were analyzed. The large-scale analysis showed a strong shadowing effect i.e. the degradation of signal strength when

the source and destination nodes are located in different arms of the L-shaped corridor. Furthermore, the result of the small-scale fading analysis showed the characteristics of multi-path signals in the L-shaped corridor. By combining the concept of both large-scale and small-scale fading characteristics, we also proposed a scheme called as RPE scheme to estimate the optimum relay location where the network can achieve its best capacity performance.

By analyzing the network performance, we also found that relaying technique is more effective in shadowing environment, while the technique is ineffective in non-shadowing environment. Moreover, the results showed that the network achieved the highest performance when the relay node is located at the corner of the L-shaped corridor. This location is also well estimated by the proposed RPE scheme. By estimating with RPE, the optimum relay placement is the location where the bottleneck link gain is maximum. Finally, based on evaluation of various relaying schemes, it was found that the two-way relay with network coding scheme can achieve the best performance while the cooperative relaying scheme is found to be ineffective in strong shadowing environments.

Chapter 4

Design of multi-hop MIMO relay networks in a realistic environment

4.1 Motivation

In the previous chapter, we consider the simple configuration of relay networks which contain single relay in the perspective of dealing with shadowing problem. In this chapter, we extend our consideration to multi-hop relay networks which contain more than two relay nodes.

Recently, MIMO has been introduced in relay networks to increase channel capacity of each relaying hop. However, one of the serious problems in conventional multi-hop relay networks is frequency-sharing interference which deteriorates the network performance as discussed in Chapter 2. In Section 2.5.2, we introduced MIMO Two-Way Multi-hop Networks (M2WMNs) which provide adjacent interference cancellation and bi-directional communication owing to the benefits of multiple antennas. Even though M2WMN can eliminate the effect of adjacent interference, over-reach interference still limits the system performance. In section 2.5.3, power control for M2WMN is proposed to alleviate the effect of over-reach interference.

The studies of M2WMN so far just theoretically assumed all channels between nodes to follow independent identically distributed (i.i.d.) Rayleigh fading model for ease of analysis. This assumption is certainly far from realistic case where the channels in different links might experience different pathloss condition including shadowing, especially for disconnected links.

In addition, nowadays, network designers are questioning about where to deploy relay nodes in a given environment in order to achieve the highest network capacity. So far, the optimal relay placement of M2WMN in practical environment has been left as an open issue,

especially for the case that power control is applied.

Moreover, several practical researches of relay networks have been performed such as one of our works in the previous chapter [59]. However, these works consider the network configuration of two-hop relay networks where there is no frequency-sharing interference problem as in M2WMN. Therefore, the study of M2WMN in the realistic environment where interference among nodes is taken into account becomes necessary.

Consequently, this chapter constructs a 3D ray-tracing simulation of channel propagation for M2WMN in a practical U-shaped indoor environment where shadowing is dominant as illustrated in Fig. 4.1. In this paper, 3D ray-tracing simulator called *Wireless Insite* [60] which can provide highly accurate 3D ray searching in indoor environments is employed. Using this semi-empirical propagation data, this chapter aims to investigate the performance of M2WMN as well as the optimum relay locations in realistic environment. Moreover, we compare the results from 3D ray-tracing simulation and channel model based on the conventional assumption of Rayleigh fading to observe the applicability of these two models. Finally, we also propose a sub-optimal scheme to estimate the optimal relay placement in this chapter.

4.2 Target environment and network topology

In this chapter, we aim to study the efficiency of MIMO multi-hop relay network in U-shaped corridor of a concrete dormitory [61], as shown in Fig. 4.1. The corridor consists of two straight corridors in the left and right hand side connected by another straight corridor in the middle. The concrete wall along the corridor consists of several wooden doors of private rooms and glass windows. The height of the corridor is 2.4 m.

In this study, the multi-hop relay network contains 5 transceiver nodes which are respectively denoted as node 1, 2, 3, 4 and 5 as in Fig. 4.2. The source node 1 and the destination node 5 are separately located at the left and right straight corridors, thus direct transmission is blocked by strong shadowing effect. Three relay nodes are employed to rescue the direct link, which are placed along the U-shaped corridor at their candidate locations around the two corners of the corridor and the middle area of the connecting corridor. These candidate locations are varied at one meter spacing with the corresponding locations numbered as 1 to 7 as in Fig. 4.2. For the rest of this paper, R_2, R_3 and $R_4 \in \{1, 2, ..., 7\}$ are respectively defined as the locations of node 2, 3 and 4.

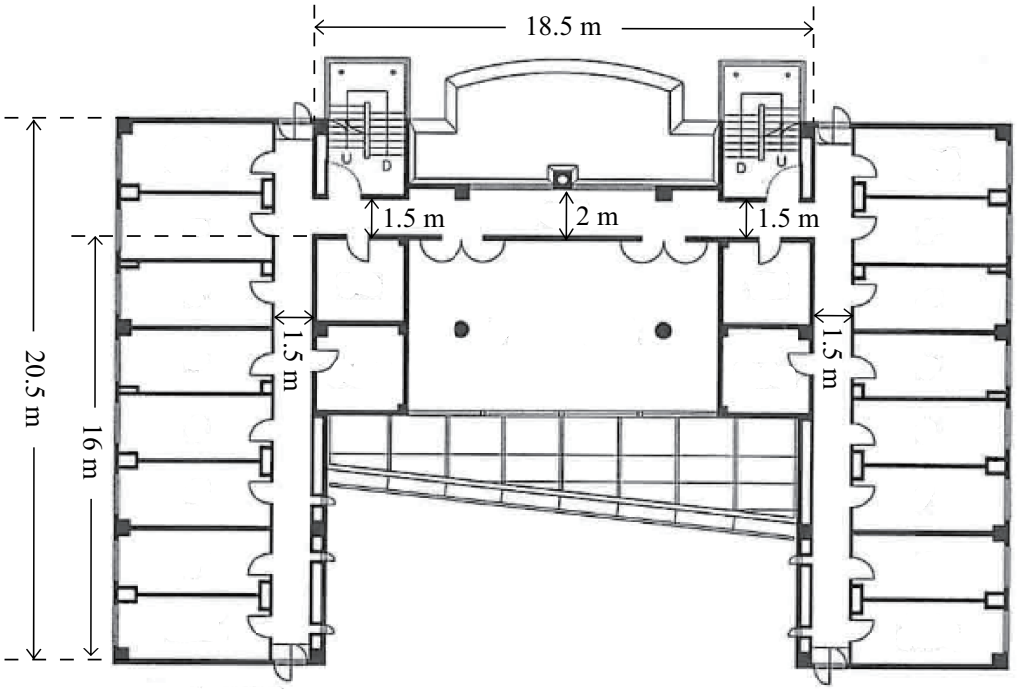

Figure 4.1 A U-shaped corridor environment for multi-hop network.

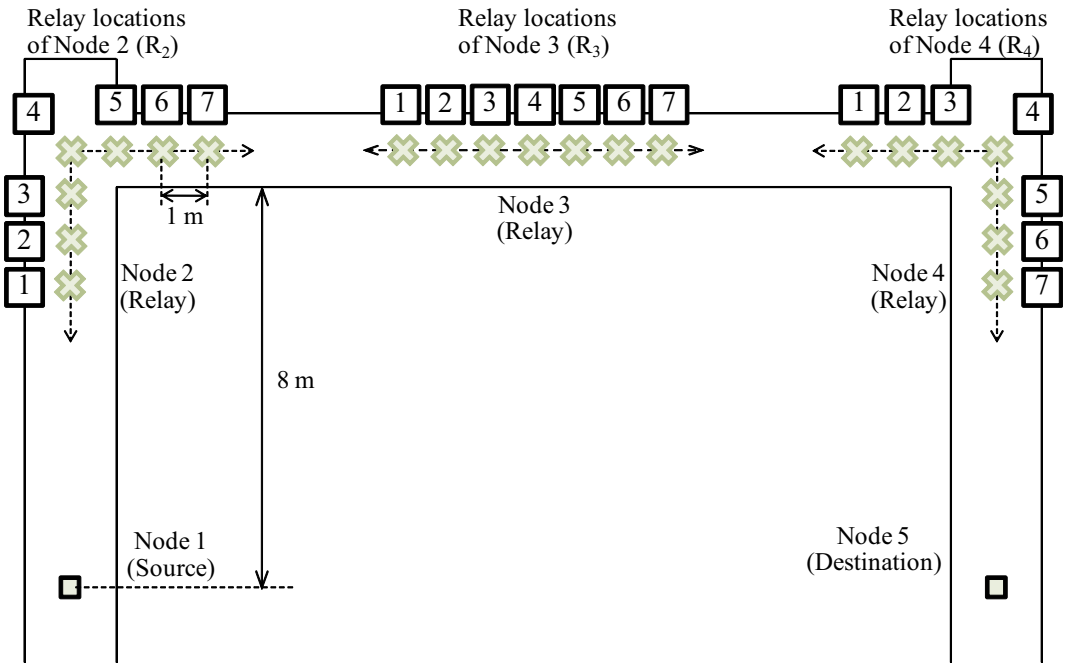

Figure 4.2 A multi-hop network topology in the U-shaped corridor environment.

Table 4.1 Simulation parameters.

Center frequency	5.06 GHz
Antenna height	2.3 m
Reflection times	8 times
Diffraction times	2 times
Penetration times	4 times

4.3 Propagation models

In this chapter, we investigate the performance as well as the optimal node placement of M2WMN based on two propagation models, i.e. 3D ray-tracing propagation model and Rayleigh fading model. 3D ray-tracing model resembles the wireless channels in real environments by geometrically reconstructing electromagnetic wave propagation paths between a transceiver pair from provided information of building shapes, obstacles, etc. On the other hands, Rayleigh fading model is considered as a reference model as it was used in the previous studies of M2WMN [25], [42].

4.3.1 3D Ray-tracing propagation model

For this model, 3D ray-tracing simulator called *Wireless Insite* [60] is used to generate the propagation channels between nodes of the multi-hop network in the target environment. Detailed information of the environment presented in the previous subsection are input into the simulator to precisely resemble the 3D U-shaped corridor. Once the propagation environment setup is completed, ray-tracing can be started. Ray-tracing simulation parameters are summarized in Table 4.1.

The simulator provides several options of propagation models, but we selected the Full 3D model which provides efficient and accurate predictions of propagation and channel characteristics in complex indoor environment. This model combines ray launching algorithm to predict the geometrical propagation paths from the transmitter to the receiver points, and Uniform Theory of Diffraction (UTD) [62]- [63] to identify diffracting edges in the study environment. By this method, 3D ray paths which include the effect of reflections, penetrations, and diffractions can be constructed. The details of ray-tracing algorithm can be referred to the user manual in [64].

By conducting the 3D ray-tracing simulation, we can obtain the information of amplitude, phase shift, Angle of Departure/Arrival (AoD/AoA) of each ray path in order to construct MIMO channels. Before describing how to construct MIMO channels, we first consider a pair of Tx-Rx with one Tx antenna and one Rx antenna (SISO) which contains V ray paths. Each path departs from the Tx antenna with an elevation angle θ_{T_v} and an azimuth angle ϕ_{T_v}, and arrives at the Rx antenna with an elevation angle θ_{R_v} and an azimuth angle ϕ_{R_v}, where $v = 1, 2, ..., V$. Each path has a distinct amplitude χ_v and phase shift φ_v. The parameters $\theta_{\mathrm{T}_v}, \phi_{\mathrm{T}_v}, \theta_{\mathrm{R}_v}, \phi_{\mathrm{R}_v}, \chi_v$ and φ_v of each ray path are generated from the 3D ray-tracing simulator. In this paper, we consider a narrowband fading system, where delay spread is very small relative to the inverse signal bandwidth, so that the channel can be characterized as the superposition of K multipath components as

$$h = \sum_{v=1}^{V} \left(\chi_v e^{-j\varphi_v} \right). \tag{4.1}$$

Next, MIMO components can be generated from the knowledge of AoA/AoD. In this paper, we consider a system of M transmit antennas and M receive antennas ($M \times M$ MIMO) in Uniform Linear Array (ULA) antenna configuration with half wavelength antenna spacing. Generally, MIMO channel can be represented as

$$\mathbf{H} = \sum_{v=1}^{V} \left(\chi_v e^{-j\varphi_v} \mathbf{a}_{\mathrm{R}}(\theta_{\mathrm{R}_v}, \phi_{\mathrm{R}_v}) \mathbf{a}_{\mathrm{T}}(\theta_{\mathrm{T}_v}, \phi_{\mathrm{T}_v})^T \right),$$

where $\mathbf{a}_{\mathrm{R}}(\theta_{\mathrm{R}_v}, \phi_{\mathrm{R}_v}) \in \mathcal{C}^M$ and $\mathbf{a}_{\mathrm{T}}(\theta_{\mathrm{T}_v}, \phi_{\mathrm{T}_v}) \in \mathcal{C}^M$ are the receive and transmit array response vectors for a plane wave, $[.]^T$ denotes transpose of a vector. The elements in these two array vectors can be estimated from the knowledge of $\theta_{\mathrm{T}_v}, \phi_{\mathrm{T}_v}, \theta_{\mathrm{R}_v}$, and ϕ_{R_v} by applying the principle of array signal processing [65].

4.3.2 Rayleigh fading model (Reference model)

MIMO channel is generally represented as $\mathbf{H} = \sqrt{\xi}\mathbf{H}_{\text{i.i.d.}}$, where $\mathbf{H}_{\text{i.i.d.}}$ denotes i.i.d. Rayleigh fading MIMO channel matrix and ξ denotes the channel pathloss. In this reference model, we employ a simple exponent pathloss model such that $\xi = Ad^{-\alpha}$, where d, α and A respectively denote the node-to-node distance, the pathloss decay exponent, and a pathloss constant

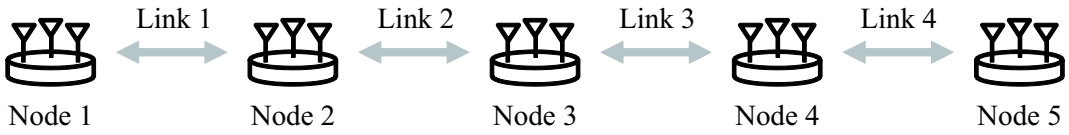

Figure 4.3 Link indices for multi-hop network.

defined by the pathloss at a reference distance of 1 m. This paper employs $\alpha = 3.5$, and $A = -46$ dB.

4.4 Relay communication schemes for MIMO multi-hop networks

This section describes relaying schemes used in the analysis in this chapter. In all schemes, all nodes are assumed to have perfect synchronization with perfect knowledge of the channel state information from the adjacent nodes. For ease of understanding, the links between all pairs of adjacent nodes are indexed as l. The details of link indices are described in Fig. 4.3. Since the network consists of 5 nodes, the number of frequency-sharing link between adjacent nodes becomes $L = N - 1 = 4$.

4.4.1 Conventional MIMO multi-hop schemes

In this chapter, we consider two conventional MIMO communication schemes for multi-hop networks, i.e. MIMO direct transmission from source to destination, and one-way MIMO multi-hop with dual frequency channels.

4.4.1.1 Direct Transmission

The direct transmission is the simplest communication scheme in which source node directly transmits signal to destination node without using relay nodes. Owing to the benefit of MIMO, M multiple streams can be simultaneously transfered from Tx to Rx. Referring to Shannon capacity formula in Eq. (2.8), the channel capacity of the MIMO direct transmission can be determined by

$$C_{\mathrm{E2E}} = \log_2 \det[\mathbf{I}_M + \frac{p_1}{M\sigma^2}\mathbf{H}_{51}\mathbf{H}_{51}^H], \tag{4.2}$$

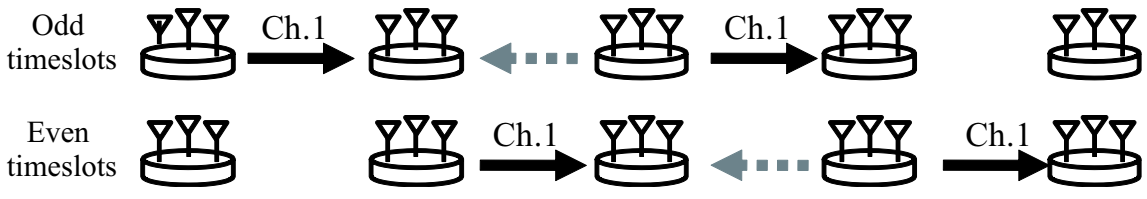

(a) Conventional one-way MIMO multi-hop network with single channel.

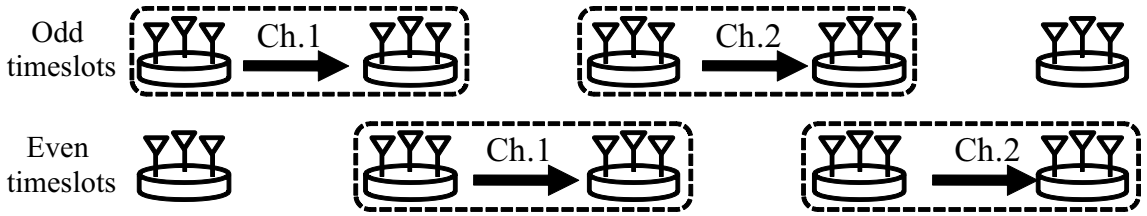

(b) Conventional one-way MIMO multi-hop network with double channels.

Figure 4.4 Conventional one-way MIMO multi-hop networks.

where p_1 is the transmit power of node 1, $\mathbf{H}_{51} \in \mathcal{C}^{M \times M}$ is the channel matrix of transmission link from node 1 to 5, and $\mathbf{I}_M$ is a $M \times M$ identity matrix. It is noted that the noise power is assumed to be equal to -90 dBm at all nodes.

4.4.1.2 One-way MIMO multi-hop with dual frequency channels

In Section 2.5.1, we learnt that the main problem occurring in conventional one-way multi-hop networks is co-channel interference. We again consider the conventional one-way MIMO multi-hop in Fig. 4.4. Figures 4.4a and 4.4b show the conventional MIMO multi-hop network with single and dual frequency channels respectively. The network contains 5 transceiver nodes ($N = 5$), which can switch their roles as a Tx and Rx. As shown in Fig. 4.4, the network spends two timeslots for data transfer by using relay in the multi-hop network.

As mentioned, signal from adjacent node severely interferes the nearby receiver, so that different frequency channels are assigned among adjacent links to avoid the interference. However, the network capacity is reduced by half indeed. It is also assumed that all nodes are capable to switch frequency channels to avoid interference.

From the end-to-end capacity described in Eq. (2.40), we reconsider it as follows. The channel capacity of link l in the one-way MIMO multi-hop network can be determined as

$$C_l = \log_2 \det[\mathbf{I}_M + \frac{p_l}{M\sigma^2}\mathbf{H}_l\mathbf{H}_l^H], \tag{4.3}$$

where p_l is the transmit power of link l, $\mathbf{H}_l \in \mathcal{C}^{M \times M}$ is the channel matrix of link l in the

considering direction, and the noise power η is assumed to be the same in all nodes. Therefore, the end-to-end capacity of the one-way MIMO multi-hop network with dual frequency channels can be determined by the bottleneck link as follow.

$$C_{\mathrm{E2E}} = \frac{1}{4} \min_{l \in \{1,2,3,4\}} C_l \text{ [bits/s/Hz]}. \tag{4.4}$$

Since the network spends two phases in order to carry the message from source to destination, the capacity is scaled by a factor of $\frac{1}{2}$. Furthermore, the network uses two frequency channels in this case, so that the capacity is again divided by two. Therefore, the end-to-end capacity is divided by four as expressed in Eq. (4.4).

In our analysis, we consider the relay nodes in various locations as introduced earlier. Using the calculation method in Eq. (4.4), the end-to-end capacity when node 2, 3 and 4 are respectively placed at location R_2, R_3 and R_4 can be described as $C_{\mathrm{E2E}}(R_2, R_3, R_4)$. Therefore, the optimum relay locations (R_2^*, R_3^*, R_4^*) and the network capacity corresponding to these locations can be respectively determined as follows,

$$(R_2^*, R_3^*, R_4^*) = \arg\max_{R_2,R_3,R_4} \left(C_{\mathrm{E2E}}(R_2, R_3, R_4)\right) \tag{4.5}$$

$$C_{\mathrm{E2E}}^* = \max_{R_2,R_3,R_4} \left(C_{\mathrm{E2E}}(R_2, R_3, R_4)\right). \tag{4.6}$$

4.4.2 MIMO Two-Way Multi-Hop Network (M2WMN) scheme

As mentioned in Chapter 2, M2WMN allows the networks simultaneously relay signal in two directions owing to the advantages of spatial multiplexing and interference cancellation of MIMO. The network model and fundamental concept of M2WMN is described in Section 2.5.2.

4.4.2.1 End-to-end capacity of the network at specific node locations and Optimum relay node locations

The network topology considered in this chapter is intrinsically non-symmetric as the weights are determined in a node-by-node consecutive manner, as shown in Fig. 2.13. In order to avoid a non-general algorithm-dependent optimal node placement due to the non-symmetricity of the M2WMN algorithm, we employs the following evaluation method for deciding optimal node placement.

Firstly, when relay nodes are placed in locations (R_2, R_3, R_4), the end-to-end capacity of the network with the Tx/Rx weight calculation starting from the source node (node 1) and

ending at the destination node (node 5), $C_{\mathrm{E2E}}^{1\to5}(R_2, R_3, R_4)$, can be determined by Eq. (2.48). Also, the end-to-end capacity with Tx/Rx weight calculation in the opposite direction (from node 5 to node 1), $C_{\mathrm{E2E}}^{5\to1}(R_2, R_3, R_4)$, can be similarly determined. Therefore, the end-to-end capacity of the network at locations (R_2, R_3, R_4) is calculated by

$$\bar{C}_{\mathrm{E2E}}(R_2, R_3, R_4) = \frac{1}{2}\left(C_{\mathrm{E2E}}^{1\to5}(R_2, R_3, R_4) + C_{\mathrm{E2E}}^{5\to1}(R_2, R_3, R_4)\right). \tag{4.7}$$

Finally, the optimum relay locations and the network capacity corresponding to these locations can be determined by

$$(R_2^*, R_3^*, R_4^*) = \underset{R_2,R_3,R_4}{\arg\max}\left(\bar{C}_{\mathrm{E2E}}(R_2, R_3, R_4)\right) \tag{4.8}$$

$$C_{\mathrm{E2E}}^* = \max_{R_2,R_3,R_4}\left(\bar{C}_{\mathrm{E2E}}(R_2, R_3, R_4)\right). \tag{4.9}$$

4.4.2.2 Power control in M2WMN

As described in Section 2.5.3, even though M2WMN can eliminate the effect of interference from adjacent nodes, the over-reach interference still limits the end-to-end capacity. Therefore, power control algorithm is applied to optimize the transmission power of each link in order to maximize SINR at the bottleneck link. The details of this algorithm can be referred to Section 2.5.3.

4.5 Numerical analysis

4.5.1 End-to-end capacity of the network based on 3D ray-tracing model

First of all, using the channels generated by 3D Ray-tracing simulator, we evaluate the relay capacity performance of the four relaying schemes, i.e. MIMO direct transmission, one-way MIMO multi-hop with dual channels, M2WMN without power control and M2WMN with power control as illustrated in Fig. 4.5. For a fair comparison, we consider the same number of antennas at all nodes $M = 3$ for all schemes in the analysis.

Figure 4.6 shows the comparison of end-to-end capacity at the optimum relay locations (R_2^*, R_3^*, R_4^*) with different transmit power constraint $p_{\max}$. As shown in the figure, M2WMN with power control outperforms the other schemes. In addition, at low Tx power region, the direct transmission which suffers from shadowing has inferior performance to the rest relaying

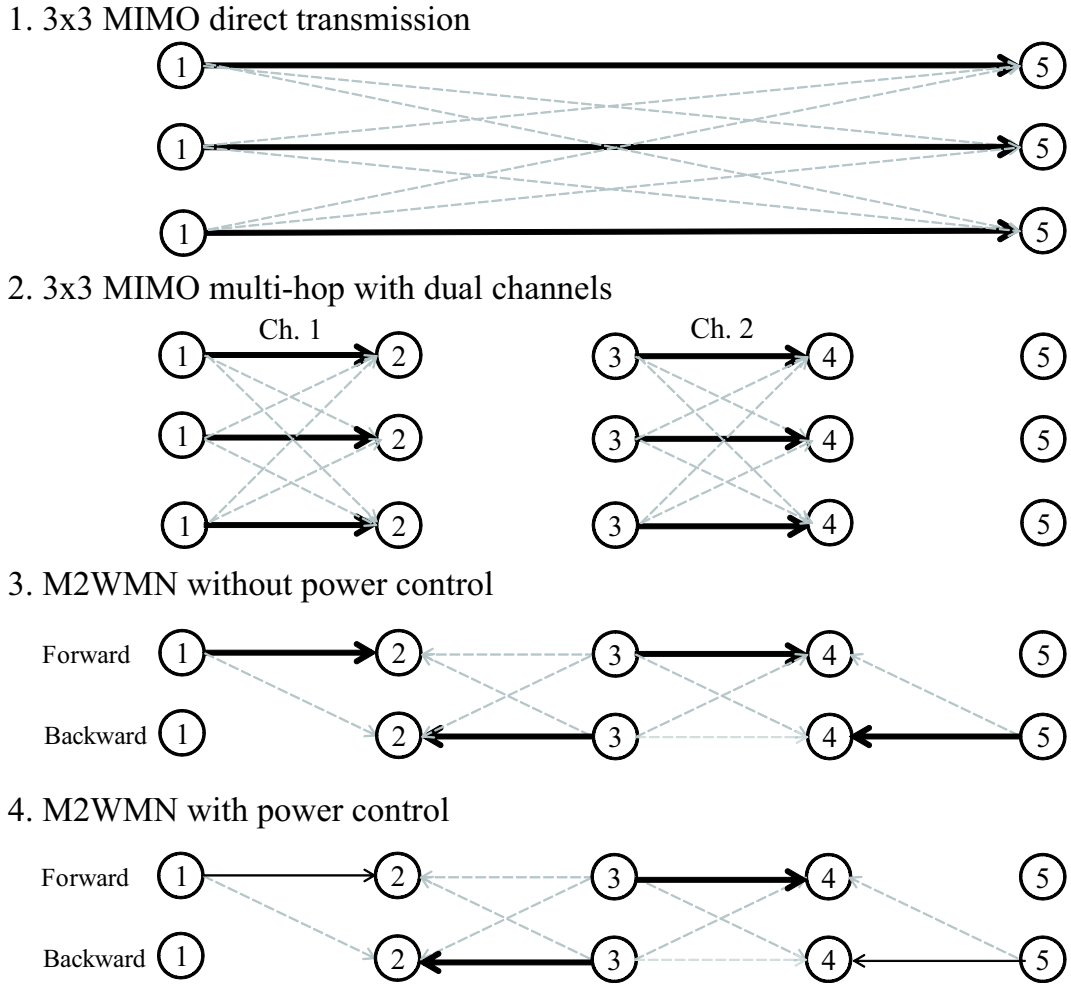

Figure 4.5 Relaying schemes of the analysis.

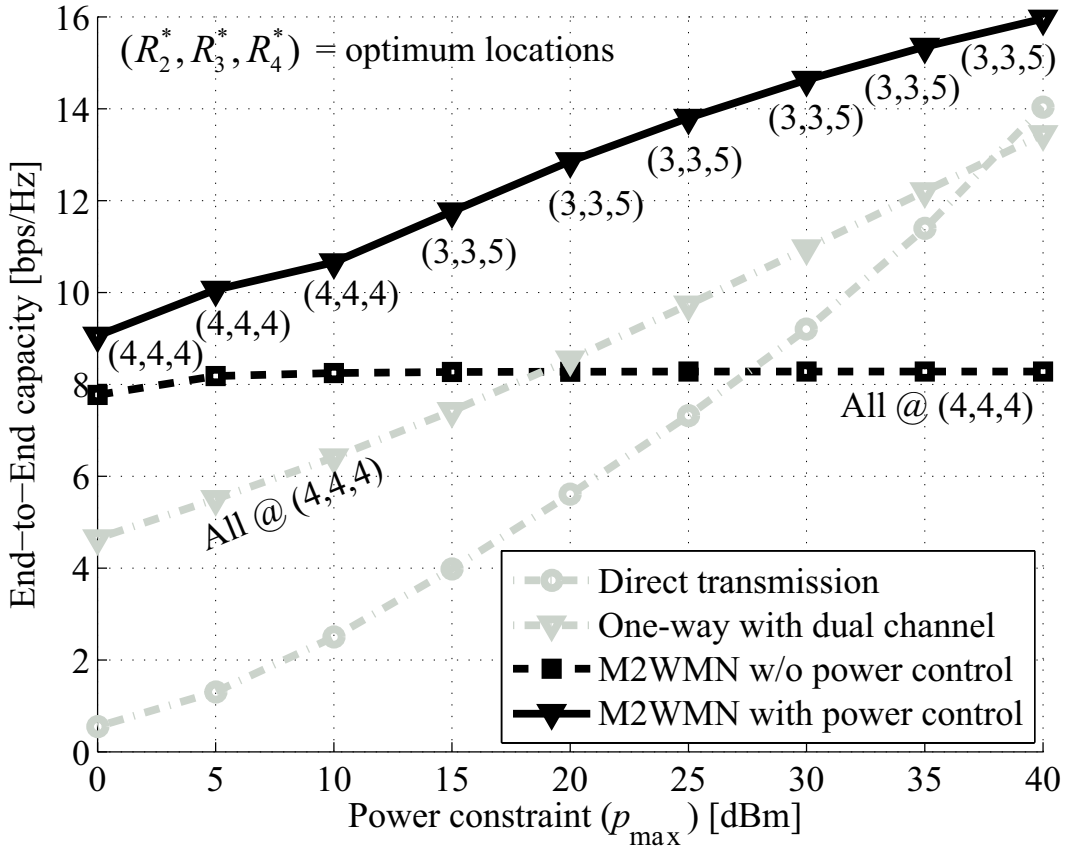

Figure 4.6 The network capacity based on 3D ray-tracing model.

schemes due to degraded SNR. The conventional one-way MIMO multi-hop can solve the problem of shadowing; however, it requires a double bandwidth to avoid frequency-sharing interference and twice the timeslots for realizing bi-directional communication as compared to M2WMN. Therefore, it has lower relay capacity as compared to the M2WMN in both cases with and without power control.

On the contrary, at the high Tx power region, the capacity of the direct transmission tends to approach that of M2WMN. For the direct transmission, since signal attenuation due to shadowing can be overcome. Furthermore, this scheme does not require so many timeslots and frequency resource for relaying so that the capacity improvement is significant in the high Tx power region. Moreover, owing to dual frequency channels in conventional one-way multi-hop scheme, interference is completely avoided so that the capacity tends to be higher than that of M2WMN in the case that power control is not applied. From this point, we can conclude that the network capacity of conventional schemes tends to be higher when the allowable Tx power increases.

4.5.2 Optimum relay placements of multi-hop network based on 3D ray-tracing model

From the results shown in Fig. 4.6, we found that the optimal relay locations are always at the corner of the corridor ($(R_2^*, R_3^*, R_4^*) = (4, 4, 4)$) in the conventional MIMO multi-hop with dual frequency channels and the M2WMN without power control. For the M2WMN with power control, the optimum locations are still at $(4, 4, 4)$ in the low Tx power region. However, the situation changes when the allowable Tx power increases. The optimal locations turn to be $(3, 3, 5)$ or $(3, 5, 5)$. It should be noted that since we consider a symmetric network topology in capacity calculation, the two locations $(3, 3, 5)$ and $(3, 5, 5)$ are equivalent.

From this result, we learn that, in the relay network without power control, the most suitable relay placement is normally where all relay links are in LOS of each other such that they can properly relay signal from their adjacent nodes without suffering from the effect of shadowing [59]. However, the situation is changed in the case of power control.

In order to understand the insight of these optimum relay locations, we introduce two parameters, i.e. the desired link power of the bottleneck, g_{r}, and the interference power at the bottleneck, g_{i}, expressed as:

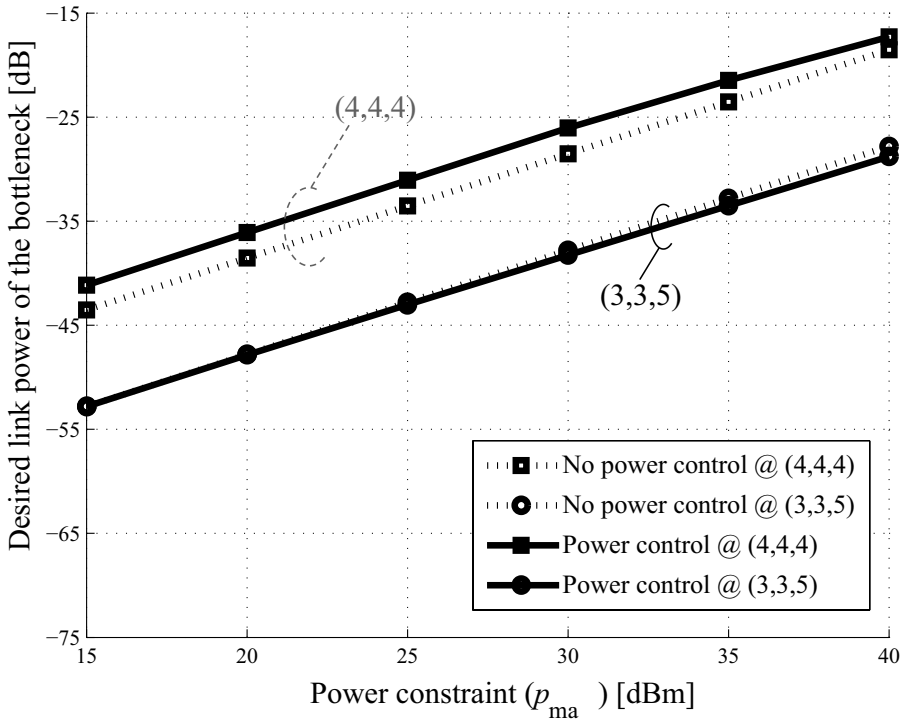

(a) Desired link power of the bottleneck.

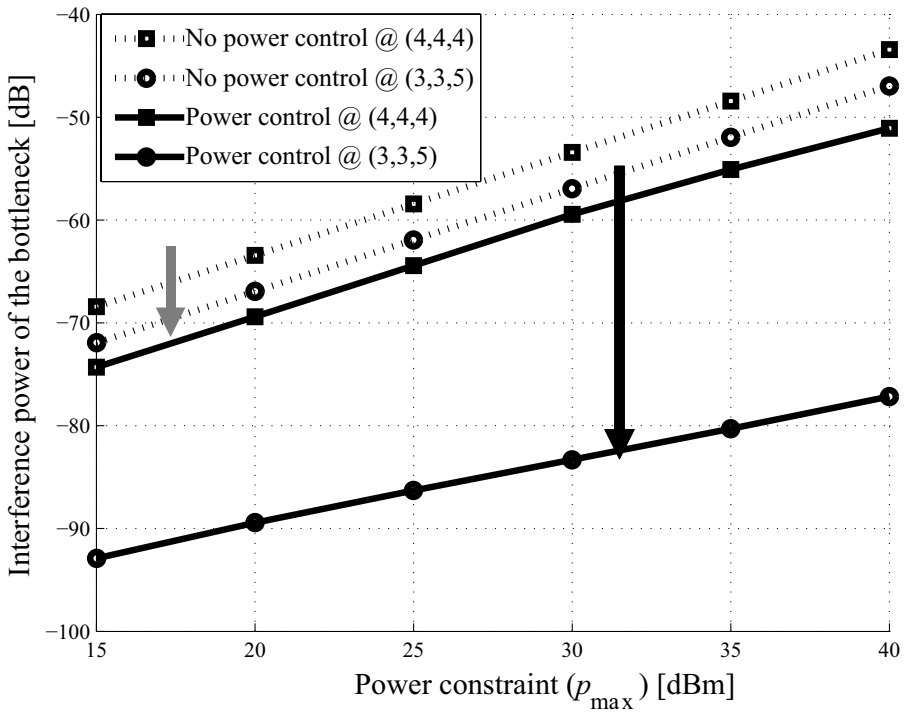

(b) Interference power of the bottleneck.

Figure 4.7 Bottleneck link characteristic at the optimum locations.

$$g_{\mathrm{r}} = \sqrt{\left(p_{\tilde{l}^{\mathrm{F}}} g_{\tilde{l}^{\mathrm{F}}}\right)\left(p_{\tilde{l}^{\mathrm{B}}} g_{\tilde{l}^{\mathrm{B}}}\right)}, \tag{4.10}$$

$$g_{\mathrm{i}} = \sqrt{\left(\sum_{\tilde{l}^{\mathrm{F}} \neq k} p_k g_{\tilde{l}^{\mathrm{F}},k}\right) \cdot \left(\sum_{\tilde{l}^{\mathrm{B}} \neq k} p_k g_{\tilde{l}^{\mathrm{B}},k}\right)}, \tag{4.11}$$

$$\tilde{l}^{\mathrm{F}} = \arg \min_{l \in I_{\mathrm{o}}^{\mathrm{F}} \cup I_{\mathrm{e}}^{\mathrm{F}}} \gamma_l^{\mathrm{F}}, \tag{4.12}$$

$$\tilde{l}^{\mathrm{B}} = \arg \min_{l \in I_{\mathrm{o}}^{\mathrm{B}} \cup I_{\mathrm{e}}^{\mathrm{B}}} \gamma_l^{\mathrm{B}}. \tag{4.13}$$

The following describes the concept of these two introduced parameters. As described in Eq. (2.48), the end-to-end capacity of the network in each stream (Fw or Bw) is determined by the capacity of bottleneck link or the link having the minimum capacity in that direction. We denote the bottleneck link of Fw and Bw streams by $\tilde{l}^{\mathrm{F}}$ and $\tilde{l}^{\mathrm{B}}$, given in Eq. (4.12) and (4.13) respectively. In Eqs. (4.10), the terms $(p_{\tilde{l}^{\mathrm{F}}} g_{\tilde{l}^{\mathrm{F}}})$ and $(p_{\tilde{l}^{\mathrm{B}}} g_{\tilde{l}^{\mathrm{B}}})$ are referred to the numerator of SINR formula in Eq. (2.47) applied for the bottleneck link in Fw and Bw streams respectively. Therefore, the geometric mean of these two values in (4.10), defined as the desired link power of the bottleneck, represents the average signal power that is used to carry the streams in both directions. On the other hand, in Eq. (4.11) the terms $\sum_{\tilde{l}^{\mathrm{F}} \neq k} p_k g_{\tilde{l}^{\mathrm{F}},k}$ and $\sum_{\tilde{l}^{\mathrm{B}} \neq k} p_k g_{\tilde{l}^{\mathrm{B}},k}$ can be referred to the denominator, ignoring the noise power term, of SINR in Eq. (2.47) applied for the bottleneck link in Fw and Bw streams respectively. The geometric mean of these two values in Eq. (4.11), defined as the interference power at the bottleneck, represents the average interference power bothering the desired signal at the bottleneck link which results in deteriorating the network capacity.

Figures 4.7a and 4.7b respectively show the characteristic of the desired link power and the interference power at the bottleneck link with respect to different power constraints when relay node placement is $(4, 4, 4)$ (the optimum placement when power control is not applied) and $(3, 3, 5)$ (the optimum placement when power control is applied). In these figures, we only consider the power constraint greater than 15dBm to differ the two optimal locations in both cases of with and without power control. The results show that power control significantly reduces the bottleneck interference while has small effect on the changes of the desired link power of the bottleneck. It implies that the optimal relay placement in power control case is the place where interference can be efficiently reduced. On the other hand, in the case of no power control, as the problem of overreach interference cannot be alleviated, the relay capacity

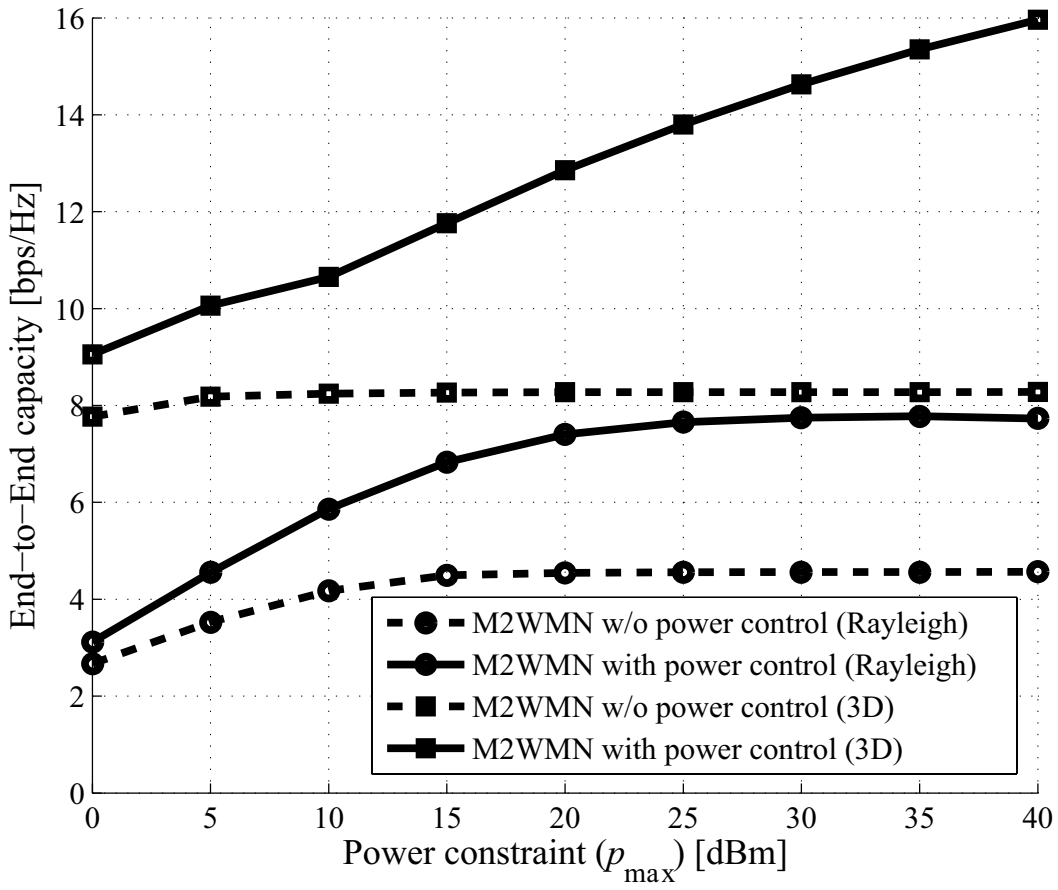

Figure 4.8 The M2WMN capacity based on 3D ray-tracing model and Rayleigh model.

is dominated by the signal strength of the desired link power. Thus, the best placement strategy is to locate relay nodes such that relay links have good channel quality, or in other words, are in LOS of each other.

4.5.3 Comparison of network performance based on 3D Ray-tracing model and Rayleigh model

Figure 4.8 shows the comparison of the network based on 3D ray-tracing model and the reference Rayleigh model. The result shows that the performance of the network performance based on 3D ray-tracing model is always superior to that of the theoretical model. It is because in Rayleigh model, all links are assumed to experience a same pathloss decay exponent so that over-reach interference significantly affects the performance. While in realistic cases e.g.

3D ray-tracing model, strong shadowing helps to suppress over-reach interference drastically. Consequently, in terms of performance evaluation of multi-hop networks, e.g. M2WMN, the assumption that all links experience a same propagation model is not so reasonable, especially for shadowing scenarios.

4.6 Sub-optimal relay location searching method

4.6.1 Methodology

The optimal location (R_2^*, R_3^*, R_4^*) in the previous section is obtained by searching for the sets of locations where M2WMN can achieve the highest network capacity. However, the search requires the comparison of totally $7^3 = 343$ combinations of locations in an exhaustive manner, which is impractical for real applications. In this section, we aim to propose a distributed search algorithm which can relax this complexity.

The proposed distributed search algorithm is described as follows.

1. Initialization:
   - Set the initial locations of node 2, 3 and 4 at the place where all nodes are in almost LOS to adjacent nodes. Therefore, $\left(R_2^{(0)}, R_3^{(0)}, R_4^{(0)}\right) = (4, 4, 4)$. Here, the initial location of node 3 is set as the middle point of the connecting corridor.
   - Assign initial node indices: $a^{(0)} := 2$, $b^{(0)} := 3$ and $c^{(0)} := 4$.
2. Iterate until convergence:
   (a) Fix location of node $a^{(i)}$, and $b^{(i)}$ as the previous iteration:
   $$R_{a^{(i)}}^{(i)} := R_{a^{(i)}}^{(i-1)}, \;\; R_{b^{(i)}}^{(i)} := R_{b^{(i)}}^{(i-1)} \tag{4.14}$$
   (b) Find the optimal location of node $c^{(i)}$ such that the end-to-end capacity is maximized:
   $$R_{c^{(i)}}^{(i)} = \underset{R'_{c^{(i)}} \in \{1,2,\ldots,7\}}{\arg\max} \; \bar{C}_{\mathrm{E2E}}\{R_{a^{(i)}}^{(i)}, \; R_{b^{(i)}}^{(i)}, R'_{c^{(i)}}\} \tag{4.15}$$
   (c) Switch the anchor index $c^{(i)}$ to other relay location consecutively as follows,
   $$c^{(i)} : 4 \rightarrow 3 \rightarrow 2 \rightarrow 3 \rightarrow 4 \rightarrow 3 \rightarrow 2 \rightarrow \ldots \tag{4.16}$$
   $$a^{(i)} \text{ and } b^{(i)} \text{ are assigned to the rest nodes.} \tag{4.17}$$

It is noted that $\{R_a, R_b, R_c\}$ represents the set of location of node a, b and c where variable positions is not placed in the order of node index, but each value is specific to the corresponding node.

In the above algorithm, the search for optimum location is done by searching the location of a relay node which can maximize capacity while the rest two nodes's locations are fixed. Then, in the succeeding iterations, the searching node is respectively changed in the sequence shown in Eq. (4.16). The algorithm is repeated until the end-to-end capacity converges. The proof of capacity increase is described in the appendix of this chapter, Section 4.8.1.

4.6.2 Estimation results and comparison

Figure 4.9 illustrates the result of the network capacity when we use the proposed searching algorithm for the location optimization compared to the exhaustive search method. As shown in the figure, the network capacity in both cases are almost similar and the optimum relay locations have a same tendency. In addition, Fig. 4.10 shows the improvement of network capacity against the searching iterations at the power constraint of 30 dBm. The figure shows that the network capacity converges after only three iterations. It implies that the search for optimal locations can be reduced to only $7 \times 3 = 21$ combinations from 343 combinations of the exhaustive search. Also, using this method, network planners can find the optimum locations by just moving only one node in each iteration rather than comparing the network capacity of all combinations in an exhaustive manner.

In order to confirm the usability of the proposed algorithm, we apply this searching algorithm to M2WMN in another virtual network topology based on Rayleigh fading model as shown in Fig. 4.11. The network consists of 5 nodes aligned in a straight line, where node 1 and 5 are separated with a 80 meter distance and node 2, 3 and 4 are respectively located in between the two end nodes with 5 candidate locations for each node as shown in the figure. We choose this network topology as an example of a network without shadowing effect.

The comparison of the search results using the exhaustive method and the proposed algorithm is shown in Fig. 4.12. The results show that the proposed algorithm can also predict the optimum relay locations by achieving almost the same network capacity performance as compared to the exhaustive search. Figure 4.13 shows the example of the network capacity improvement with respect to searching iteration until convergence at the power constraint of 30 dBm, which confirms the fast convergence performance of the proposed searching algorithm.

It is noted that in both the case of M2WMN in U-shaped corridor and in straight topology,

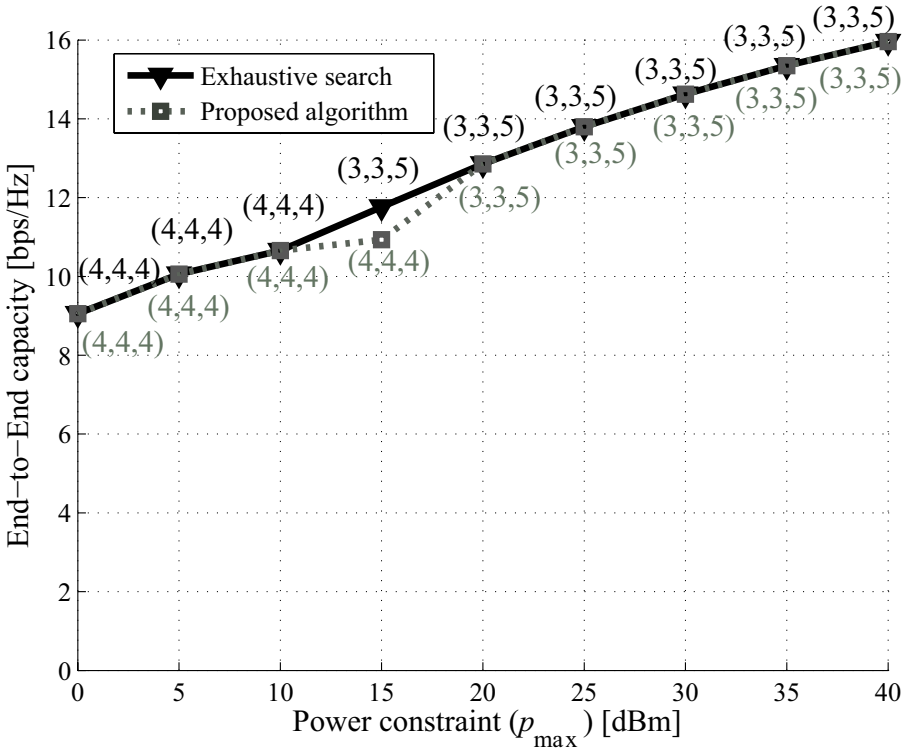

Figure 4.9 The end-to-end capacity and optimal locations obtained by the proposed method.

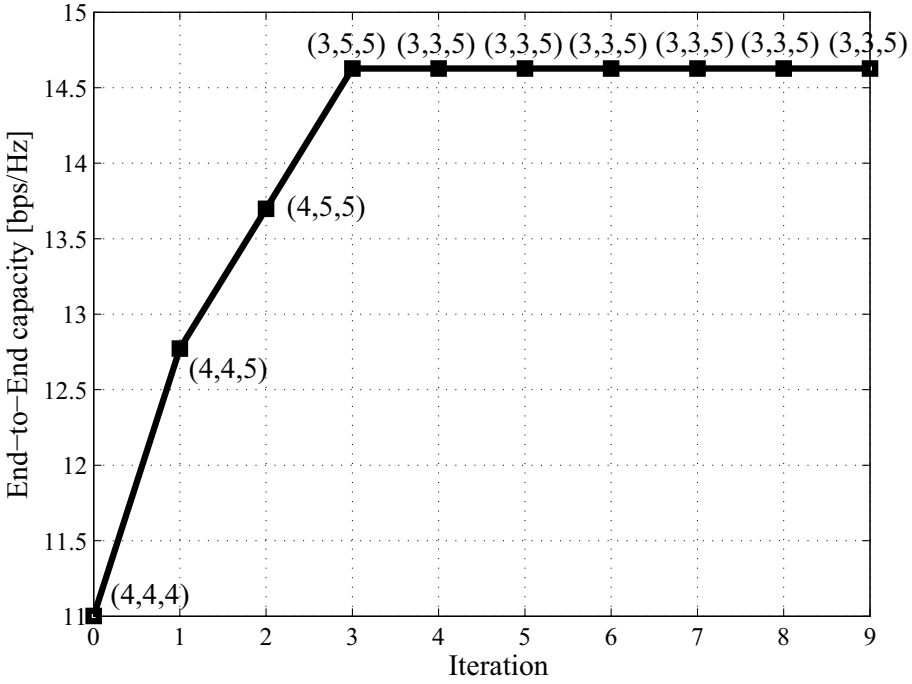

Figure 4.10 The capacity of the network against searching iteration at $p_{\max} = 30$ dBm.

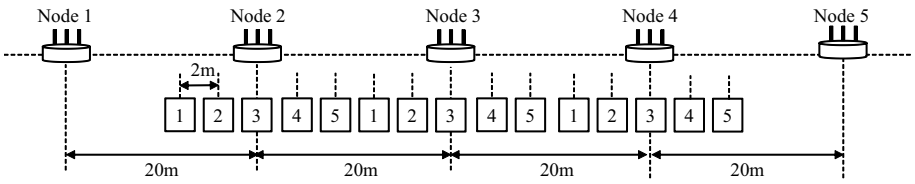

Figure 4.11 M2WMN in a straight topology with Rayleigh fading model.

the proposed algorithm predicts the different locations from the exhaustive search at $p_{\max} = 15$ dBm. It implies that the searching algorithm possibly yields to different locations from the optimum ones when Tx power is in between low and high power region, however, the difference of capacity is not significant.

4.7 Chapter summary

This chapter investigated M2WMN in a practical U-shaped corridor environment dominated by shadowing. The result confirmed that the assumption that all links in the network experience a same propagation model, e.g. Rayleigh fading model, is not proper for evaluating network performance in real scenarios with the existence of shadowing. Moreover, this chapter investigated the open problem of choosing optimum relay locations maximizing the performance of M2WMN in the real scenario. The analysis results showed that without power control, the optimal locations are where adjacent nodes are in Line-of-Sight (LOS) to each other. Interestingly, the optimum locations are not necessarily LOS locations anymore when power control is applied. Finally, we proposed a sub-optimal relay placement searching method which reduces the complexity of the conventional exhaustive search.

4.8 Chapter appendix

4.8.1 The proof of the proposed sub-optimal location search algorithm

The capacity of the network at the optimal location obtained from step b) in the iterative algorithm can be expressed as:

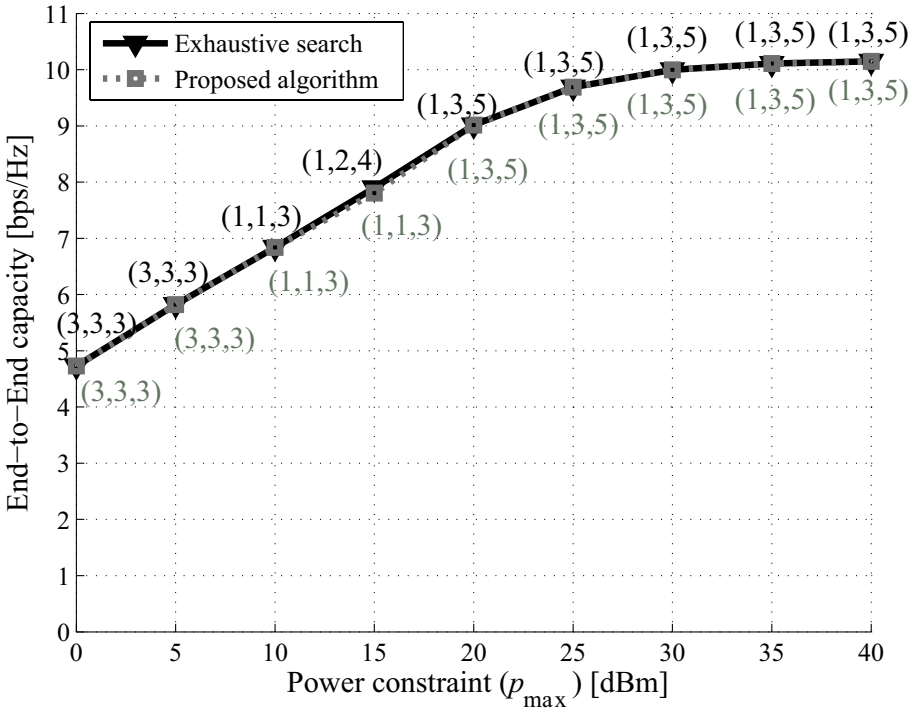

Figure 4.12 The network capacity and its corresponding optimum locations obtained by the proposed method in straight topology.

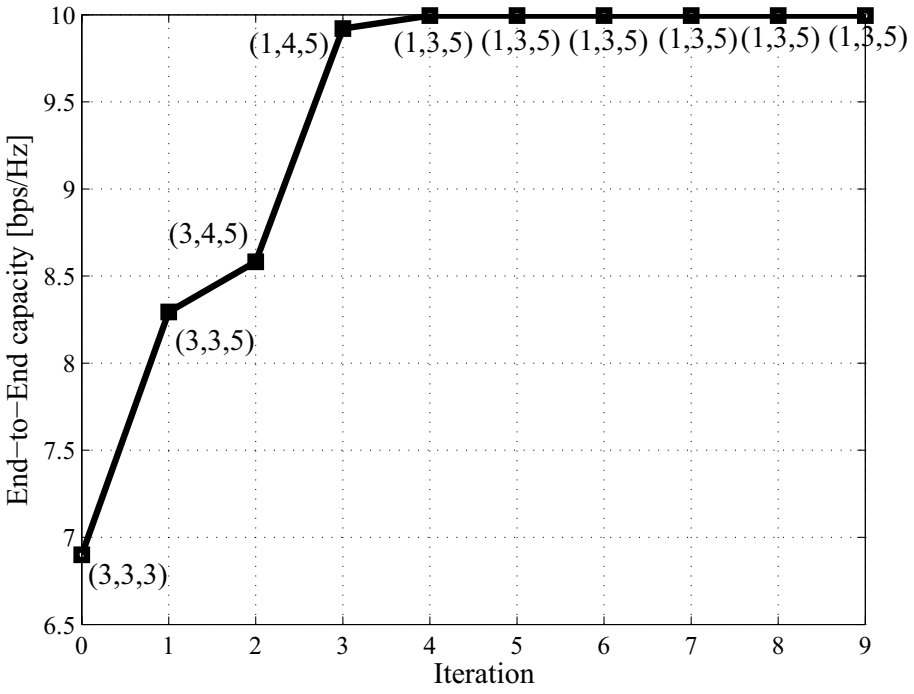

Figure 4.13 The capacity of the network in the straight topology against searching iteration at $p_{\max} = 30$ dBm.

$$
\begin{aligned}
C_{\text{sub}}^{(i)} &= C_{\text{E2E}}\{R_{a^{(i)}}^{(i)},\ R_{b^{(i)}}^{(i)}, R_{c^{(i)}}^{(i)}\} \\
&= \max_{R_{c^{(i)}}^{'} \in \{1,2,...,7\}} C_{\text{E2E}}\{R_{a^{(i)}}^{(i)},\ R_{b^{(i)}}^{(i)}, R_{c^{(i)}}^{'}\}, \qquad (4.18)
\end{aligned}
$$

where $a^{(i)}$ and $b^{(i)}$ are the fixed node indices at iteration i respectively, $c^{(i)}$ denotes the node index of the searching node at iteration m, $R_{a^{(i)}}^{(i)}$ and $R_{b^{(i)}}^{(i)} \in \{1, 2, ..., 7\}$ are the fixed locations of node a and b at iteration i respectively, $R_{c^{(i)}}^{(i)}$ is the estimated location of node c at iteration i, $R_{c^{(i)}}^{'}$ denotes a variable of location of node c at iteration i and $C_{\text{E2E}}\{R_{a^{(i)}}^{(i)},\ R_{b^{(i)}}^{(i)}, R_{c^{(i)}}^{'}\}$ denotes the end-to-end capacity at the location $\{R_{a^{(i)}}^{(i)},\ R_{b^{(i)}}^{(i)}, R_{c^{(i)}}^{'}\}$.

The following expression shows the proof:

$$
\begin{aligned}
C_{\text{sub}}^{(i)} &= \max_{R_{c^{(i)}}^{'} \in \{1,2,...,7\}} C_{\text{E2E}}\{R_{a^{(i)}}^{(i-1)},\ R_{b^{(i)}}^{(i-1)}, R_{c^{(i)}}^{'}\} && (4.19) \\
&\geq C_{\text{E2E}}\{R_{a^{(i)}}^{(i-1)},\ R_{b^{(i)}}^{(i-1)}, R_{c^{(i)}}^{(i-1)}\} && (4.20) \\
&= C_{\text{E2E}}\{R_{a^{(i-1)}}^{(i-1)},\ R_{b^{(i-1)}}^{(i-1)}, R_{c^{(i-1)}}^{(i-1)}\} && (4.21) \\
&= C_{\text{sub}}^{(i-1)} && (4.22)
\end{aligned}
$$

The equality in (4.19) is based on the fact that the locations of the fixed nodes are the same as that obtained from the previous iteration, $R_{a^{(i)}}^{(i-1)} = R_{a^{(i)}}^{(i)}$ and $R_{b^{(i)}}^{(i-1)} = R_{b^{(i)}}^{(i)}$. From (4.20), we know that the value of capacity that we obtain in (4.19) at iteration i should be larger or equal to that obtained from the location in the previous iteration, $i-1$. Since the node indices a, b, and c in the expression $\{.,.,.\}$ is not placed in order, when anchor indices change in step c) of the iterative algorithm, the expression in (4.20) can be rewritten in (4.21) which also denotes the capacity in the previous iteration $i-1$ as expressed in (4.22).

From this algorithm, we know that when we run the iterative algorithm, the capacity will increase until convergence to a certain supremum (not necessarily the global one, or the optimum one) after several iterations.

Chapter 5

Deployment methodology of multi-hop relay networks for sensor networks in practical environments

5.1 Motivation

In the two previous chapters, we have discussed about MIMO relay networks for several configurations in specific practical environments. In this chapter, we extend our consideration to the relay networks, which are applied for WSNs in more general environments.

As mentioned, several studies [17]- [20], as well as IEEE 802.15.4 standard [21] suggest cluster-tree topology for the efficient communications in WSNs. In a practical deployment, however, network designers still confront with the problem of how to determine the appropriate locations to place relays. Several studies show that the good strategy of relay deployment helps the network improve the system performance [31]- [34], [66]- [67]. In [31]- [32], [66], the studies propose the algorithm to determine the optimum placement of relays by considering WSNs with channel model, where the signal varies by the distance between transceiver nodes. However, these methods are inapplicable to the realistic environments, where signals in WSNs also affected by shadow fading. Also, network topology in these studies are in 2-dimensional geometry. In [33]- [34], [67], the optimization problems to determine relay placements are NP-hard problems, some of which can be solved by simplified methods to find sub-optimal results and based on graph theory. However, they are also impractical since we cannot have all information in graphs to create the optimization problems.

In previous two chapters, we have studied about the good condition of the optimum relay placement to maximize the network performance. Therefore, this chapter aims to apply the analogy learnt in previous chapters to propose a novel methodology of relay deployment, which can be simply performed by using a simple measurement tool and determination of three dimentional geometric structure of the environment of interest. By the proposed method, we can determine the minimum number of relay nodes to cover all sensor nodes in which locations of sensor and sink nodes are pre-assigned and packet loss rate can be minimized. Moreover, we learnt from the previous chapters that MIMO technique can increase the network capacity with diversity or multiplexing gain, so that we aim to employ multiple antenna to the sink and relay nodes which are assumed to have more capability than sensor nodes equipped with single antenna due to the limitation of battery. Applying multiple antenna at the relay nodes also enables the network to perform two-way relaying introduced in Section 2.4.2.1 and increases the network performance from the conventional relaying schemes. Therefore, the application of multiple antenna technique is also one of the methods to optimize the network performance in this chapter.

5.2 Target environment

We consider a factory model [68] illustrated in Fig. 5.1 as our target environment. The factory consists of 4 main areas, i.e. two warehouse areas, a convey area and a production area, as shown in Fig. 5.2. Due to the large size of the factory, one sink node connected to the central server via the backhaul network is installed in each area. We assume that sensor nodes deployed in each area are assigned to transfer sensing data to the sink in that area and different frequency channels are assigned to each area to avoid the interference between nodes in different areas. Here, we can treat a group of sensor nodes coordinating with the sink in each area as one distinct network.

For the ease of our explanation and analysis, we consider only the network in the warehouse area 1 illustrated in Fig. 5.3. In this area, sensor nodes are randomly deployed along the shelves with different height and each shelf is filled with several objects with different kinds of materials. In addition, the sink node is deployed at the middle of this area with the ceiling height. It is certain that some sensors are hidden from the sink by objects in the environment resulting in the degradation of receive signal, so that they need relays to help them transfer data to/from the sink. Therefore, in our scenario, we aim to propose a methodology to deploy

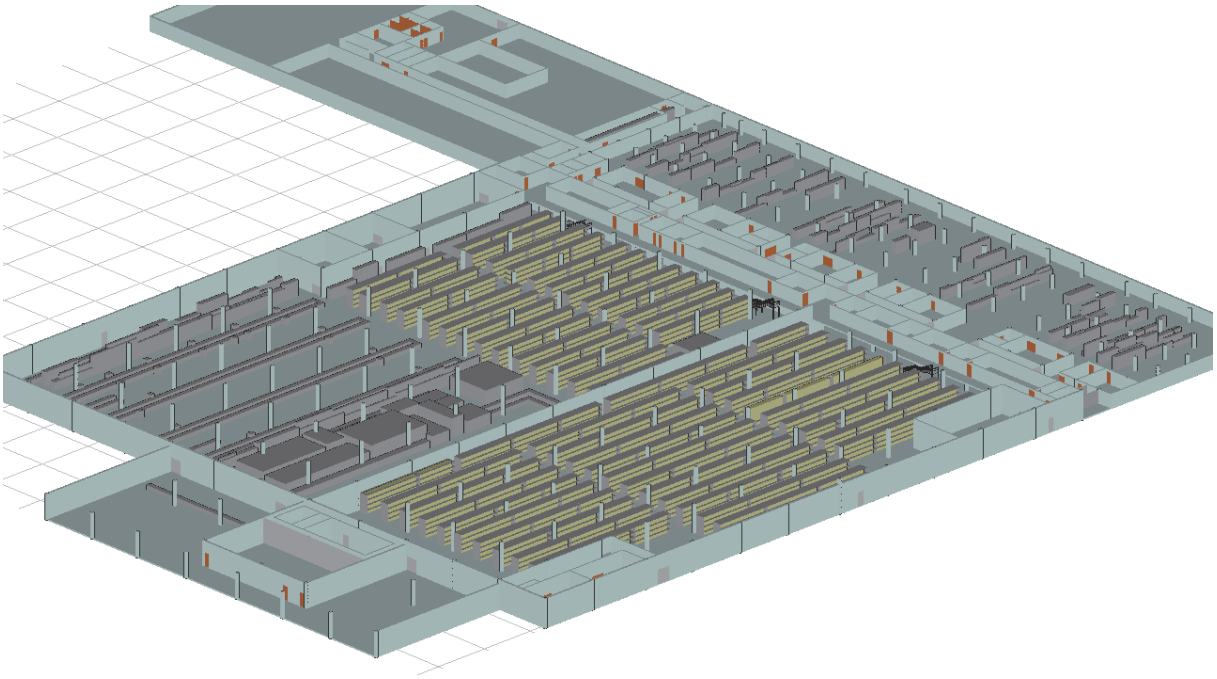

Figure 5.1 Target factory environment.

multi-hop relay network to cover all sensor nodes whose location are pre-assigned.

5.3 Channel model

Similar to the previous section, 3D ray-tracing simulator called Wireless Insite [60] is used to generate propagation channel of between transceiver nodes in the target environment since we cannot perform the real measurement in the field. With this simulator, the information of the target environment described in the previous section can be constructed in three dimensions and the position of sensor nodes, sink and relay can be defined. For suitability of the factory environment and application in this chapter, the simulation parameter used in this chapter is described in Table 5.1. It is noted that we assume that the WSN in this work operates in 2.4 GHz band which is specified by IEEE 802.15.4 standard.

By the simulation, the information of ray paths for each Tx-Rx pair with single antenna can be obtained. Since we aim to employ multiple antennas in some transceiver nodes for reason of performance optimization, which would be explained later, MIMO channel is reconstructed by using the knowledge of AoD/AoA, amplitude, and phase shift of each ray path as described

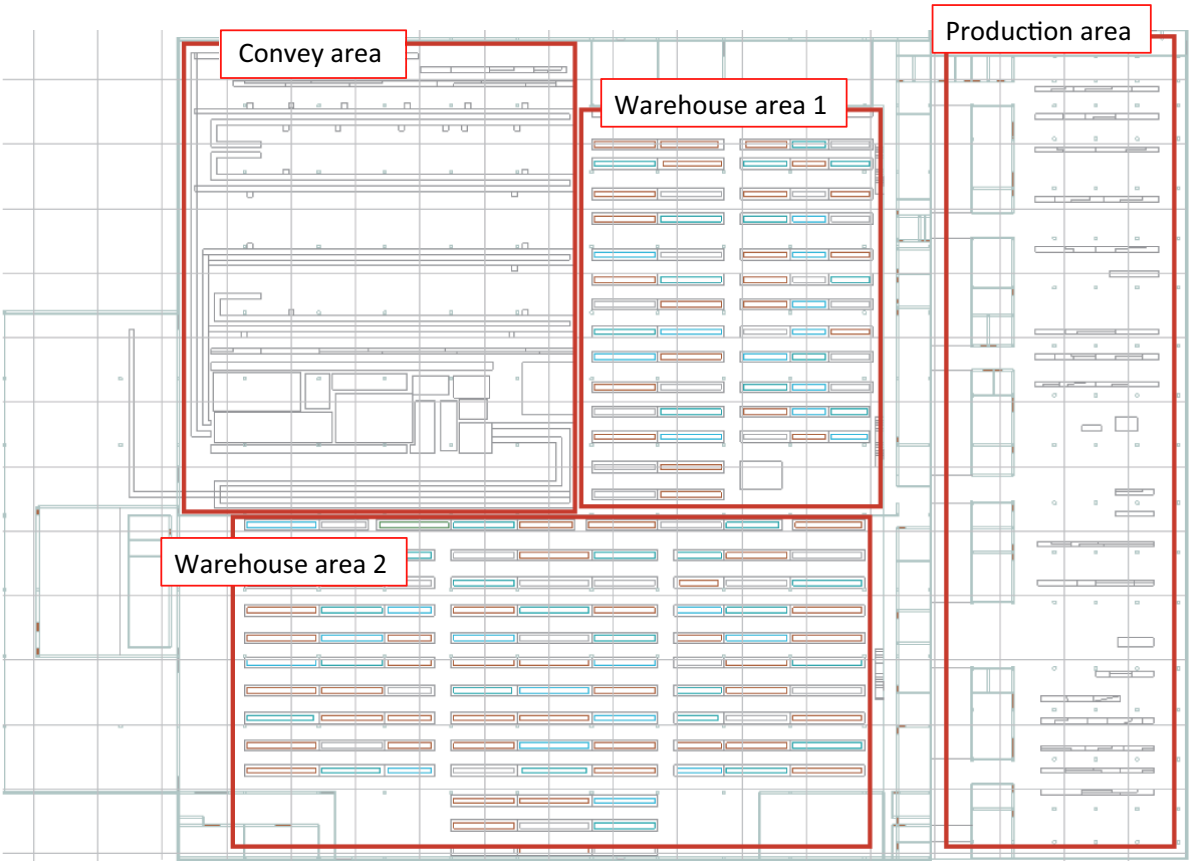

Figure 5.2 Factory layout.

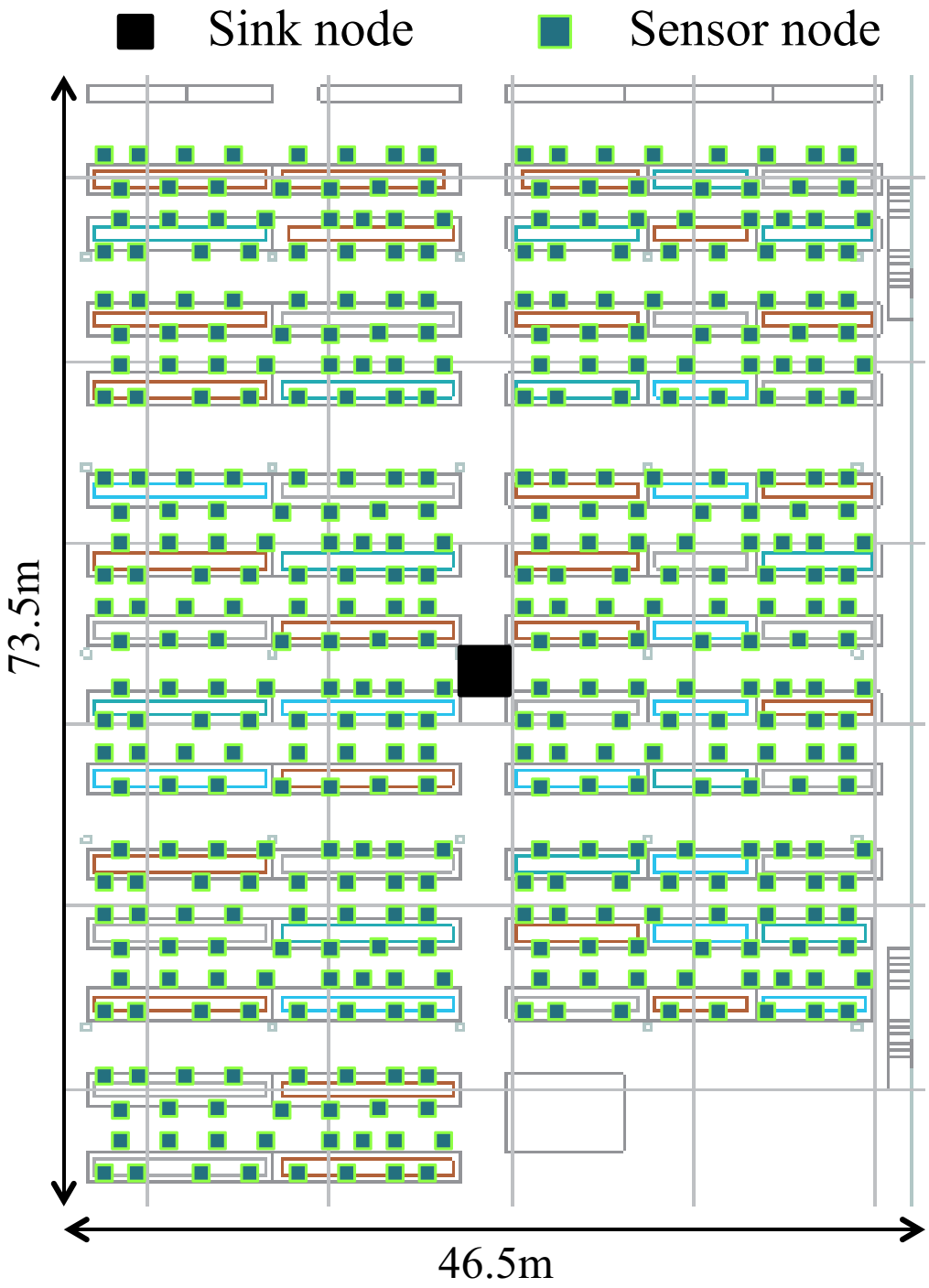

Figure 5.3 Layout of the warehouse area 1.

Table 5.1 Simulation parameters.

Center frequency	2.4 GHz
Reflection times	6 times
Diffraction times	1 times
Penetration times	4 times

in Section 4.3.1. Here, the antenna configuration is designed as antenna with one-wavelength spacing linear array antenna.

5.4 System model

Since we aim to optimize the relay node placement and performance of WSNs from the baseline of IEEE 802.15.4 standard, we firstly clarify the network model we consider in this chapter based on the specification of the standard. In this chapter, we consider the sensor in cluster-tree topology as illustrated in Fig. 5.4, and the network operates in beacon-enable mode where all devices in the network are synchronized. The first coordinator node, which we called so far as sink node, acts as the parent of all devices in the network which has greater computational resources than any other device in the PAN. The sink forms the first cluster with its children sensor nodes and provides them synchronization services.

For the sensor nodes that cannot directly connect to the sink, the additional PAN coordinators, which we call them as relay nodes, are employed to connect them to the central sink. These PAN coordinators also provide synchronizations to their children in their incivilities and receive synchronization frame, called beacon, from the parent PAN coordinators. Anyway, how each sensor chooses its PAN coordinator is not defined by the standard so that this is one part of the network optimization.

In our considering factory environment, the sensor network consists of N sensor nodes, M relay nodes and one sink node. Let s_n denote the index of sensor node n, $n \in \{1, \ldots, N\}$, $r_m(l_m)$ denote the index of relay node m, $m \in \{1, \ldots, M\}$, at candidate location $l_m \in \{1, 2, \ldots, L_m\}$, where L_m is the number of candidate locations of relay r_m and r_0 denote the index of the sink node. In this chapter, candidate locations are defined as all possible locations to place relay which is described in more details in the next section. $h_{\mathrm{Rx,Tx}} \in \mathcal{C}$ denotes complex response of transmission from node Tx to node Rx in the case of single

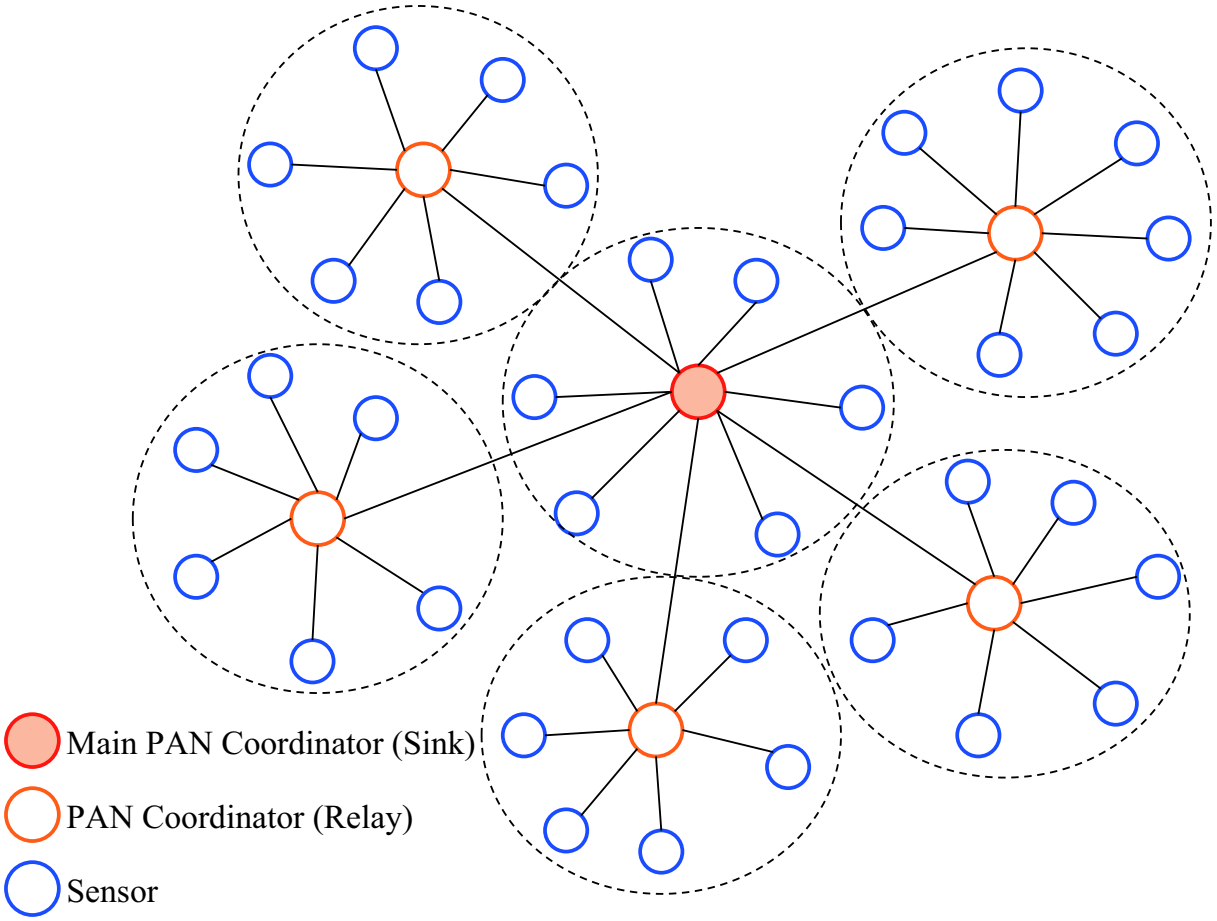

Figure 5.4 Cluster-tree topology of WSNs.

antenna configuration, $\mathbf{h}_{\mathrm{Rx,Tx}} \in \mathcal{C}^{M_\mathrm{r}\times 1}$ or $\mathbf{h}_{\mathrm{Rx,Tx}} \in \mathcal{C}^{1\times M_\mathrm{t}}$ denotes the channel vector of SIMO or MISO transmission from node Tx to node Rx in the case of multiple antenna configuration at only Tx or Rx side respectively, and $\mathbf{H}_{\mathrm{Rx,Tx}} \in \mathcal{C}^{M_\mathrm{r}\times M_\mathrm{t}}$ denotes the channel vector of MIMO transmission from node Tx to node Rx in the case of multiple antenna configuration at both Tx and Rx side, where M_t and M_r denote the number of transmit and receive antenna respectively. P_{Tx} denotes the transmit power of node Tx. Since devices in WSN have low power consumption and should not be so complicated, we assume that CSI is known only at Rx side for all transceiver nodes.

5.5 Relay node placement optimization

In this section, we introduce the novel methodology to determine the optimum relay node placement of multi-hop relay networks for sensor networks in practical environments. In order to make a comparison with the optimized network, we define a reference case where the relay locations are not optimized.

5.5.1 Proposed network planning methodology

Our proposed methodology consists of three main steps, i.e. sink coverage check, initial relay location assignment and network optimization. In the first step, we observe the coverage from the sink node to determine how much sensor nodes in the network cannot connect to the sink. In the second step, the number of relays and all candidate locations for each relay are assigned. In the final step, we aim to optimize the network performance by determining the appropriate communication scheme and also optimum relay locations.

5.5.1.1 Sink coverage check

The coverage from the sink is determined by Packet Error Rate (PER) of receive signal where sensor nodes which has PER less than 1 % are defined as connected node, and the rest are defined as non-connected nodes. Here, PER can be determined by Signal to Noise Ratio (SNR), γ, of the receive signal as $\mathrm{PER} = 1 - (1 - \mathrm{BER})^{(\text{Packet size(byte)}\times 8)}$, where BER stands for Bit Error Rate which is calculated by $\mathrm{BER} = Q(\sqrt{\gamma})$ for Offset-Quadrature Phase Shift Keying (O-QPSK) modulation, $Q(.)$ is Q function, and packet size is assumed to be 20 bytes. It is noted that the calculation is based on the specification of sensor networks definded by

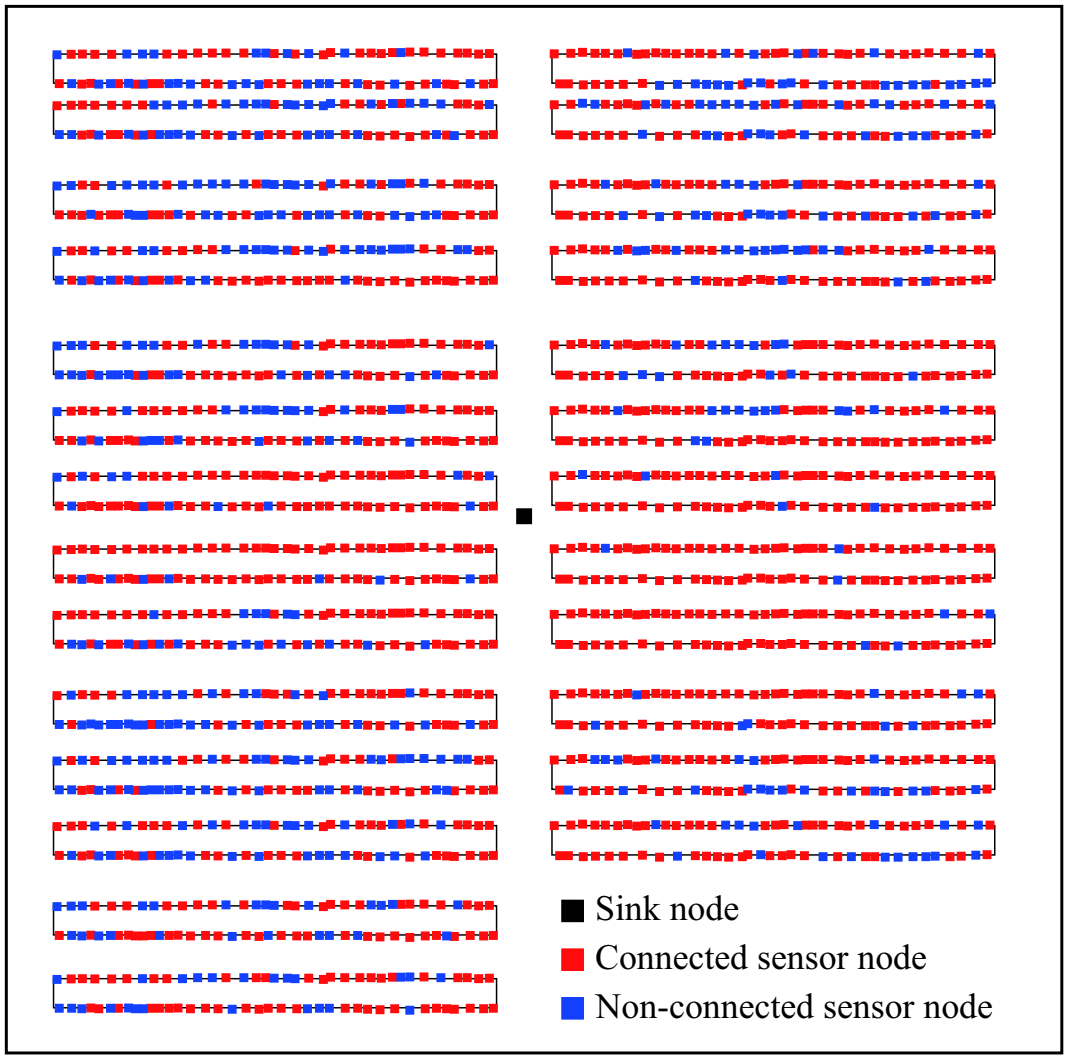

Figure 5.5 Coverage from the sink in the network in single antenna configuration.

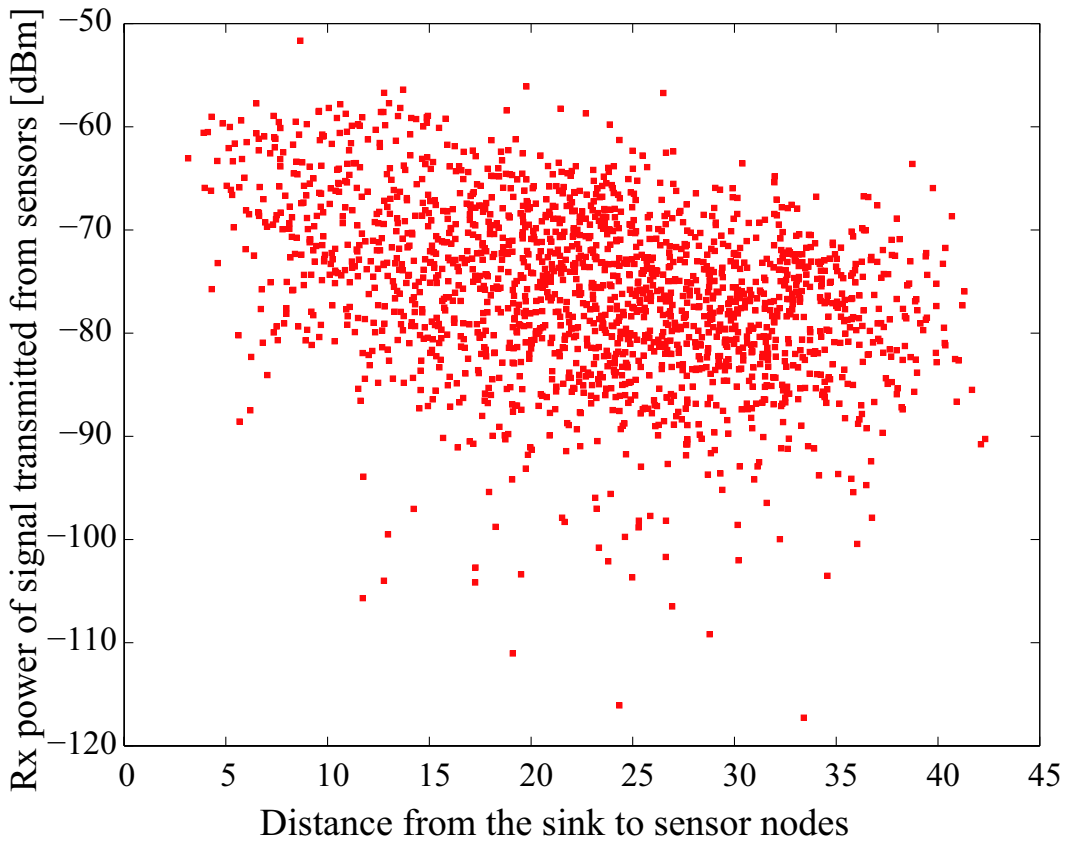

Figure 5.6 Rx power of signal transmitted from sensor nodes against distance in single antenna configuration.

IEEE 802.15.4 standard.

The result of coverage is shown in Fig. 5.5. Also, the receive power at the sink node of the signal transmitted from sensor node s_n, P_{r_0,s_n} with respect to distance from transmitting sensor node s_n is plotted in Fig. 5.6. By these results, we can observe the strong multipath fading in the network since there are several nodes are non-connected even they are in Line-of-Sight to the sink, as shown in Fig. 5.5, and the fluctuation of receive power is obvious, as shown in Fig. 5.6.

From the above results, the determination of network coverage is difficult due to the effect of multipath fading. To reduce this effect, we decide to install an additional antenna at the sink node to achieve receive diversity gain by Maximum Ratio Combination (MRC)

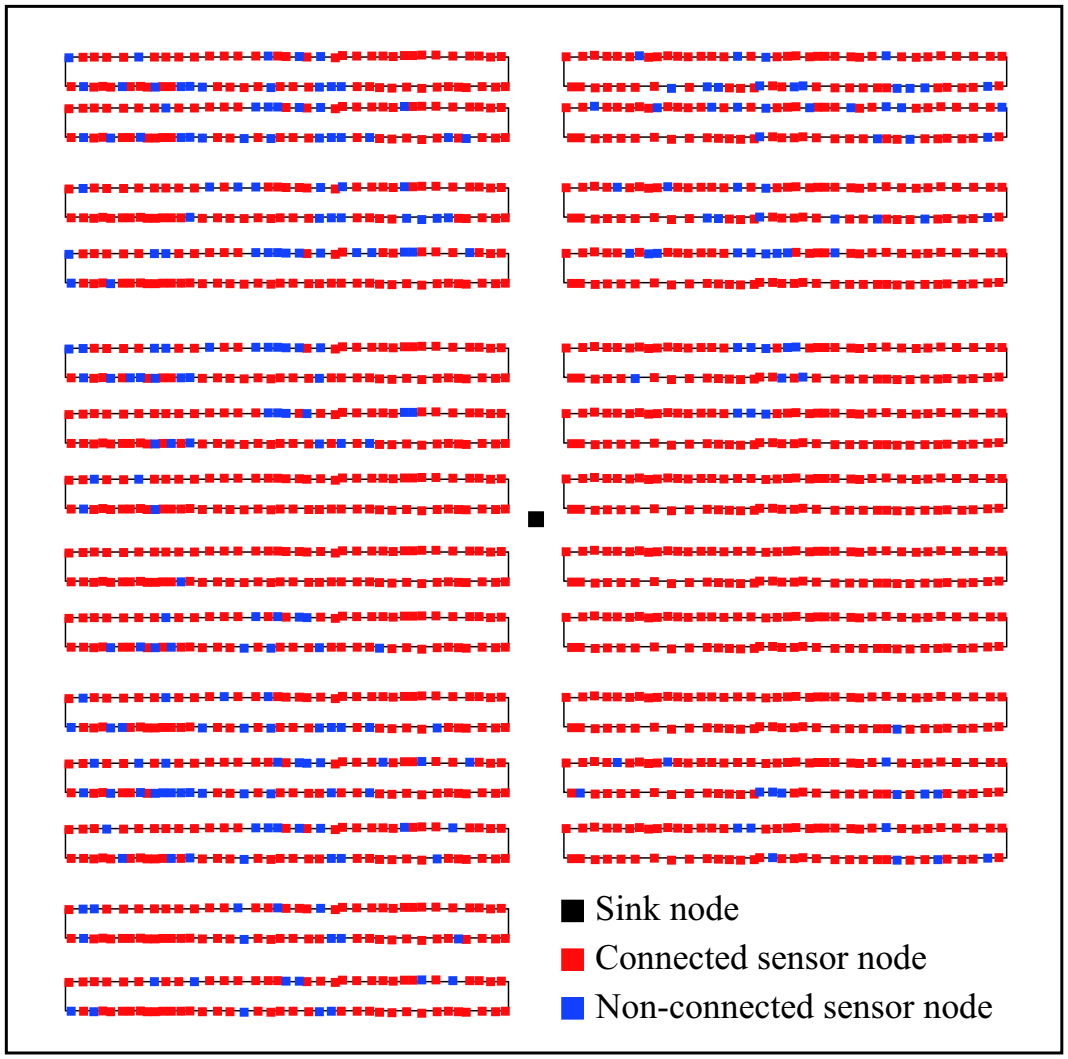

Figure 5.7 Coverage from the sink in the network with diversity gain.

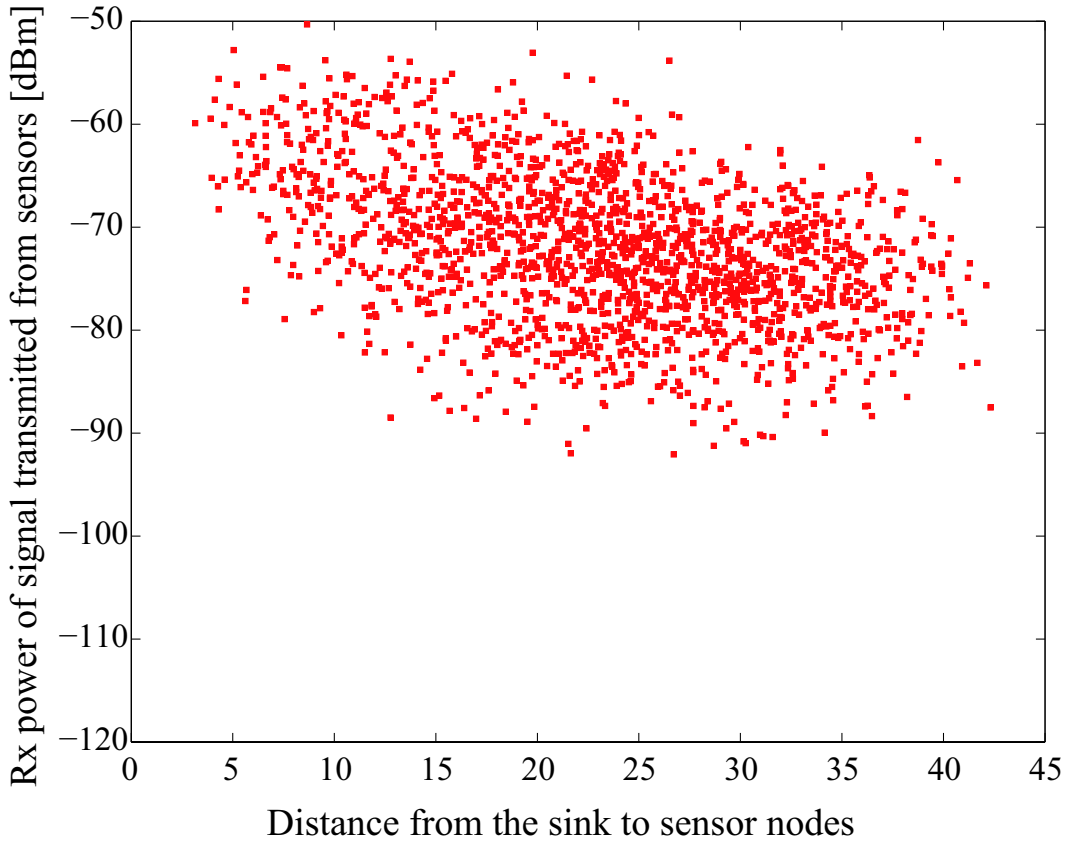

Figure 5.8 Rx power of signal transmitted from sensor nodes against distance with diversity gain.

mechanism [71], and the receive power can be determined as,

$$P_{r_0,s_n} = P_{s_n} \sum_{i=1}^{2} |h^i_{r_0,s_n}|^2, \tag{5.1}$$

where $h^i_{r_0,s_n}$ is the channel response of the transmission from s_n to r_0 at receive antenna i. The result of the connectivity of sensor nodes and receive power against distance from sensor nodes are shown in Fig. 5.7 and 5.8 respectively. From the results, we can confirm that the effect of multipath is significantly reduced. Since the purpose of deploying relays in the network is to enlarge the network coverage, so that the relay nodes in the network are also equipped with double antennas. It is noted that we do not employ multiple antennas at sensor nodes since they are expected to consume low power due to the limitation of battery resource.

5.5.1.2 Initial relay location assignment

In Fig. 5.7, we found that non-connected sensor nodes are mostly located far from the sink node due to the effect of distance pathloss and shadowing from warehouse. Figure 5.9 shows the histogram of the number of non-connected nodes and the height of their locations, and we found that most of the non-connected nodes exist in low locations where they have high possibility to be hidden from the sink. In chapter 3, it was proved that the appropriate location to place relay in the case of two-hop relay network is where relay is in LOS to both the source and destination nodes. However, since we cannot achieve double LOS condition for all sensor nodes due to the number of sensor nodes, our strategy to deploy relay nodes is to determine that relay which has higher probability to achieve double LOS condition. The following describes how to assign the relay locations in the network. For the ease of the consideration, we decide to deploy relays at the same height as the sink, which can guarantee the LOS condition for the transmission from relays to the sink. In addition, we create grid points on the plane at the sink and relay height with one meter of distance between grid points, as shown in Fig. 5.10. The procedure of relay assignment with candidate locations is concluded below.

- Initialize:
  - $S \leftarrow s_n, \forall n \in \{\mathrm{PER}_{r_0,s_n} < 1\%\}$ %Allocate sensor nodes that are connected with the sink node to the set S

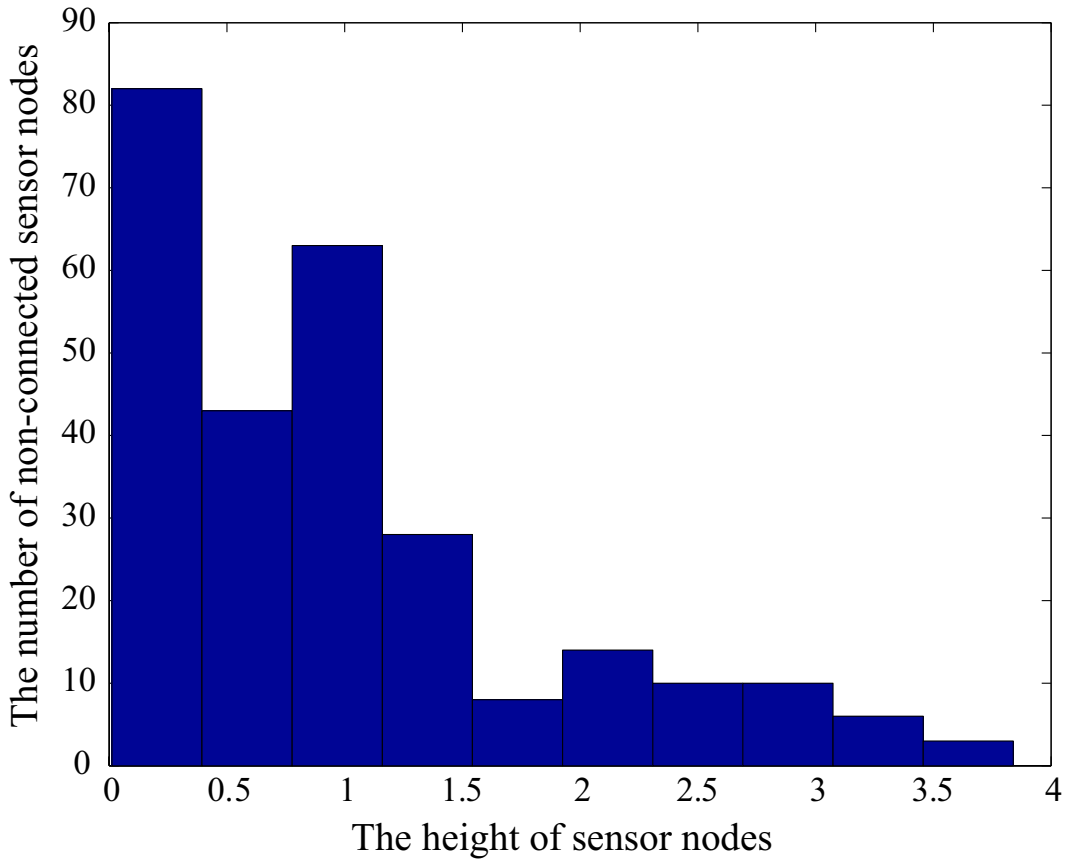

Figure 5.9 Histogram of the number of non-connected nodes against the height of sensor locations.

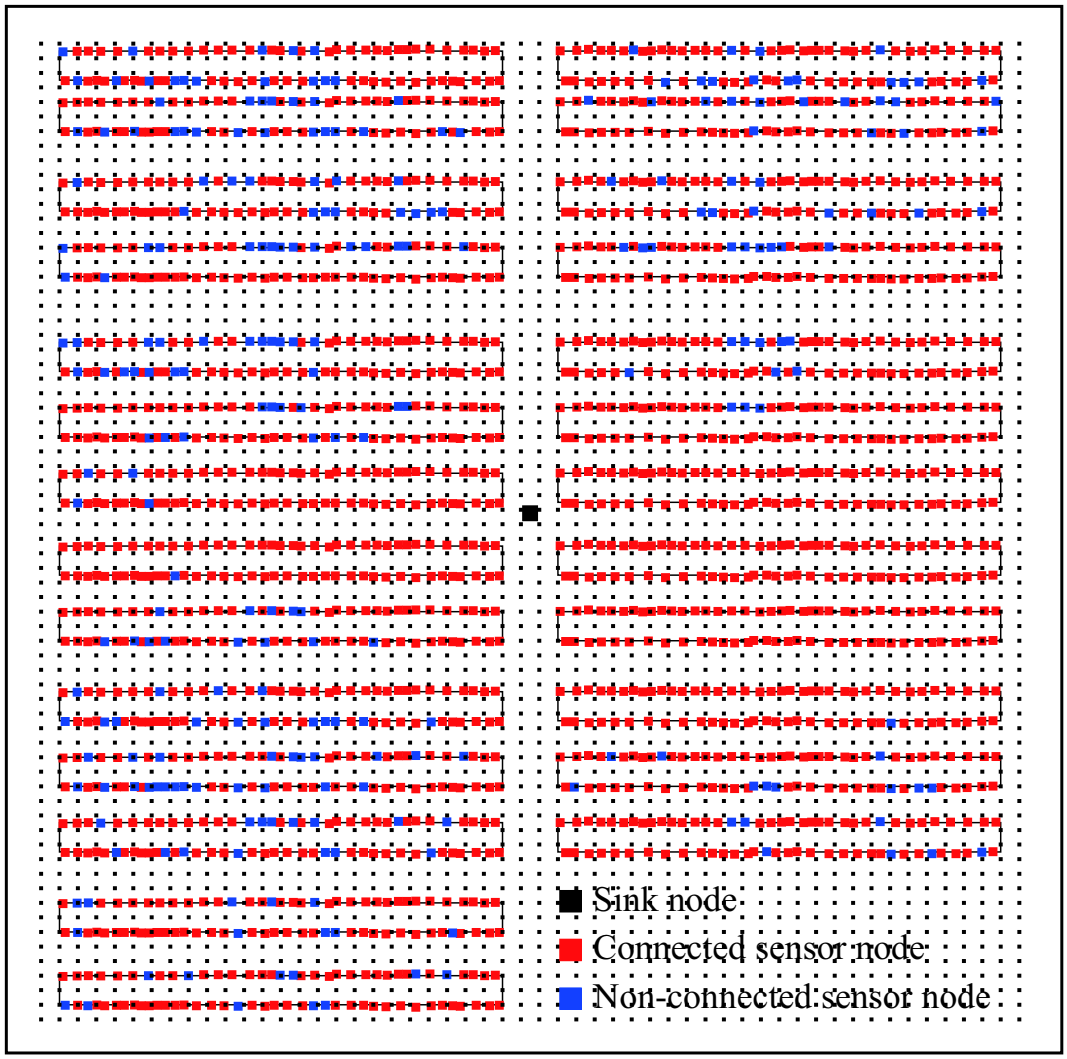

Figure 5.10 Virtual grid points over the geometric of the target area.

– $m = 1$ %Assign the index for the first relay

- Repeat until $|S| = N$ % Repeat until all sensor nodes are connected to the sink or relays.

  1. Scope down the area that non-connected nodes exist.
  2. At each grid point in the area assigned in 1, determine how much sensor nodes are in double LOS by the geometric of the environment.
  3. Assign the locations that have the maximum number of sensor nodes in double LOS condition with the sink as candidate locations $l_m \in \{1, \ldots, L_m\}$ of relay node r_m. It is noted that there can be one or more than two locations.
  4. Check the coverage of the network from the sink and relay at each location by measuring received signal strength. (In our consideration, we use 3D ray-tracing simulation instead).
  5. $S_{r_m(l_m)} \leftarrow s_n, \forall n \in \{\text{PER}_{r_m(l_m),s_n} < 1\%\}$
     $S_{r_m(l_m)} = S_{r_m(l_m)} \cup S$ %Allocate all sensor nodes that are connected with the sink or the previous relay nodes $m-1, \ldots, 1$ to the set $S_{r_m(l_m)}$.
  6. $l_m^{(0)} = \arg\max_{l_m \in \{1,\ldots,L_m\}} \left|S_{r_m(l_m)}\right|$ %Assign the initial location for relay node r_m as the location that can most cover the network.
  7. $S = S_{r_m(l_m^{(0)})}$ %Update the coverage of the network.
  8. $m = m+1$ %Change the index of relay to determine the coverage of the next relay.

5.5.1.3 Network optimization

From the previous procedure, we can obtain the candidate locations of each relay node and the initial location has been assigned. Among candidate relay locations, we aim to find the location which mininmize the packet loss rate when the communication schemes which will be described in Section 5.6 is applied. Here, the overall packet error rate of the network at relay locations $\{l_1, l_2, \ldots, l_M\}$ of relay nodes $r_1, r_2, \ldots, r_M$, $\text{PER}_{\text{all}}(l_1, l_2, \ldots, l_M)$, is used to evaluate the network performance. Therefore, the optimum relay locations which can minimize overall packet error rate, and the performance of the optimum locations can be

respectively determined as,

$$\{l_1^*, l_2^*, \ldots, l_M^*\} = \underset{\forall l_m \in \{1,\ldots,L_m\}}{\arg\min} \mathrm{PER}_{\mathrm{all}}(l_1, l_2, \ldots, l_M), \tag{5.2}$$

$$\mathrm{PER}_{\mathrm{all}}(l_1^*, l_2^*, \ldots, l_M^*) = \min_{\forall l_m \in \{1,\ldots,L_m\}} \mathrm{PER}_{\mathrm{all}}(l_1, l_2, \ldots, l_M). \tag{5.3}$$

5.5.2 Non-optimized relay node placement (Reference case)

For a fair comparison, we consider the non-optimized location case by using the same number of relay nodes with the case of proposed method. The results, which would be described later, show that the network needs four relays to cover all of the sensor nodes in the network. Since the location of the sink is at the center of the rectangle area, so that we divide the area into four sub-areas as shown in Fig. 5.11, each of which is aimed to deploy a relay node. In each sub-area, since sensor nodes are randomly distributed in 3 dimensions, so that in the case of non-optimized locations, we simply locate a relay at the middle point between the sink to the farthest sensor node in each dimension axis as shown in Fig. 5.12.

5.6 Communication schemes

In the previous section, we described the optimization methodology of relay placements to optimize the network performance. In this section, the communication schemes considered for performance optimization are described. Here, we consider two communication schemes adapted from MAC protocol of IEEE 802.15.4 standard, i.e. conventional Time Division Duplex (TDD) scheme and MIMO Two-way relay employing Network Coding (M2W/NC) scheme. In addition, we also apply the Hybrid-Automatic Repeat reQuest (ARQ) protocol to perform retransmission in the case that error occur in each transmission.

5.6.1 Relaying schemes

5.6.1.1 Conventional Time Division Duplex (TDD) scheme

Before describing the details of the conventional communication scheme considered in this chapter, we firstly introduce the concept of channel access algorithm in MAC protocol of IEEE 802.15.4 standard and clarify the assumption we use for our consideration. The standard defines the superframe structure illustrated in Fig. 5.13 to allocate the time distribution mechanism for beacon-enable mode, where all nodes in the network are synchronized [21].

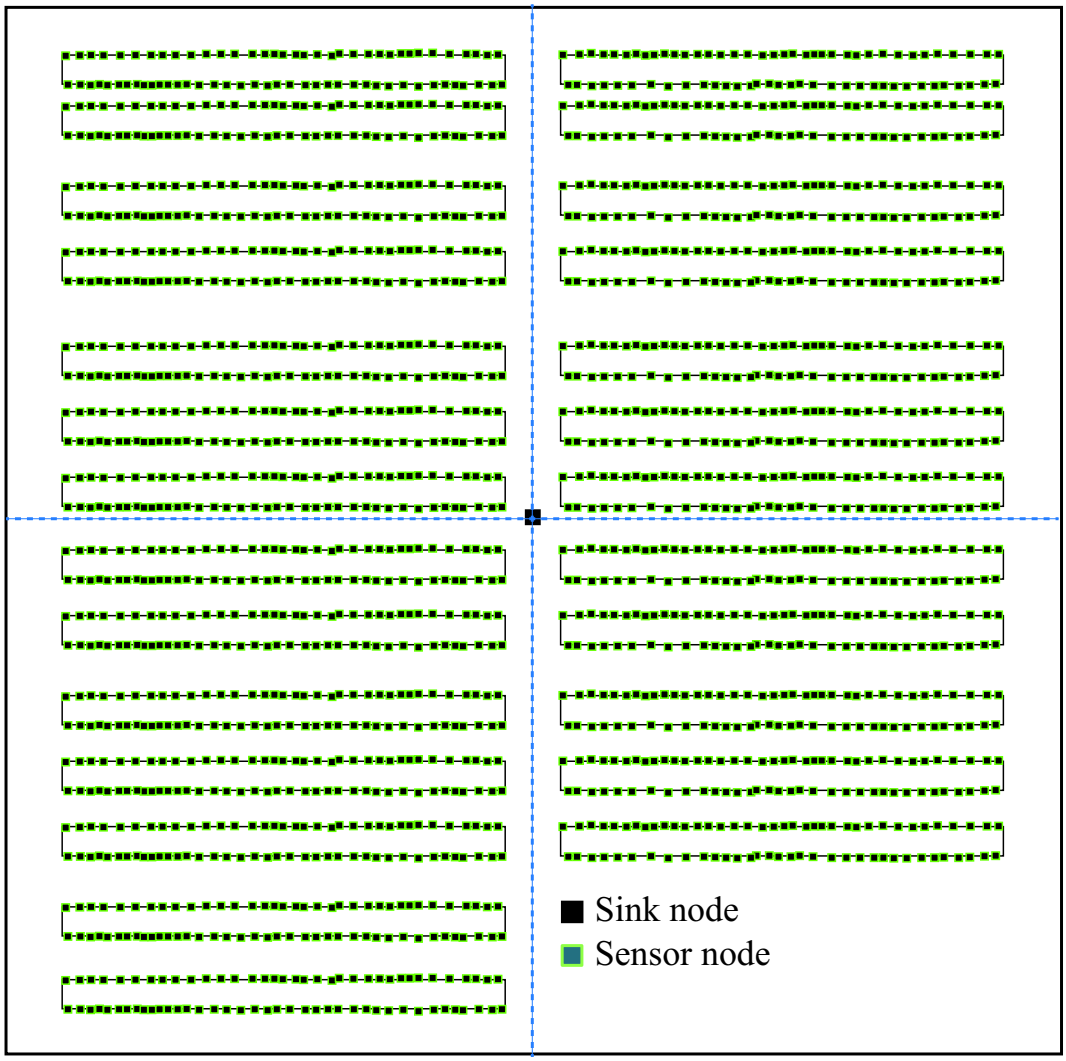

Figure 5.11 Sub-areas for determining relay locations in non-optimized case.

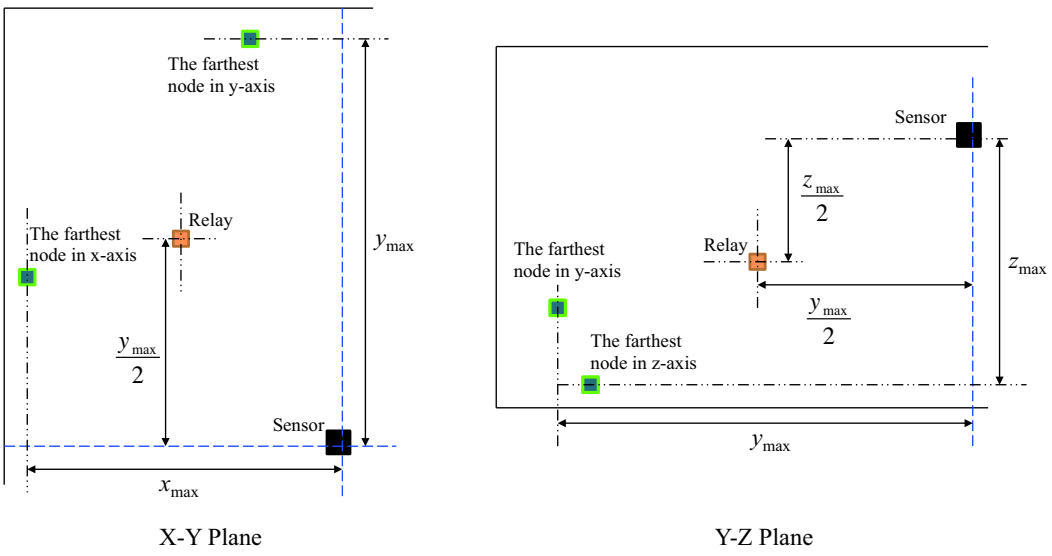

Figure 5.12 The relay location in each sub-area.

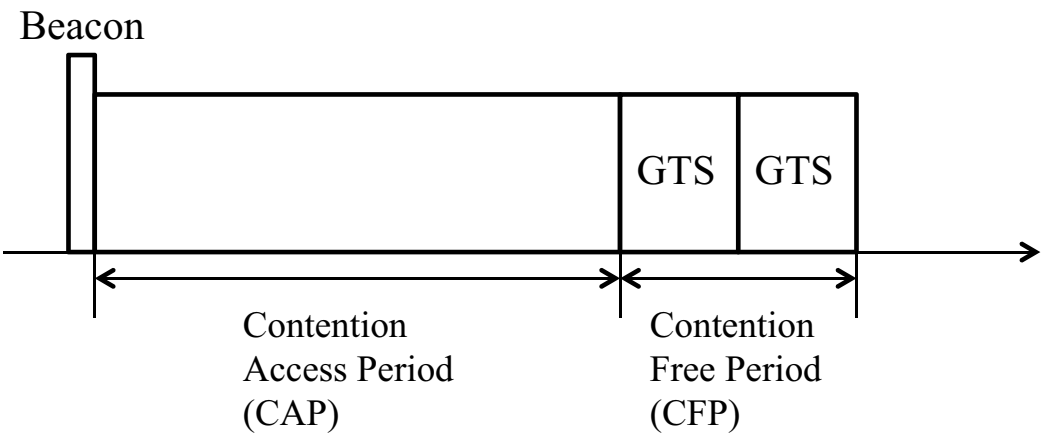

Figure 5.13 The superframe structure.

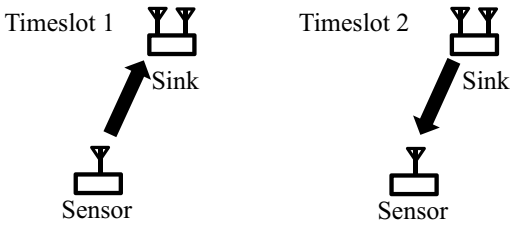

(a) Direct transmission.

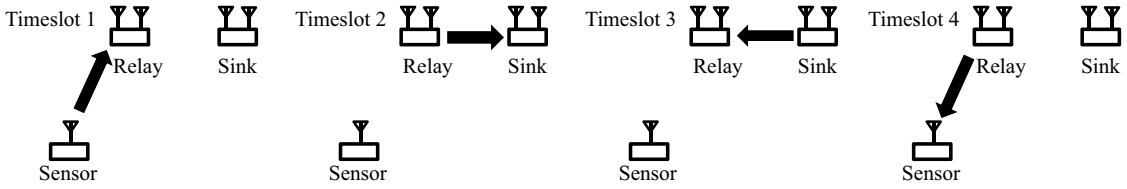

(b) Relay-assisted transmission.

Figure 5.14 Up/downstream data transfer in TDD case.

Each superframe consists of active and inactive portion which allows the coordinator to enter low-power mode for energy saving. The active portion composes of three parts, i.e. a beacon, a Contention Access Period (CAP), and a Contention-Free Period (CFP). Beacon frame is transmitted for the synchronization purpose. During CAP, the system allows sensor nodes to compete freely to access the channel with slotted Carrier Sense Multiple Access with Collision Avoidance (CSMA/CA) mechanism. During CFP, the system provides the sensor nodes exclusive access to the channel within its allocated Guaranteed Time Slots (GTSs), without competing each other to access channel.

In this chapter, we are considering the WSN for autonomous control system in the industrial field, which needs to guarantee stable control. The nondeterministic contention-based channel access cause unpredictable performance bounds. Therefore, we assume that data flows in the network are sequential time-bounded and must be pre-determined when the network operation is initiated. Therefore, all devices sequentially access the wireless medium during CFP through GTS, while CAP is left for any nodes, which have abrupt data, to freely access the medium with CSMA/CA mechanism. For the ease of the analysis, we omit the time during beacon frame, CAP, and assume that in one sequence each device transmit one packet data via GTS in one superframe, where frame header is neglected.

Data flows in the network are categorized into two types, i.e. direct data flows, and relay-assisted data flows. Direct data flows correspond to flows sent/received by sensor nodes,

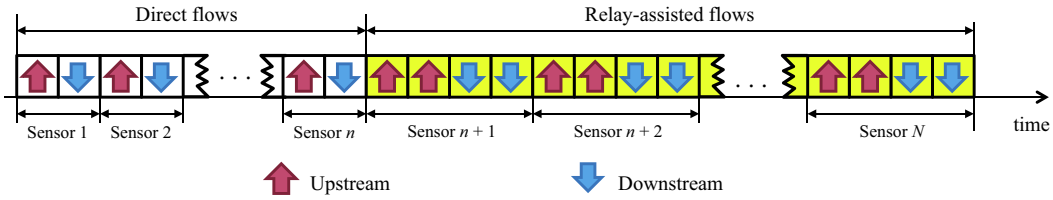

Figure 5.15 Timeslots of data flows in each sequence for TDD case.

which need no relay to connect to the sink, while relay-assisted data flows correspond to flows sent/received by sensor nodes, which transfer data via relays. During a sequence, each sensor sends one packet data to the sink (considered as upstream), and receives one packet data from the sink (considered as downstream). Each sensor node responsible for direct flows spends two timeslots for up/downstream, while each sensor node responsible for relay-assisted flows needs up to four timeslots to complete up/downstream transfer, as shown in Fig. 5.14. Therefore, timeslots for data flows in the network in each sequence can be concluded in Fig. 5.15.

As mentioned, data flows in the network needed to be pre-determined during network setup, so that firstly, each sensor needs to decide whether it will directly transfer to the sink or which relay it should connect to. Since the devices operating in receiver mode can measure the SNR from transmitters, each sensor determines its appropriate route as follows. Firstly, sensor node s_n consider the case of direct flows by the following formula,

$$C_{s_n \to r_0} = \log_2 \left(1 + \frac{P|\mathbf{h}_{r_0,s_n}|^2}{\sigma^2} \right) \tag{5.4}$$

$$C_{r_0 \to s_n} = \log_2 \left(1 + \frac{P|\mathbf{h}_{s_n,r_0}|^2}{2\sigma^2} \right) \tag{5.5}$$

$$C_{(s_n,r_0)} = \frac{1}{2}(C_{s_n \to r_0} + C_{r_0 \to s_n}), \tag{5.6}$$

where $C_{s_n \to r_0}$ and $C_{r_0 \to s_n}$ correspond to the channel capacity of direct transmission from sensor node s_n to the sink node r_0 (upstream) and from the sink node r_0 to sensor node s_n (downstream) respectively, and the Tx power of sensor node, and sink node are set to be equal $P_{s_r} = P_{r_0} = P$. In the case of upstream, multiple antenna is equipped at receiver side, so that the Rx can gain Maximum Ratio Combination (MRC) diversity gain as shown in Eq. (5.4). In the case of downstream, since we assume that Tx does not know the CSI, the Rx can obtain the transmitter gain from STBC mechanism as expressed in Eq. (5.5). The proof

of this equation is shown in the appendix of this chapter (Section 5.9). Consequently, the capacity of s_n in direct transmission case, $C_{(s_n,r_0)}$, is calculated by Eq. (5.6). The capacity is divided by 2 since it takes 2 timeslots to transfer data in up/downstream.

Next, the case of relay-assisted flows is considered by the following formula,

$$C_{s_n \to r_m} = \log_2 \left(1 + \frac{P|\mathbf{h}_{r_m,s_n}|^2}{\sigma^2}\right) \tag{5.7}$$

$$C_{r_m \to r_0} = C_{r_0 \to r_m} = \log_2 \left(1 + \frac{P\|\mathbf{H}_{r_0,r_m}\|_{\mathrm{F}}^2}{2\sigma^2}\right) \tag{5.8}$$

$$C_{r_m \to s_n} = \log_2 \left(1 + \frac{P|\mathbf{h}_{s_n,r_m}|^2}{2\sigma^2}\right) \tag{5.9}$$

$$C_{s_n \to r_m \to r_0} = \min\left(C_{s_n \to r_m}, C_{r_m \to r_0}\right) \tag{5.10}$$

$$C_{r_0 \to r_m \to s_n} = \min\left(C_{r_0 \to r_m}, C_{r_m \to s_n}\right) \tag{5.11}$$

$$C_{(s_n,r_m)} = \frac{1}{4}\left(C_{s_n \to r_m \to r_0} + C_{r_0 \to r_m \to s_n}\right), \tag{5.12}$$

where $\|.\|$ denotes the Frobenius norm of the matrix, $C_{s_n \to r_m}$ and $C_{r_m \to r_0}$ correspond to the channel capacity of transmission in upstream from s_n to relay node r_m and relay node r_m to r_0 respectively, and $C_{r_0 \to r_m}$ and $C_{r_m \to s_n}$ correspond to the channel capacity of transmission in downstream from r_0 to relay node r_m and relay node r_m to s_n respectively. Similar to Eqs. (5.4) and (5.5), channel capacity is gained by MRC diversity in Eq. (5.7), and by STBC in Eq. (5.9) respectively. In Eq. (5.8), since the sink and relay are both equipped with multiple antennas but only single streams is sent over MIMO channel, the channel capacity of transmission between sink and relay is gained by both STBC transmitter diversity and receiver diversity. The prove of the equation can be seen in the appendix of this chapter (Section 5.9). Consequently, the capacity of data transmission in upstream and downstream can be determined by the bottleneck capacity of two-hop transmission as in Eqs. (5.10) and (5.11) respectively and the capacity of s_n in relay-assisted case with relay node r_m can be calculated by Eq. (5.12). The capacity is divided by 4 since it takes 4 timeslots to transfer data in up/downstream.

In conclusion, each sensor will select which parent node it will connect to by determining the route where capacity is maximized as,

$$r_m^n = \underset{m \in \{0,1,2,\ldots,M\}}{\arg\max} \left(C_{(s_n,r_m)}\right), \tag{5.13}$$

where r_m^n is the selected relay node by s_n. It is noted that if $r_m^n = 0$, it means that the route of direct transmission to the sink is selected.

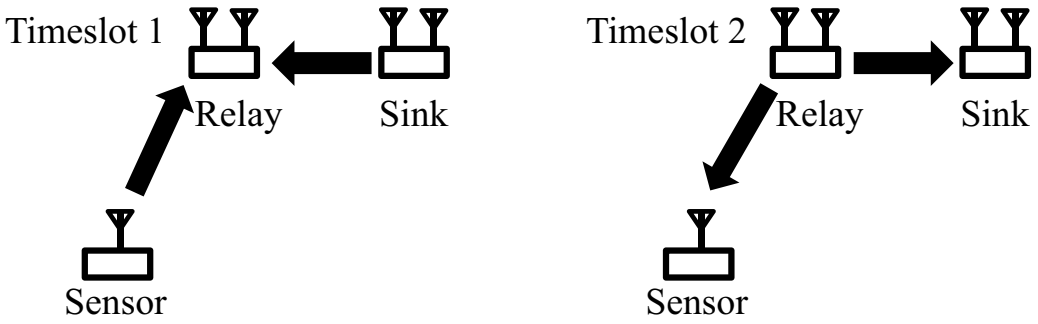

Figure 5.16 Up/downstream data transfer of relay-assisted flows in M2W/NC case.

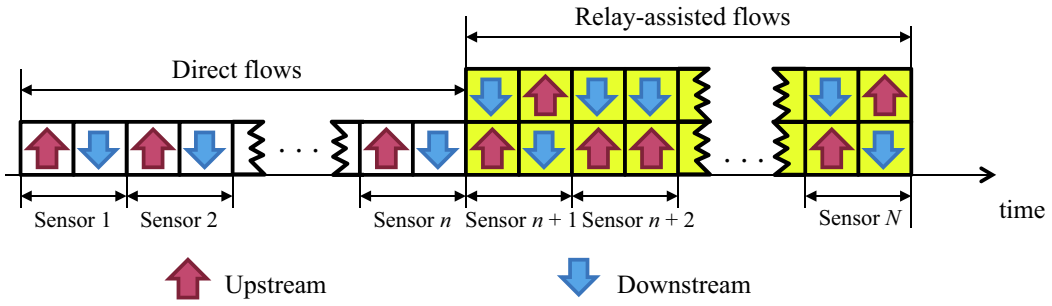

Figure 5.17 Timeslots of data flows in each sequence for M2W/NC case.

5.6.1.2 Two-way Relay Networks with Network Coding

In Chapter 2, we introduced MIMO two-way relay network schemes which allow the network simultaneously communicate in bi-direction owing to multiple antennas. In this chapter, since we are considering the network where CSI is known at Rx side only and two-hop relaying configuration is enough for covering sensor nodes in the network, we aim to adopt MIMO Two-Way relaying with Network Coding (M2W/NC) scheme introduced in Section 2.4.2.1 to our WSN. The mechanism of transmission in direct flow is similar to TDD case and that in relay-assisted flows can be concluded in Fig. 5.16. By applying M2W/NC, the required timeslots relay-assisted data flow in up/downstream can be reduced by half, as shown in Fig. 5.17. Here, relay is equipped with two antennas, which is enough for performing M2W/NC, so that no additional antenna is required.

Similar to the conventional scheme, each sensor decide whether it should directly connect to the sink or connect to which relay by determining the capacity in direct transmission

case and relay-assisted case. The capacity in direct transmission case can be calculated by Eqs. (5.4), (5.5) and (5.6), while the capacity of the relay-assisted case can be determined as follows.

The M2W/NC scheme in this section is adapted from the scheme explained in Section 2.4.2.1. Since the sink node, which can be treated as the source node of two-hop relay network, is also equipped with two-array antenna, we apply STBC mechanism to obtain Tx diversity gain with single stream transmission. In the first timeslot, the sink node and sensor node s_n transmit signals to relay node r_m with multiple access mechanism. At the sink node, in the first symbol period, two different symbols $x_{r_0}(1)$ and $x_{r_0}(2)$ of the transmit signal x_{r_0} are simultaneously transmitted over antenna 1 and 2 respectively, and over the second symbol period, $x^*_{r_0}(2)$ and $-x^*_{r_0}(1)$ are simultaneously transmitted over antenna 1 and 2 respectively. The transmit signal of the sink can be expressed as,

$$\mathbf{x}_{s_n}^{\text{STBC}} = \begin{bmatrix} x_{r_0}(1) & x_{r_0}(2) \\ x_{r_0}(2)^* & -x_{r_0}(1)^* \end{bmatrix}. \tag{5.14}$$

Therefore, the equivalent channel matrix from r_0 to r_m can be written as,

$$\mathbf{H}_{r_m,r_0}^{\text{STBC}} = \begin{bmatrix} h^{11}_{r_m,r_0} & -\left(h^{12}_{r_m,r_0}\right)^* & h^{21}_{r_m,r_0} & -\left(h^{22}_{r_m,r_0}\right)^* \\ h^{12}_{r_m,r_0} & \left(h^{11}_{r_m,r_0}\right)^* & h^{22}_{r_m,r_0} & \left(h^{21}_{r_m,r_0}\right)^* \end{bmatrix}^T, \tag{5.15}$$

where $h^{ab}_{\text{X,Y}}$ is a channel response of transmission from Tx antenna b at Y node to Rx antenna a at X node, and the notation $[.]^*$ refers to conjugate operation.

At the sensor node s_n, transmit signals in the first and second symbol period are $x_{s_n}(1)$ and $x_{s_n}(2)$ respectively, and the channel of the transmission from s_n to r_m is $\mathbf{h}_{r_m,s_n} = \left[h^1_{r_m,s_n}\ h^2_{r_m,s_n}\right]$, where $h^1_{r_m,s_n}$, and $h^2_{r_m,s_n}$ denote the channel response elements of the channel at antenna 1 and 2 respectively.

Finally, the receive signal at the relay node r_m can be concluded by the following expression as,

$$\begin{aligned} \mathbf{y}_{r_m} &= \mathbf{H}_{r_m}\mathbf{x}_{r_m} + \mathbf{n}_{r_m} \\ &= \begin{bmatrix} h^{11}_{r_m,r_0} & h^{12}_{r_m,r_0} & h^1_{r_m,s_n} & 0 \\ -(h^{12}_{r_m,r_0})^* & (h^{11}_{r_m,r_0})^* & h^2_{r_m,s_n} & 0 \\ h^{21}_{r_m,r_0} & h^{22}_{r_m,r_0} & 0 & h^1_{r_m,s_n} \\ -(h^{22}_{r_m,r_0})^* & (h^{21}_{r_m,r_0})^* & 0 & h^2_{r_m,s_n} \end{bmatrix} \begin{bmatrix} x_{r_0}(1) \\ x_{r_0}(2) \\ x_{s_n}(1) \\ x_{s_n}(2) \end{bmatrix} + \mathbf{n}_{r_m}, \end{aligned} \tag{5.16}$$

where $\mathbf{y}_{r_m} = \left[y^1_{r_m}(1)\ y^1_{r_m}(2)\ y^2_{r_m}(1)\ y^1_{r_2}(2)\right]$ is the receive signal vector, the element $y^a_{r_m}(b)$ stands for the receive signal at antenna a at symbol period b, $\mathbf{H}_{r_m}$ denotes the equivalent

receive channel matrix, $\mathbf{x}_{r_m}$ denotes the equivalent transmit signal vector, and $\mathbf{n}_{r_m}$ is complex AWGN with zero mean and σ^2 variance element vectors, where typically $\mathrm{E}[\mathbf{n}_{r_m}\mathbf{n}_{r_m}^H] = \sigma^2\mathbf{I}_{4\times4}$.

The detection of data streams can be performed at node r_m by applying ZF weight which is

$$\mathbf{W}_{r_m} = \mathbf{H}_{r_m}(\mathbf{H}_{r_m}^H\mathbf{H}_{r_m})^{-1}. \tag{5.17}$$

After applying the weight to the received signal, the estimated signal vector becomes

$$\begin{aligned}\tilde{\mathbf{x}}_{r_m} &= \mathbf{W}_{r_m}^H\mathbf{H}_{r_m}\mathbf{x}_{r_m} + \mathbf{W}_{r_m}^H\mathbf{n}_{r_m} \\ &= \mathbf{x}_{r_m} + \mathbf{W}_{r_m}^H\mathbf{n}_{r_m},\end{aligned} \tag{5.18}$$

where $\tilde{\mathbf{x}_{r_m}} = [\tilde{x}_{r_0}(1)\ \tilde{x}_{r_0}(2)\ \tilde{x}_{s_n}(1)\ \tilde{x}_{s_n}(2)]$, and $\mathbf{W}_{r_m}^H = \left[\mathbf{w}_{r_m,r_0}^H\ \mathbf{w}_{r_m,s_n}^H\right]^T$.

Hence, the capacity of transmission from r_0 to r_m and s_n to r_m can be calculated as

$$C_{r_0\to r_m} = \frac{1}{2}\log_2\det[\mathbf{I}_{2\times2} + \frac{P}{2\sigma^2}(\mathbf{w}_{r_m,r_0}^H\mathbf{w}_{r_m,r_0})^{-1}] \tag{5.19}$$

$$C_{s_n\to r_m} = \frac{1}{2}\log_2\det[\mathbf{I}_{2\times2} + \frac{P}{2\sigma^2}(\mathbf{w}_{r_m,s_n}^H\mathbf{w}_{r_m,s_n})^{-1}]. \tag{5.20}$$

In the next timeslot, the network encodes signal $x_{r_m} = x_{r_0} \oplus x_{s_n}$ and broadcast the signal to the sink node and sensor node s_n. The channel from relay node r_m to the sink node can be considered as 2×2 MIMO STBC diversity channel, and channel from relay node r_m to sensor node s_n can be considered as 2×1 MISO STBC diversity channel and the channel capacity respectively becomes,

$$C_{r_m\to r_0} = \log_2\left(1 + \frac{P\|\mathbf{H}_{r_0,r_m}\|_{\mathrm{F}}^2}{2\sigma^2}\right) \tag{5.21}$$

$$C_{r_m\to s_n} = \log_2\left(1 + \frac{P|\mathbf{h}_{r_m,s_n}|^2}{2\sigma^2}\right). \tag{5.22}$$

The proof of the above expression can be referred to the appendix in Section 5.9.

Finally, the capacity of the network can be calculated from the following equations,

$$C_{s_n\to r_m\to r_0} = \min\left(C_{s_n\to r_m}, C_{r_m\to r_0}\right) \tag{5.23}$$

$$C_{r_0\to r_m\to s_n} = \min\left(C_{r_0\to r_m}, C_{r_m\to s_n}\right) \tag{5.24}$$

$$C_{(s_n,r_m)} = \frac{1}{2}\left(C_{s_n\to r_m\to r_0} + C_{r_0\to r_m\to s_n}\right), \tag{5.25}$$

where $C_{s_n\to r_m\to r_0}$ and $C_{r_0\to r_m\to s_n}$ denote the capacity of upstream and downstream respectively, and $C_{(s_n,r_m)}$ denotes the capacity of the sensor node s_n which is divided by 2 since it takes 2 timeslots to transfer data in up/downstream.

Similar to the conventional scheme, each sensor can select its parent node by Eq. (5.13).

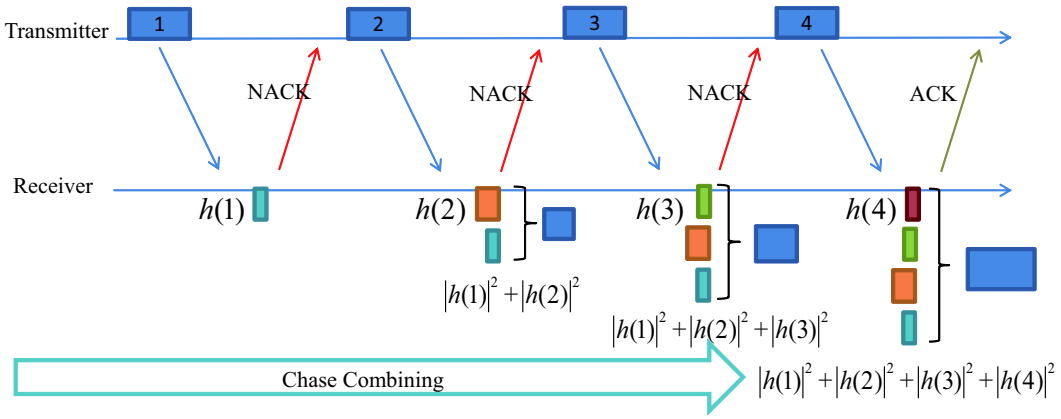

Figure 5.18 The concept of Chase Combining scheme of H-ARQ protocol.

5.6.2 Retransmission Protocol

In wireless transmission, generally, a receiver requests retransmission from the transmitter when the receiver found the error in the received packet to ensuring reliable transmission in each link. In our analysis, we apply Chase Combining (CC) scheme of Hybrid-Automatic Retransmission reQuest (H-ARQ) protocol to perform retransmission [69]. The following describes the fundamental concept of this protocol.

Figure 5.18 shows the concept of H-ARQ protocol for a pair of Tx-Rx. In this case, the Rx detects the signal sent from the Tx and determine the SNR of the signal. If the received SNR creates PER $>$ 1%, the Rx sends Negative ACKnowledgement (NACK) packet for retransmission, otherwise the Rx sends ACK packet to Tx. In each retransmission by H-ARQ in CC scheme, the Tx transmits the same code bits and the Rx uses MRC mechanism to combine the retransmitted signals to decode the code bits. The retransmission is continued until the received SNR can be gained until it provides PER less than 1%.

By the concept described above, CC scheme of H-ARQ can be directly applied to the transmission in direct flows. For the transmission in relay-assisted flows, the consideration is different in TDD and M2W/NC relaying scheme. In TDD case, since the data transfer is in hop-by-hop manner, retransmission is performed (if needed) in the first hop before transfer to the destination in the second hop, as illustrated in Fig. 5.19a. In M2W/NC case, the retransmission pattern is adapted from the retransmission scheme for M2W/NC described in [70] as illustrated in Fig. 5.19b. The acknowledgement packet contains the acknowledgment information from both A and B. In this figure, error occurs in the transmission from B in

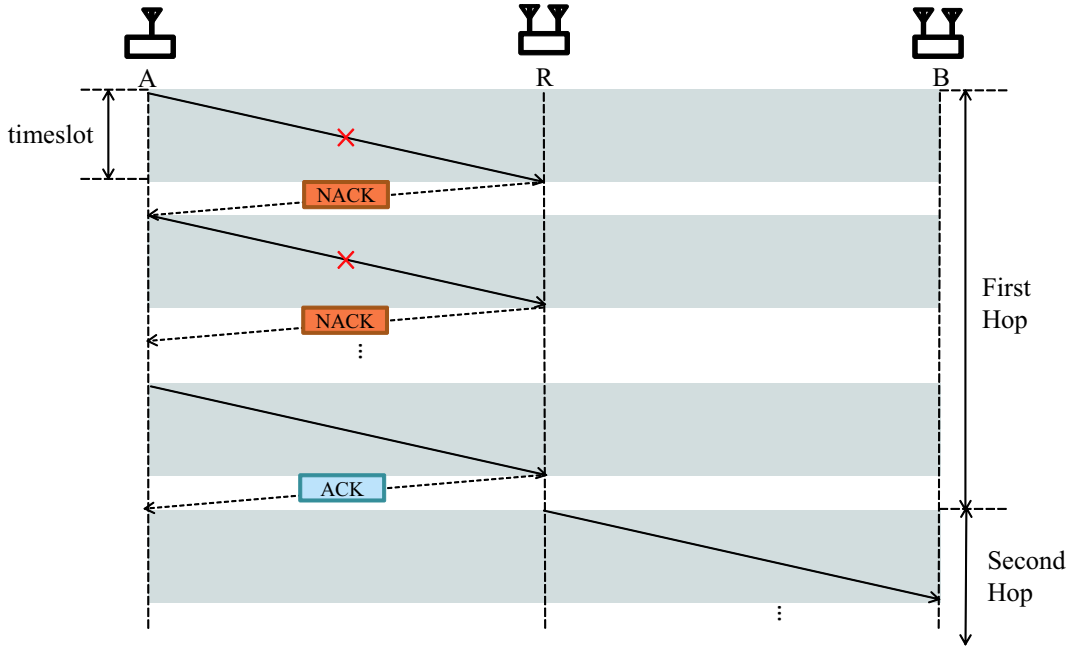

(a) TDD case.

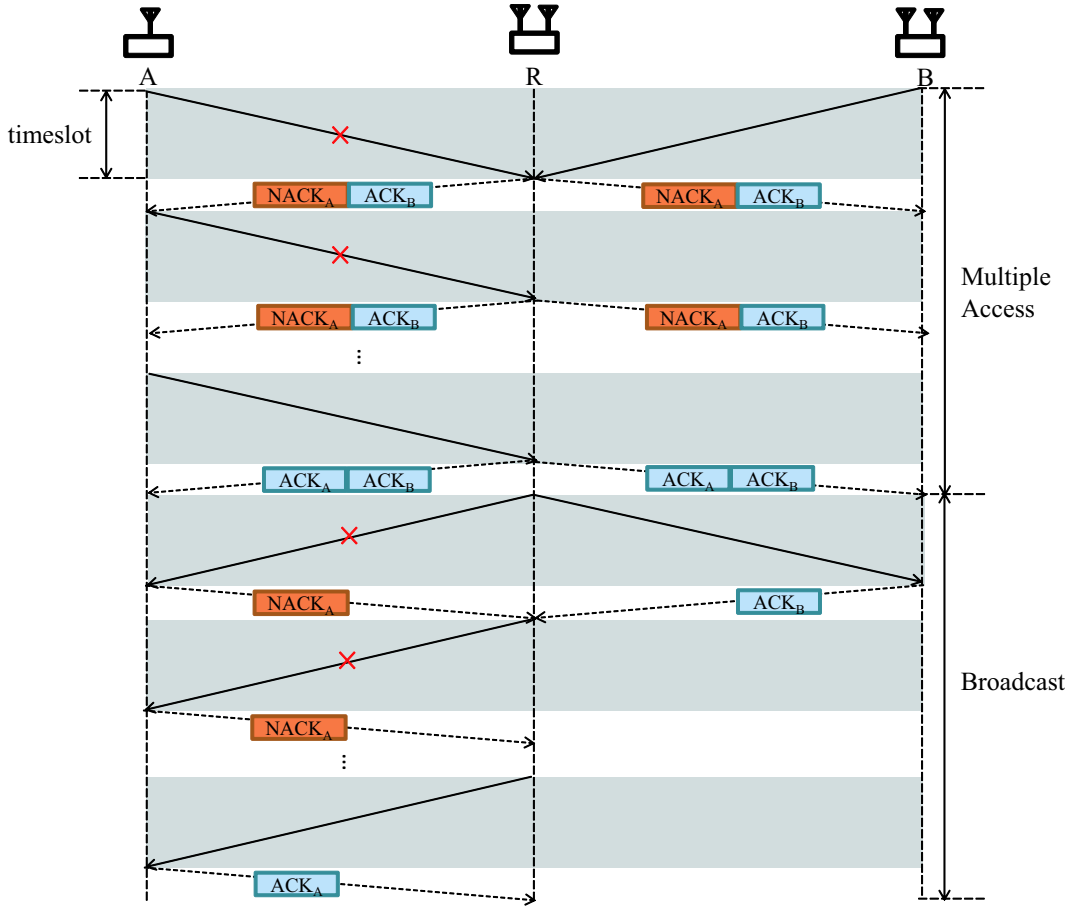

(b) M2W/NC case.

Figure 5.19 Retransmission pattern in relaying networks.

the first timeslot, so that R broadcasts ACK information for A and NACK information for B. In the second timeslot, B performs retransmission and the retransmission continues until the received SNR at B provide PER less than 1%. After R can decode packets from A and B, R turns to broadcast phase to send the encoded signal to A and B. If there is error in transmission to A or B, the receiver node sends NACK packet to R to request retransmission and the retransmission is continued until total received SNR is acceptable.

5.7 Performance evaluation

5.7.1 Evaluation method

In this section, we discuss how we evaluate the network performance when each sensor node can decide which parent node to connect. In this chapter, the network performance is determined by the overall packet error rate as follows.

In the previous section, the network capacity of each transmission link in each communication scheme can be determined. As acknowledged, the channel capacity can be calculated from the SNR of the receive signal as, $C = \log_2(1 + \gamma)$, where γ denotes the SNR, so that we already know the SNR of each transmission link. Here, PER of each link can also be calculated.

With the information of PER, we determine the packet loss in one sequence by the following condition.

- In each sequence, each sensor node aims to send/receive one packet in up/downstream.
- If PER of receive signal is less than 1 %, the receiver requests a retransmission to the transmitter.
- The packet that needs retransmission is considered as error packet.
- The overall packet error rate is defined as,

$$\text{PER}_{\text{all}} = \frac{\text{The number of error packets}}{\text{The number of sent packets}}. \tag{5.26}$$

From the above simulation, the overall packet error rate in one sequence, PER_{all}, is determined to evaluate the network performance. It is noted that this value is used to substitute in Eqs. (5.2)-(5.3) for network performance optimization described in Section 5.5.1.3.

5.7.2 The evaluation of the proposed deployment method

In this section, we discuss the optimization results after we apply our proposed algorithm described in Section 5.5.

5.7.2.1 Relay placement assignment results

Regarding to the proposed algorithm in Section 5.5, the algorithm begins by confirming the coverage from the sink and the results shown in Fig. 5.7. In the next step in Section 5.5.1.3, the number of relay nodes and candidate locations with initial placement of each relay node are determined. Figure 5.20 illustrates the placement of relays. The results show that this environment needs four relay nodes to enable the connectivity of all sensor nodes and the candidate locations of each relay node are near to each other.

5.7.2.2 Comparison of three node deployment methods

After relay locations are assigned, the optimization of network performance and relay placement is performed as described in Section 5.5. In our analysis, we compare the performance of the network by using two different communication schemes introduced in Section 5.6 in three cases of deployment: 1. Relay node is not deployed, 2. Relay placement is not optimized as described in Section 5.5.2 (Reference case), and 3. Relay placement is optimized by the proposed scheme.

Figure 5.21 shows the overall packet error rate against the change of transmission power, and Fig. 5.22 shows the time required in one sequence, where each sensor attempts to send/receive one packet in up/down stream. From these results, we can observe that the network in the case of no relay has worst performance in comparison to the other cases in both terms of overall packet error rate and sequence time. This can be implied that since there are a number of non-connected nodes in this case, these nodes, which are in bad channel condition, have high opportunity of unsuccessful transmission, so that they spend so much effort in performing retransmissions. Therefore, the introduction of relay nodes to the network improves the network performance as can be seen in Figs. 5.21 and 5.22.

Furthermore, the results also show that the network deployed with the proposed method has lower packet loss rate and sequence time than the non-optimized location case. The results show that the reduction of sequence time is obvious in low Tx region while in very high Tx regime the different is not significant. From these results, it can be implied that

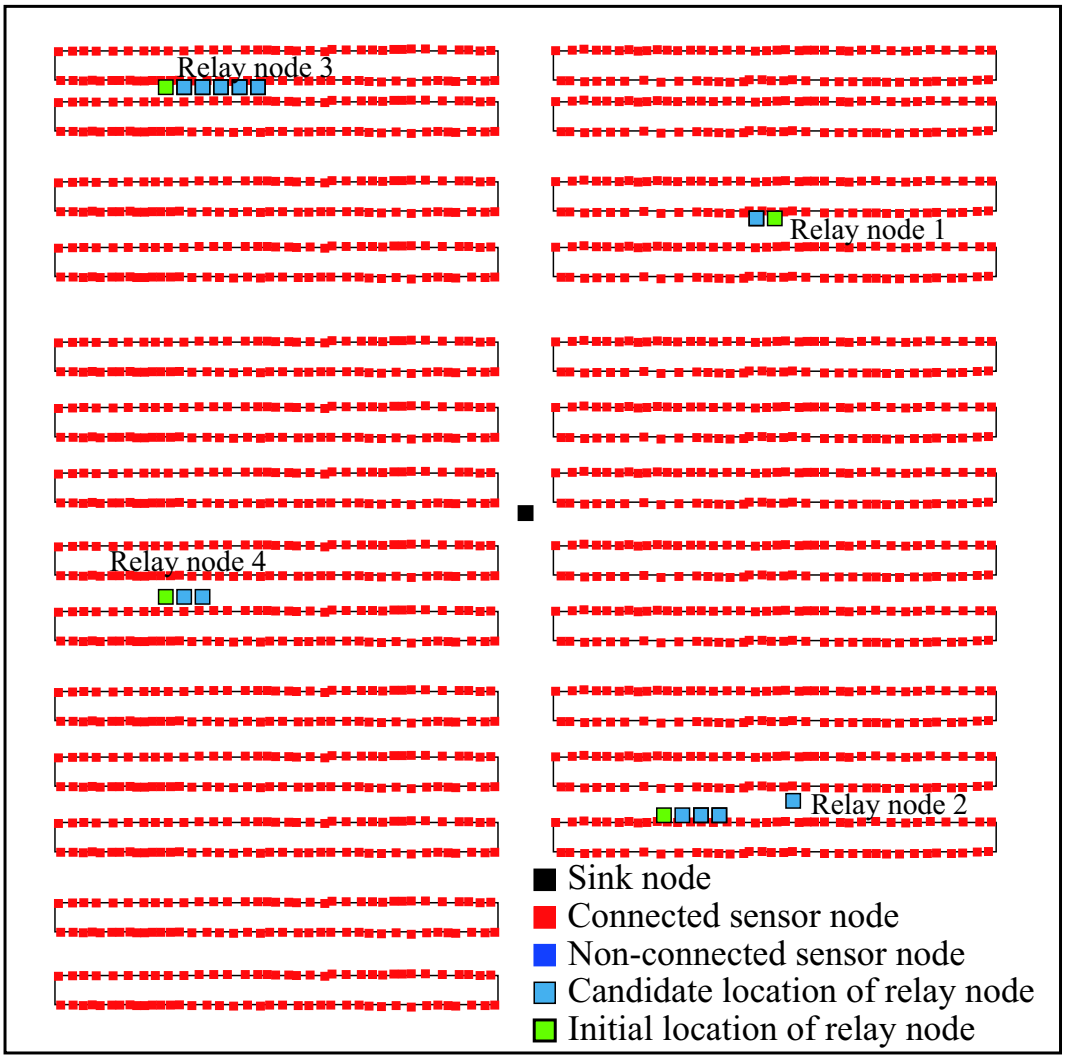

Figure 5.20 Relay locations estimated by the proposed algorithm.

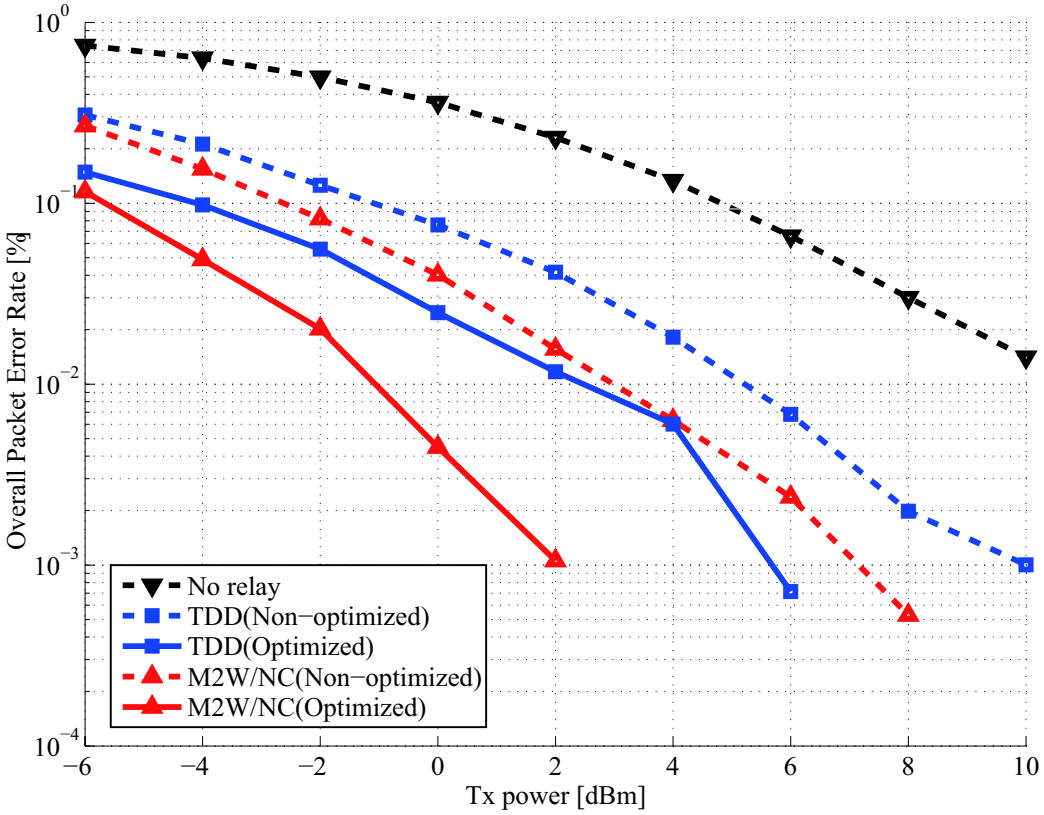

Figure 5.21 The characteristic of overall packet loss.

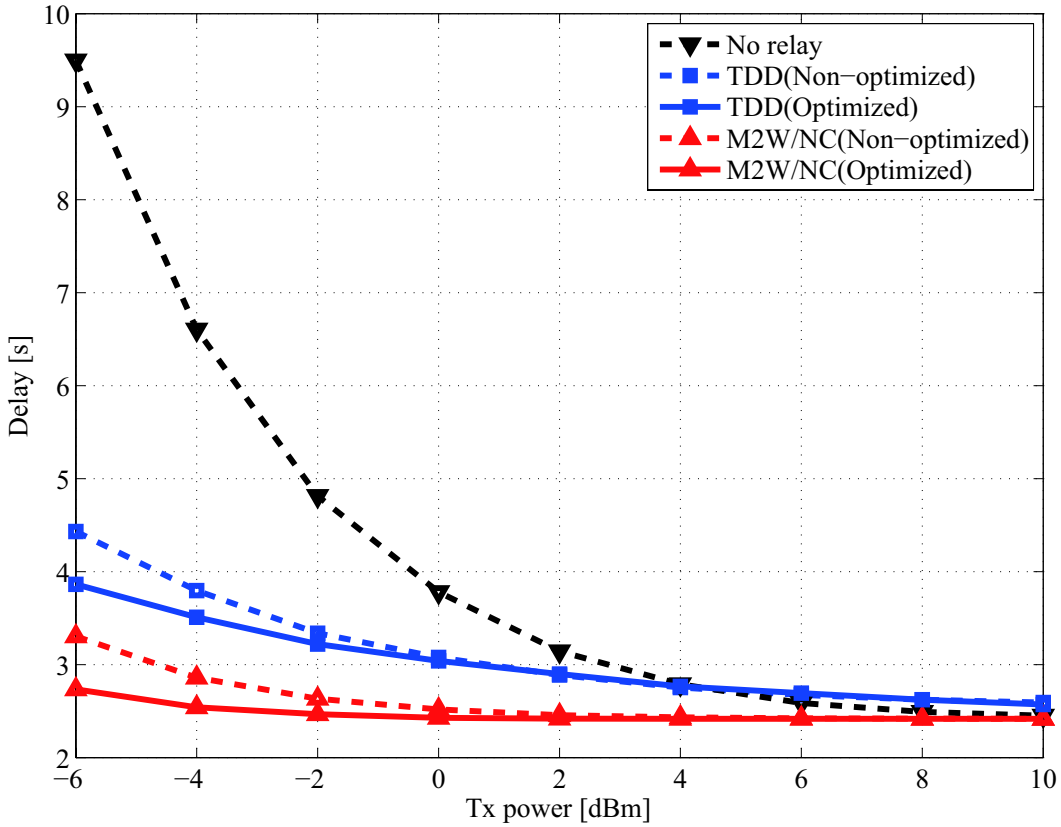

Figure 5.22 The characteristic of average sequence time.

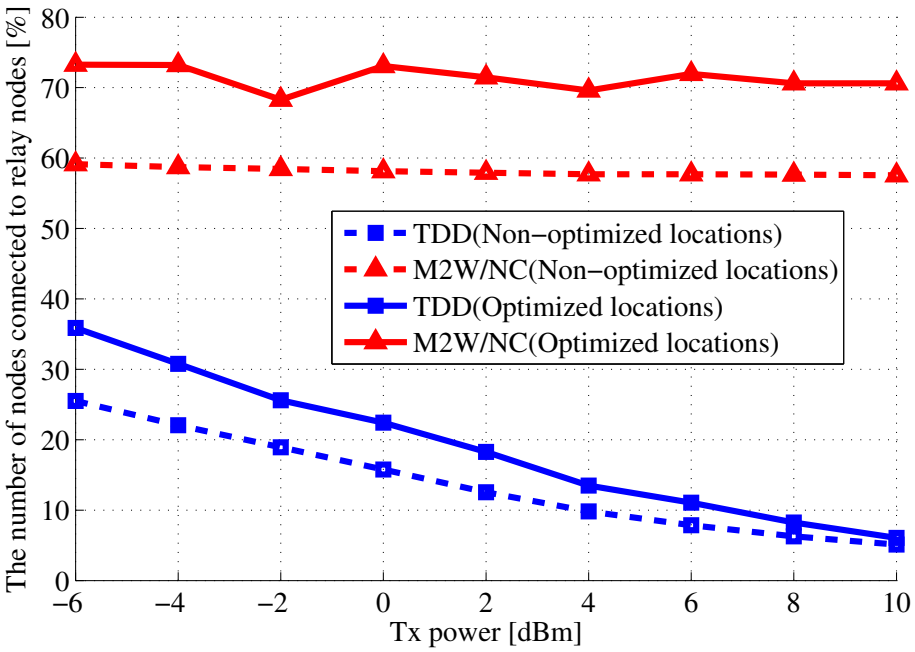

Figure 5.23 The number of sensor nodes connected to relay nodes.

since the proposed method to find the optimum locations is to reduce the condition of NLOS together with the awareness of connectivity of sensors in the network, the performance of the network can be optimized. Therefore, we can confirm the efficiency of the proposed method.

5.7.2.3 Comparison between TDD and M2W/NC schemes

Next, the comparison between TDD and M2W/NC is discussed. Before discussing about this issue in details, we first observe the number of nodes selecting to connect to relay nodes for transmission as shown in Fig. 5.23. In this figure, the results show that the number of relay-assisted nodes in M2W/NC is more than that in TDD. The reason can be explained as follows. Normally, in TDD case, sink-connected sensor nodes spend 2 timeslots and relay-assisted sensor nodes spend 4 timeslots for up/downstream, while in M2W/NC case, both sink-connected and relay-assisted nodes both spend equally 2 timeslots for up/downstream. Therefore, since each sensor node decides to select its parent node by capacity, sensor nodes in M2W/NC case will choose to connect to the relay nodes which is located nearer than the sink and provide better channel condition without the reduction of end-to-end capacity by the number of timeslots. On the contrary, sensor nodes in TDD case might rather choose to

connect to the sink even channel condition may not better than the connection to relay nodes nearby but capacity is not reduced by the number of timeslots.

Moreover, when Tx power is higher, capacity of direct transmission is improved to be more than relay-assisted link, so that the number of sensor nodes select relay nodes as their parents is reduced in TDD scheme, while the number of sensor nodes connected to relays in M2W/NC scheme has no significant change.

From the above explanation, we can imply that the reduction of packet loss rate of M2W/NC scheme from TDD scheme is that sensors in M2W/NC scheme can choose parent nodes which have the best channel condition without the constraint of the number of timeslots. In addition, by comparing the number of sensor nodes choosing to connect to relay nodes between optimized location and non-optimized location cases in Fig. 5.23, we found that sensor nodes in the optimized location tend to select more relay nodes in optimized location case rather than in the other case. This can also confirm the efficiency of the proposed scheme.

In addition, the characteristic of sequence time in two schemes is discussed. Since the relay-assisted sensor nodes in M2W/NC scheme spend a half number of timeslots of those in TDD scheme, the sequence time of M2W/NC scheme should be lower from TDD scheme. This situation obviously happens in low Tx power regime as shown in Fig. 5.22, however, the sequence time of TDD scheme approaches to that of M2W/NC in the high Tx power regime. The reason can be explained by the reduction of number of relay-assisted nodes in high Tx power regime as shown in Fig. 5.23. Consequently, we can conclude that M2W/NC scheme provides a better performance than the conventional TDD scheme.

5.8 Chapter summary

This chapter proposed the deployment methodology of relay nodes to support WSNs in the target factory environments. The results showed that the network optimized with the proposed methodology can perform better than the network where relay locations are not optimized. Moreover, the network optimization by the upcoming M2W/NC scheme shows better performance than the conventional TDD scheme. The reduction of timeslots by M2W/NC does not only result in a shorter delay, but it also increases the chance of sensor nodes to select a better route to perform transmission by the same number of timeslots with the direct transmission.

5.9 Chapter appendix

Rather than the advantage of spatial multiplexing explained so far in previous chapters, MIMO can provide the feature of diversity. As described in Section 5.5, we apply multiple antenna technique in order to combat with multipath problem [71]- [72]. In this chapter appendix, we briefly discuss about the mechanism of diversity and the calculation method of channel capacity in Eqs. 5.4-5.5, and 5.7-5.9.

Basically, diversity at receiver and transmitter side is considered separately. In the case of receiver diversity, or SIMO channels, each receiver antenna receives the same signal from transmitter with the different fading condition. The receiver combines these independent signals and it results in the increase of SNR at the receiver over SNR obtained with single antenna. On the contrary, in the case of transmitter diversity, or MISO channels, the design of transmitter diversity depends on the channel knowledge at the transmitter. If the channel is known at transmitter, the diversity gain can be obtain similarly to the SIMO case, however, without channel knowledge, diversity gain is achieved by a combination of space and time diversity via a STBC technique, which is adapted in some MIMO two-way relaying schemes previously. Since we assumed that there is no channel feedback for all transmission to reduce the complexity of the devices, the discussion of transmitter diversity in this section would focus only the case of no channel knowledge at Tx. In addition, the configuration of multiple antennas at both Tx and Rx side, or MIMO, can also provide diversity gain by combining the mechanism of diversity at Tx and Rx side.

5.9.1 Receiver diversity

We consider a system with single antenna at the transmitter and multiple antennas at the transceiver (SIMO), as shown in Fig. 5.24. The channel vector of the SIMO channel can be written as,

$$\mathbf{h} = [h_1 \; h_2 \ldots h_{M_\mathrm{r}}]^T, \tag{5.27}$$

where M_r is the number of receive antenna, h_i is complex channel response at antenna i. Once again, the transmit signal x is sent from the transmitter, so that the receive signal can be written as

$$\mathbf{y} = \mathbf{h}x + \mathbf{n}, \tag{5.28}$$

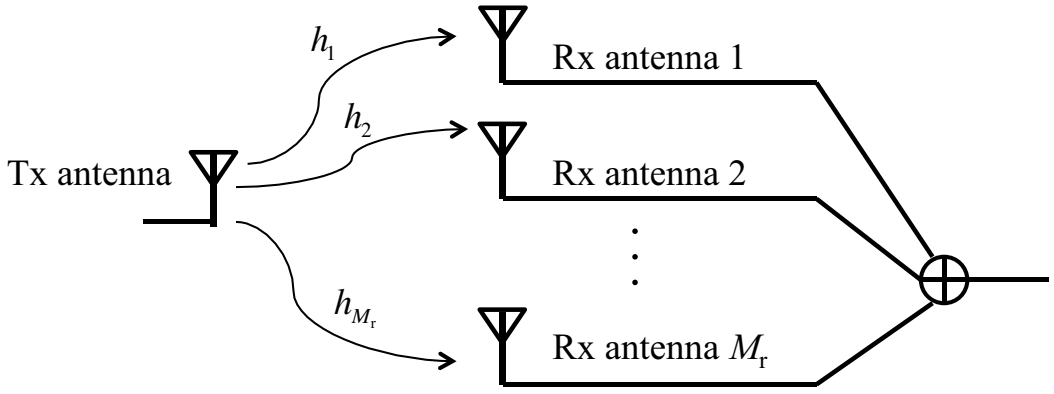

Figure 5.24 The diagram of Rx diversity.

where $\mathbf{y} \in \mathcal{C}^{M_r}$ is receive signal vector, and $\mathbf{n} \in \mathcal{C}^{M_r}$ is the noise signal vector. To maximize the received SNR, the receiver perform Maximum Ratio Combining(MRC) [] by applying receive weight $\mathbf{w} = \mathbf{h}$ such that the receive signal becomes

$$\begin{aligned} \mathbf{h}^H\mathbf{y} &= \mathbf{h}^H\mathbf{h}x + \mathbf{h}^H\mathbf{n} && (5.29) \\ &= |\mathbf{h}|^2 x + \mathbf{h}^H\mathbf{n}. && (5.30) \end{aligned}$$

Therefore, the output SNR and channel capacity can be concluded as

$$\begin{aligned} \gamma &= \frac{|\mathbf{h}|^4 P}{|\mathbf{h}^H\mathbf{h}|\sigma^2} = \frac{|\mathbf{h}|^4 P}{|\mathbf{h}|^2\sigma^2} = \frac{|\mathbf{h}|^2 P}{\sigma^2}, && (5.31) \\ C &= \log_2\left(1 + \frac{|\mathbf{h}|^2 P}{\sigma^2}\right). && (5.32) \end{aligned}$$

This expression is applied to the capacity calculation in Eqs. 5.4, and 5.7.

5.9.2 Transmitter diversity

In the case of no channel knowledge at Tx side, we use the STBC technique to obtain diversity gain. Since the consideration of STBC is different by the number of antennas, we apply an algorithm originally proposed by Alamoti [73] as follows to perform diversity in 2 transmit antenna configuration used in this chapter. In this technique, two different symbols x_1 and x_2 of symbol period 1 and 2 is simultaneously transmitted from Tx antenna 1 and 2 respectively in the first symbol period, and symbols $-x_2^*$ and x_1^* from Tx antenna 1 and 2 respectively in the next symbol period, as shown in Fig. 5.25. In this system, the MISO channel is

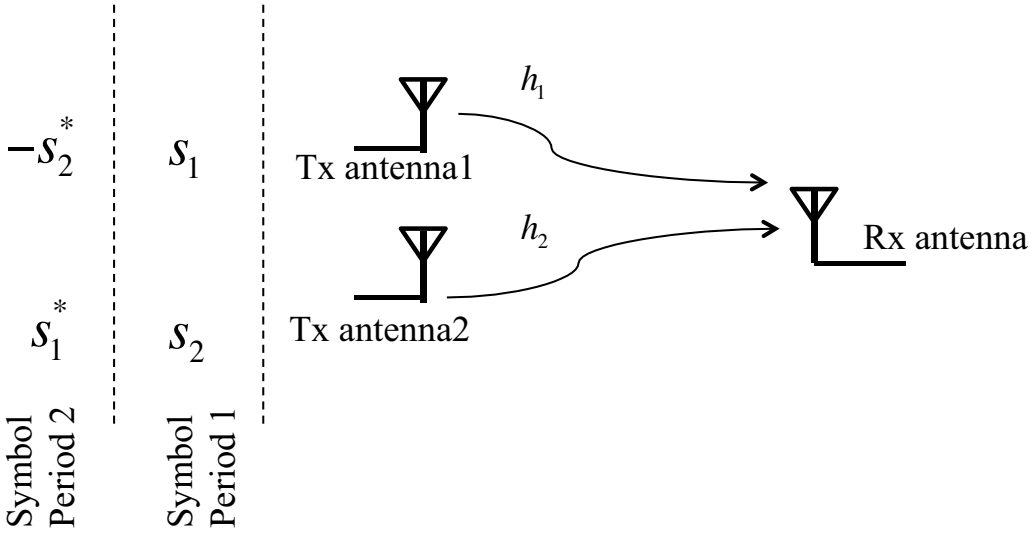

Figure 5.25 The diagram of Tx diversity in 2 Tx antenna configuration.

expressed as $\mathbf{h} = [h_1\ h_2]$ and the receive signal at symbol period 1 and 2, $y(1)$ and $y(2)$ can be respectively expressed as,

$$y(1) = h_1 x_1 + h_2 x_2 + n(1), \tag{5.33}$$

$$y(2) = -h_1 x_2^* + h_2 x_1^* + n(2), \tag{5.34}$$

where $n(1)$ and $n_(2)$ is complex AWGN with zero mean and σ^2 variance element vectors, where typically $\sigma^2 = \mathrm{E}[n[1]^2] = \mathrm{E}[n[2]^2]$. The receive signal can be rearranged and expressed in vector as,

$$\mathbf{y} = \begin{bmatrix} y(1) \\ y^*(2) \end{bmatrix} = \begin{bmatrix} h_1 & h_2 \\ h_2^* & -h_1^* \end{bmatrix} \begin{bmatrix} x_1 \\ x_2 \end{bmatrix} + \begin{bmatrix} n(1) \\ (n(2))^* \end{bmatrix} \tag{5.35}$$

$$= \mathbf{H}_{\mathrm{STBC}}\mathbf{x} + \mathbf{n}, \tag{5.36}$$

where $\mathbf{x} = [x_1\ x_2]^T$ and $\mathbf{n} = [n(1)\ (n(2))^*]^T$. The STBC channel matrix $\mathbf{H}_{\mathrm{STBC}}$ is orthogonal matrix, which satisfies $\mathbf{H}_{\mathrm{STBC}}^H \mathbf{H}_{\mathrm{STBC}} = \|\mathbf{h}\|_F^2 \mathbf{I}_{2\times 2}$, where $\|.\|$ stands for Frobenious norm. In order to maximize SNR of each symbol signal, we apply receive weight $\mathbf{W} = \mathbf{H}_{\mathrm{STBC}}$ and the receive signal becomes

$$\mathbf{H}_{\mathrm{STBC}}^H \mathbf{y} = \mathbf{H}_{\mathrm{STBC}}^H \mathbf{H}_{\mathrm{STBC}}\mathbf{x} + \mathbf{H}_{\mathrm{STBC}}^H \mathbf{n} \tag{5.37}$$

$$= \|\mathbf{h}\|_F^2 \mathbf{x} + \mathbf{H}_{\mathrm{STBC}}^H \mathbf{n}. \tag{5.38}$$

Finally, the received SNR and channel capacity can be respectively concluded as,

$$\gamma = \frac{\|\mathbf{h}\|_F^2 P}{2|\mathbf{H}_{\text{STBC}}^H \mathbf{H}_{\text{STBC}}|\sigma^2} = \frac{\|\mathbf{h}\|_F^4 P}{2\|\mathbf{h}\|_F^2 \sigma^2} = \frac{2\|\mathbf{h}\|_F^2 P}{\sigma^2}, \tag{5.39}$$

$$C = \log_2\left(1 + \frac{\|\mathbf{h}\|_F^2 P}{2\sigma^2}\right). \tag{5.40}$$

It is noted that the SNR is divided by two to average out the capacity per one symbol period. The above expression is applied to the capacity calculation in Eqs. 5.5, and 5.9.

5.9.3 MIMO diversity

In the case of multiple antennas are equipped at both Tx and Rx sides, the mechanism is the combination of Rx and Tx diversity explained in the previous subsections. At Tx side, the transmit symbols in the first and second symbol period is the same as in Tx diversity case. Therefore, the receive signal can be rearranged and written as,

$$\begin{bmatrix} y_1(1) \\ (y_1(2))^* \\ y_2(1) \\ (y_2(2))^* \end{bmatrix} = \begin{bmatrix} h_{11} & h_{12} \\ (h_{12})^* & -(h_{11})^* \\ h_{21} & h_{22} \\ (h_{22})^* & -(h_{21})^* \end{bmatrix} \begin{bmatrix} x_1 \\ x_2 \end{bmatrix} + \begin{bmatrix} n_1(1) \\ (n_1(2))^* \\ n_2(1) \\ (n_2(2))^* \end{bmatrix} \tag{5.41}$$

$$\tilde{\mathbf{y}} = \mathbf{H}_{\text{STBC}}\mathbf{x} + \tilde{\mathbf{n}}, \tag{5.42}$$

where $\tilde{\mathbf{y}} = [y_1(1)\ (y_1(2))^*\ y_2(1)\ (y_2(2))^*]^T$, where $y_a(b)$ is receive signal at antenna a in period symbol b, $\mathbf{H}_{\text{STBC}}$ is equivalent channel, where the element h_{ab} corresponds to channel response of signal transmitted from Tx antenna b to receive antenna a, $\mathbf{x} = [x_1\ x_2]^T$ is transmit vector, and $\tilde{\mathbf{n}} = [n_1(1)\ (n_1(2))^*\ n_2(1)\ (n_2(2))^*]^T$ is assumed to be complex AWGN with zero mean and σ^2 variance element vectors, where typically $\sigma^2 = \mathrm{E}[n^2]$.

Similar to Tx diversity case, the STBC channel matrix $\mathbf{H}_{\text{STBC}}$ is orthogonal matrix, which satisfies $\mathbf{H}_{\text{STBC}}^H \mathbf{H}_{\text{STBC}} = \|\mathbf{h}\|_F^2 \mathbf{I}_{2\times 2}$. Similarly, we aim to maximize SNR by applying receive weight $\mathbf{W} = \mathbf{H}_{\text{STBC}}$ such that receive signal becomes

$$\mathbf{H}_{\text{STBC}}^H \mathbf{y} = \|\mathbf{h}\|_F^2 \mathbf{x} + \mathbf{H}_{\text{STBC}}^H \mathbf{n}, \tag{5.43}$$

where the equivalent channel gain becomes $\|\mathbf{h}\|_F^2 = |h_{11}|^2 + |h_{12}|^2 + |h_{21}|^2 + |h_{22}|^2$. In this case, we can observe that the receiver achieve receiver diversity from the summation of first two terms and that of last two terms, and each receive antenna corresponding to each two terms

can also achieve transmitter diversity. Consequently, the received SNR and channel capacity can be respectively concluded as,

$$\gamma = \frac{\|\mathbf{h}\|_F^2 P}{2|\mathbf{H}_{\mathrm{STBC}}^H \mathbf{H}_{\mathrm{STBC}}|\sigma^2} = \frac{\|\mathbf{h}\|^4 P}{2\|\mathbf{h}\|_F^2 \sigma^2} = \frac{2\|\mathbf{h}\|_F^2 P}{\sigma^2}, \tag{5.44}$$

$$C = \log_2\left(1 + \frac{\|\mathbf{h}\|_F^2 P}{2\sigma^2}\right). \tag{5.45}$$

It is noted that the SNR is divided by two to average out the capacity per one symbol period. The above expression is applied to the capacity calculation in Eq. 5.8.

Chapter 6

Conclusion and suggestions for future studies

6.1 Conclusion of this dissertation

Deploying multi-hop relay networks as supporting backbone becomes an essential technique for the future WSNs in autonomous control systems. In addition, owing to the advantage of spatial multiplexing, employing MIMO in multi-hop relay networks can also enable the feature of bi-directional relaying as well as enhance the channel capacity. So far, there have been several theoretical studies on the achievement of high efficiency by utilizing MIMO in multi-hop networks in several ways. However, the deployment of multi-hop relay networks in the practical environments still has some difficulties. Firstly, the existence of obstacles between any pairs of Tx-Rx results in degradation of transmission, so that relay is needed. As acknowledged, locations of relay nodes has a direct effect to the network performance, however, the network designers still confront to the problem of how to verify the optimum relay placement in the awareness of connectivity of transceiver nodes in the network to their destination nodes as well as maximizing the network performance. Moreover, so far, the study of MIMO in multi-hop relay networks has not been realized in the practical environment, so that the network designer need to know how to fully exploit multiple antennas into multi-hop network, such that the network performance can be optimized. Therefore, this dissertation investigates these issues and proposes a methodology for deploying multi-hop networks in practical environments. Below are the summaries of this dissertation.

Chapter 2 reviewed the basic concept of MIMO communication systems. The proposed

communication schemes employing MIMO technique, which were used in Chapter 3, 4 and 5, were introduced. In addition, this chapter also presented the calculation method of end-to-end capacity of each relaying scheme.

Chapter 3 presented the practical study of MIMO relay networks in basic two-hop relay network in the perspective of solution for shadowing problem. The study was conducted by the MIMO channel measurement in an L-shaped corridor environment where shadowing is dominant. This chapter showed the propagation characteristics of MIMO relay networks and proved the efficiency of relay node in shadowing environment. Moreover, two-way relaying scheme was proved to be the most efficient scheme in comparison to the other schemes and the optimum relay placement was verified to be where relay is located in LOS to both Tx and Rx nodes for the case of two-hop relay networks.

Chapter 4 extended the study of MIMO relay networks into multi-hop configuration in the practical environment. The main problem in multi-hop relay network is the existence of overreach interference from far nodes. This chapter evaluated the M2WMN in practical environment and proved the efficiency of power control in order to deal with overreach interference in the realistic environment. Moreover, the optimum relay placement is proved to be in LOS locations when power control is not applied. However, we learnt that the optimum locations for relay nodes are changed to be other locations in high SNR regime when power control is applied due to the effect of reduction of overreach interference.

Chapter 5 provided the deployment methodology of relay nodes for sensor networks in practical environments. The method was designed from the idea of the appropriate condition for relay node placement learnt in Chapter 3 and 4. From the results proved that by using the proposed methodology to precisely assign relay locations, the network performance could be improved from the reference case where locations were assigned just from distance range. Moreover, two-way relaying scheme was also proved to be the appropriate scheme in the scenario of relay networks for densely deployed sensor networks.

6.2 Suggestions for future studies

In this dissertation, we extended the research of multi-hop relay networks from theory to practical study. However, our studies were based on propagation measurement which takes cost and time and is still not close to the realistic applications. Below is the suggestion for the further studies.

- Relaying schemes in our studies are all TDD based and need the precise synchronization mechanism, especially for two-way relaying schemes. The synchronization schemes right now are mostly in centralized mechanism which might not be flexible during network setup period, so that in multi-hop relay networks the synchronization method in distributed manner is necessary.

- In our study of M2WMN, we assumed that all Tx and Rx nodes have perfect knowledge of channel information. However, in the real situation, channel knowledge feedback cannot be perfectly performed due to fluctuations in coherence time. The effect of imperfect channel knowledge in M2WMN under the realistic condition has to be further investigated.

- Since the channel information exchange of power control is performed in distributed manner, the network needs some times in iterative process to determine the optimum power during network initialization. The algorithm is designed for static environment situation, however, in non-static situation, channel information is not stable in during the iterative process and the solution to deal with this situation is necessary.

- In Chapter 5, we considered the network performance of WSN during the operation. However, for the real implementation, the mechanism of network setup to perform scheduling, network synchronization and routing is necessary. Also, since we assumed the full traffic load in our consideration to see the performance of the network in the worst case, this assumption might not always be applicable for the real usage. In the real application of WSN, some nodes may need QoS and some nodes do not need symmetric data streams, so that these issues should be taken into account for the future studies.

- In the proposed methodology in Chapter 5, we estimate the relay locations by using channel data from the simulation. For the network planning in the real site, we need to develop a tool based on the proposed methodology to help the site planner select the location for deploying relays.

Appendix I

List of Publications

I.1 Publications

I.1.0.0.1 Journal papers

- N. Lertwiram, G. K. Tran, K. Mizutani, K. Sakaguchi, K. Araki, "Performance Analysis of MIMO Relay Network via Propagation Measurement in L-shaped Corridor Environment", IEICE Trans. Commun., Vol. E95-B, No. 04, Apr. 2012.

- N. Lertwiram, P. Popovski, K. Sakaguchi, "A Study of Trade-Off Between Opportunistic Resource Allocation and Interference Alignment in Femtocell Scenarios", IEEE Wireless Commun. Letters, Vol. 1, No. 4, pp. 356 - 359, Aug. 2012.

- N. Lertwiram, G. K. Tran, K. Sakaguchi, K. Araki, "An Efficient Relay Node Placement Scheme for Two-way MIMO Multi-hop Networks in Practical Environment", IEEE Trans.Wireless Commun., Vol. 12, No. 6, pp. 2977 - 2987, June 2013.

I.1.0.0.2 International conferences

- N. Lertwiram, G. K. Tran, K. Mizutani, K. Sakaguchi, K. Araki, "MIMO Radio Propagation Measurement for Two-Hop Relay Network on L-shaped Corridor with Network Performance Analysis", IEEE VTC2010-Spring, May. 2010.

- N. Lertwiram, G. K. Tran, K. Sakaguchi, K. Araki, "Relay Placement of Two-Way Multi-Hop Relay Network with Power Adaptation in a Realistic Shadowing Environment", IEEE VTC2012-Spring, May. 2012.

I.1.0.0.3 Domestic conferences

- N. Lertwiram, G. K. Tran, K. Mizutani, K. Sakaguchi, K. Araki, "Propagation Measurement of MIMO Relay Network in Strong Shadowing Indoor Environment at 5 GHz Band", IEICE RCS Technical Conf., vol. 109, no. 440, pp. 161-166, Mar. 2010 Propagation Environment," IEICE Society Conference, B-1-4, Sep. 2007.
- N. Lertwiram, G.K. Tran, K. Sakaguchi, K. Arkai, "Practical Relay Node Placement for MIMO Two-way Relay Networks in a U-Shaped Corridor Environment", IEICE SR Technical Conf., 2012-07-SR, Jul. 2012.
- N. Lertwiram, G.K. Tran, K. Sakaguchi, K. Arkai, "Network Planning Methodology for Wireless Multi-hop Networks in Practical Environments", IEICE SR Technical Conf., 2013-07-SR, Jul. 2013.

I.2 Awards

- IEEE VTS Japan Young Researcher's Encouragement Award (2010)

Reference

[1] K. Doppler, M. Rinne, C. Wijting, C. Ribeiro, K. Hugl, "Device-to-device communication as an underlay to LTE-advanced networks," *IEEE Commun. Mag.*, vol. 47, no. 12, pp. 42–49, Sept., 2009.

[2] I. F. Akyildiz, W. Su, Y. Sankarasubramaniam, E. Cayirci, "A survey on sensor networks," *IEEE Commun. Mag.*, vol. 40, no. 8, pp. 102–114, 2002.

[3] J. Cortes, S. Martinez, T. Karatas, F. Bullo, "Coverage control for mobile sensing networks," *IEEE Trans. Robotics and Automation*, vol. 20, no. 2, pp. 243–255, 2004.

[4] S. Chen, M. Huang, S. Tang, Y. Wang, "Capacity of data collection in arbitrary wireless sensor networks," *IEEE Trans. Parallel and Sistributed Systems*, vol. 23, no. 1, pp. 52–60, 2012.

[5] A. Willig, "Recent and emerging topics in wireless industrial communications: A selection," *IEEE Trans. Ind. Inforamt.*, vol. 4, no. 2, pp. 102–124, 2008.

[6] M. Kohvakka, M. Hannikainen, T. Hamalainen, "Wireless sensor network implementation for industrial linear position metering," in *Proc. 8th Euromicro Conf. Digital System Design (DSD)*, pp. 267–275, 2005.

[7] L. Q. Zhuang, K. M. Goh, J. B. Zhang "The wireless sensor networks for factory automation: Issues and challenges," in *Proc. IEEE Conf. on Emerging Technologies and Factory Automation (ETFA)*, pp. 141–148, 2007.

[8] *IEEE P802.15 Wireless Personal Area Networks: Proposal for Factory Automation*, Working Draft Proposed Standarad, Rev. 802.15.4-15/08/0571r0, 2009.

[9] W. Luan, "Smart grid communication network capacity planning for power utilities," *Transmission and Distribution Conf. and Expo.*, pp. 1–4, Burnaby, Canada, 2010.

[10] Z. Zhu, S. Lambortharan, W.H. Chin, Z. Fan, "Overview of demand management in smart grid and enabling wireless communication technologies," *IEEE Trans. Wireless. Commun.*, vol. 19, no. 3, pp. 48–56, 2012.

[11] K. Sakaguchi, V. K. Nguyen, Y. Tao, G. K. Tran, K. Araki, "Distributed power control network and green building test-bed for demand response in smart grid," *IEICE Trans. Fund.*, vol. E96-A, no. 5, 2013.

[12] T.S. Rappaport, "Wireless Communications: Principles & Practice," *Prentice Hall*, 2nd ed., 2001.

[13] J. Boyer, D.D. Falconer and H. Yanikomeroglu, "Multihop diversity in wireless relaying channels," *IEEE Trans. Commu.*, vol.52, no.10, pp.1820–1830 , 2004.

[14] R. Pabst, B.H. Walke, D.C. Schultz, P. Herhold, H. Yanikomeroglu, S. Mukherjee, H. Viswanathan, M. Lott, W. Zirwas, M. Dohler, H. Aghvami, D.D. Falconer, G.P. Fettweis, "Relay-based deployment concepts for wireless and mobile broadband radio," *IEEE Commun. Mag.*, vol.42, no.9, pp.80–89, 2004.

[15] M. Hasna and M. Alouini, "End-to-end performance of transmission systems with relays over Rayleigh fading channels," *IEEE Trans. Wireless Commun.*, vol.2, pp.1126–1131, 2003.

[16] T. He, J. A. Stankovic, C. Lu, T. F. Abdelzaher, "A spatiotemporal communications over cluster-tree sensor networks with mobile sink behavior," in *Proc. 14th IEEE Int. Conf. Embedded and Real-Time Comput. Syst. Appl. (RTCSA)*, pp. 401–412, 2008.

[17] M. Yarvis, N. Kushalnagar, H. Singh, A. Rangarajan, Y. Liu, S. Singh, "Exploting Heterogeneous in Sensor Networks," in *Proc. INFOCOM 2005*, vol.2, pp.878, 2005.

[18] L. Yu, N. Wang, W. Zhang, C. Zeng, "Deploying a Heterogeneous Wireless Sensor Network," in *Proc. Int. Conf. on Wireless. Commu., Networking and Mobile Computing*, WiCom 2007, pp. 2588–2591, 2007.

[19] O. Younis, M. Krunz, S. Ramasubramanian, "Node clustering in wireless sensor networks: recent developments and deployment challenges," *IEEE Network*, vol. 20, no. 3, pp. 20–25, 2006.

[20] S. Banerjee, S. Khuller, "A clustering scheme for hierarchical control in multi-hop wireless networks," in *Proc. IEEE Conf. INFOCOM 2001*, vol. 2, pp. 1028–1037, 2001.

[21] *IEEE Standard for Local and metropolitan area networks - Part 15.4: Low-Rate Wireless Personal Area Networks (LR-WPANs)*, IEEE Std 802.15.4]2011, 2011.

[22] D. Christin, P.S. Mogre, M. Hollick, "Survey on Wireless Sensor Network Technologies for Industrial Automation: The Security and Quality of Service Perspectives," *Future Internet 2010*, no. 2, pp. 96–125, 2010.

[23] I.E. Telatar, "Capacity of multi-antenna Gaussian channels," *Eur. Trans. Telecommun.*, vol. 10, no. 6, pp. 585–595, 1999.

[24] J. Winters, "On the capacity of radio communications systems with diversity in a Rayleigh fading environment," *IEEE Journal on Selected Areas in Commun.*, vol. 5, no. 5, pp. 871–878, 1987.

[25] F. ono, K. Sakaguchi, "MIMO spatial spectrum sharing for high efficiency mesh network," *IEICE Trans. Commun.*, vol.E91-B, pp.62–69, 2008.

[26] D. Gunduz, A. Goldsmith, H.V. Poor, "MIMO two-way relay channel: Diversity-multiplexing tradeoff analysis," *Proc. Asilomar Conf. on Signals, Systems and Computers*, 2008.

[27] F. Ono, K. Sakaguchi, "STBC MIMO Network Coding for Bi-directional Multi-Hop Relay Networks," *IEICE Trans. Commun.*, vol.E92-B, no.12, pp. 3676–3682, 2009.

[28] L. Jiang, L. Thiele, V. Jungnickel, "Modeling and measurement of MIMO relay channels," *Proc. IEEE Veh. Technol. Conf. (VTC)*, pp.419–423, 2008.

[29] F.S. Gonzalez, B. Bandemer, G. Matz, C. Oestges, F. Kaltenberger, N. Czink, "Performance of transmission-time optimized relaying schemes in real-world channels," *Proc. IEEE Antennas and Propagation (EuCAP)*, pp.1–5, 2010.

[30] X. Nie, J. Zhang, Z. Liu, P. Zhang, Z. Feng, "Experimental investigation of MIMO relay transmission based on wideband outdoor measurement at 2.35 GHz," *Proc. IEEE WCNC 2010*, pp.1–6, 2010.

[31] X. Cheng, D.Z. Du, L. Wang, B. Xu, "Relay sensor placement in wireless sensor networks," *ACM/Springer Journal of Wireless Networks*, vol. 14, no. 3 , pp. 347–355, 2008.

[32] J. Cannons, L. B. Milstein, K. Zeger, "An algorithm for wireless relay placement," *IEEE Trans. Wireless Commun.*, vol. 8, no. 11 , pp. 5564–5574, 2009.

[33] E.L. Lloyd, G. Xue, "Relay node placement in wireless sensor networks," *IEEE Trans. Compu.*, vol. 56, no. 1, pp. 134–138, 2007.

[34] Q. Wang, K. Xu, G. Takahara, H. Hassanein, "Locally optimal relay node placement in heterogeneous wireless networks," in *Proc. IEEE GLOBECOM 2005*, 2005.

[35] C. E. Shannon, "A Mathematical Theory of Communication," *Bell Sys. Tech. Journal*, pp. 379–423, 623–656, 1948.

[36] G.J. Foschini, "Layered space-time architecture for wireless communication in a fading environment when using multi-element antennas," *Bell Sys. Tech. Journal*, pp. 41–59, 1996.

[37] T. Cover and A. Gamal, "Capacity theorems for the relay channel," *IEEE Trans. Inf. Theory*, vol.25, no.5, pp. 572–584, 1979.

[38] G. Kramer, M. Gastpar and P. Gupta, "Cooperative Strategies and Capacity Theorem for Relay Network," *IEEE Trans. Signal Processing*, vol.51, no.9, pp. 3037–3063, 2005.

[39] J. N. Laneman, D. N. C. Tse, and G. W. Wornell, "Cooperative diversity in wireless networks: Efficient protocols and outage behavior," *IEEE Trans. Inf. Theory*, vol.50, no.12, pp. 3062–3080, 2004.

[40] L. Lai, K. Liu and H. El Gamal "The Three-Node Wireless Network: Achievable Rates and Cooperation Strategies," *IEEE Trans. Inf. Theory*, vol.52, no.3, pp. 805–828, 2006.

[41] S. Katti, H. Rahul, W. Hu, D. Katabi, M. Medard, J. Crowcroft, "XORs in the air: Practical wireless network coding," *ACM SIGCOMM'06*, pp. 243–254, 2006.

[42] J. Lee, G.K. Tran, K. Sakaguchi and K. Araki, "Effect of power allocation schemes on MIMO two-way multi-hop network," *IEICE Trans. Commun.*, vol.E93-B, pp. 3362–3370, 2010.

[43] C. Mung, "Geometric programming for communication systems," *Now Publishers*, 2005.

[44] P. Sadeghi, and M. Soleymani, "An Autonomous Power Control for Achieving the Maximum Uniform SIR in Wireless Networks," *IEEE Commun. Letters*, vol.14, no.2, pp. 166–168, 2005.

[45] Y. Fan and J. S. Thompson, "MIMO configurations for relay channels: theory and practice," *IEEE Trans. Wireless Commun.*, vol.6, no.5, pp. 1774, 2007.

[46] Y. Wang, F. Liu, S. Xu, X. Wang, Y. Qian and P. Wang, "Performance Analysis of Multi-Hop MIMO Relay Network," *Proc. IEEE ICC Workshops 2008*, pp. 6–10, 2008.

[47] Y. Fu, L. Yang and Z. He, "Amplify-and-forward relaying scheme based on GSVD for MIMO relay networks," *Proc. IEEE Neural Networks & Signal Processing*, pp. 506–511, 2008.

[48] A.S. Behbahani, R. Merchedand and A.M. Eltawil, "Optimizations of a MIMO Relay Network," *IEEE Trans. Signal Processing*, vol.56, no.10, pp. 5062–5073, 2008.

[49] H. Bolcskei, R. U. Nabar, O. Oyman, and A. J. Paulraj, "Capacity scaling laws in MIMO relay networks," *IEEE Trans. Wireless Commun.*, vol.5, no.6, pp. 1433–1443, 2006.

[50] J. Zhang, D. Dong, Y. Liang, C. Huang, G. Liu and W. Dong, "Propagation Characteristics of Wideband Relay Channels in Urban Micro-Cell Environment," *IEEE Letters, AP.*, vol.9, pp. 657–661, 2010.

[51] Z. Wu, J. Zhang, X. Nie and C. Huang, "A Novel Relay Channel Modeling Method with Validation of Micro-Cell MIMO Relay Measurement Results at 2.35 GHz," *Proc. IEEE CHINACOM 2010*, pp. 1–5, 2010.

[52] P. Wang,Y. Zhou, X. Yin, X. Huang and F. Liu, "Measurement and Analysis of Relay Channels in Indoor Environments," *Proc. IEEE WiCOM 2010*, pp. 1–5, 2010.

[53] X. Yin, "Spatial Cross-Correlation of Multilink Propagation Channels in Amplify-and-Forward Relay Systems," *Proc. IEEE CHINACOM 2010*, pp. 1–5, 2010.

[54] K. Mizutani, K. Sakaguchi, J. Takada and K. Araki, "Development of MIMO-SDR Platform and Its Application to Real-Time Channel Measurements," *IEICE Trans. Communication*, vol.E89B, no.12, pp. 3197–3207, 2006.

[55] G. K. Tran, N. D. Dao, K. Sakaguchi, K. Araki, H. Iwai, T. Sakata and K. Ogawa, "Performance Analysis of MIMO Schemes in Residential Home Environment via Wideband MIMO Propagation Measurement," *IEICE Trans. Fundamental of Electronics, Communications and Computer Science*, vol.E93-A, No.4, 2010.

[56] G. Strang, "Linear Algebra and Its Applications," *Thomson Learning Inc.*, 3rd ed., 1988.

[57] K. Sakaguchi, H. Chua, K. Araki, "MIMO Channel Capacity in an Indoor Line-Of-Sight (LOS) environment," *IEICE Trans. Commun.*, vol.E88-B, no.7, pp. 3010–3019, July., 2005.

[58] R.M. Buehrer, "The impact of angular energy distribution on spatial correlation," in *Proc. IEEE VTC-Fall 2002*, vol. 2, pp. 1173 – 1177, 2002.

[59] N. Lertwiram, G. K. Tran, K. Mizutani, K. Sakaguchi, K. Araki, "Performance Analysis of MIMO Relay Network via Propagation Measurement in L-shaped Corridor Environment," *IEICE Trans. Commun.*, vol. E95-B, no. 04, 2012,

[60] *http://www.remcom.com/wireless-insite*

[61] K. Baba, "Data file of architectural design and details: [37] Organization residences and dormitory (In Japanese)," ISBN 0288-4267, *Kenchiku Shiryo Kenkyusha*, 2ed., 1994.

[62] J. B. Keller, "Geometrical theory of diffraction," *Journal of the Optical Society of America*, vol. 52, pp. 116–130, 1962.

[63] R. G. Kouyoumijian and P. H. Pathak, "A uniform geometrical theory of diffraction for an edge in a perfectly conducting surface," *IEEE Proc.*, vol. 62, pp. 1448–1461, 1974.

[64] "The Wireless InSite users manual: Release 2.5.11," *Remcom Inc.*, 2009.

[65] D. G. Manolakis, V. K. Ingle, S. M. Kogon, "Statistical and Adaptive Signal Processing," ISBN 1-58053-610-7, *Artech House, Inc*, 2005.

[66] K. Xu, H. Hassanein, G. Takahara, Q. Wang, "Relay node deployment strategies in heterogeneous wireless sensor networks," *IEEE Trans. Mobile Computing*, vol. 9, no. 2, pp. 145–159, 2010.

[67] J. Tang, B. Hao, A. Sen, "Relay node placement in large scale wireless sensor networks," *Computer Communications*, vol. 29, no. 4, pp. 490–501, 2006.

[68] "Entwurf und Planung 1: Industriebau Fertigungsbetriebe von Friedemann Wild (In German)," *Verlag Georg D.W. Callwey*, 1969

[69] D. Chase, "A Combined Coding and Modulation Approach for Communication over Dispersive Channels," *IEEE Trans. Wireless Commun.*, vol. COM-21, no. 3, pp. 159–174, 1973.

[70] G.K. Tran, K. Sakaguchi, K. Araki, "MIMO Network Coding-Based PHY/MAC Protocol for Replacement of CSMA/CA in Efficient Two-Way Multi-hop Relay Networks," *EURASIP Journal on Wireless Communications and Networking*, pp. 1–20, 2010.

[71] D. Tse, P. Viswanath, "Fundamentals of wireless communications," *Cambridge University Press*, 2005.

[72] A. Paulraj, R. Nabar, D. Gore, "Introduction to Space-Time Wireless Communications," *Cambridge University Press*, 2003.

[73] S. Alamouti, "A simple transmit diversity technique for wireless communications," *IEEE J. Select. Areas Commun.*, vol. 16, no. 8, pp. 1451–1458, 1998.